Fractional Solidification for Recycled Aluminium Alloys

A thesis submitted for the degree of Doctor of Philosophy

by

Susanna Venditti

Supervisor: Professor Dmitry Eskin

Academic year 2019/2020

BCAST- Brunel Centre for Advanced Solidification Technology

Department of Mechanical, Aerospace and Civil Engineering

Brunel University London

United Kingdom

Rita Levi Montalcini una volta ha detto “non temete i momenti difficili, il meglio viene da lì”

Nella mia vita, ci sono due persone che mi hanno sempre incoraggiata a non arrendermi mai davanti alle difficoltà: Olivia ed Eleonora.

Se sono riuscita a tenere duro, e ad arrivare fino a questo punto, lo devo soprattutto a loro. Grazie.

Ad maiora... il meglio, deve ancora venire.

Abstract

Climate change, and the need of recycling, are two interconnected topics that are gaining more and more relevance nowadays. In order to decrease the CO_2 emissions and reduce, or contain, the pollution that is having devastating effects on our climate, recycling seems to be a necessity that can not be postpone or diminished anymore. In the effort of reducing pollution, the aluminium world (industry and Academia) is playing an important role. Recycling aluminium, in fact, require only 10% of the energy necessary to extract it form the bauxite ore, leading to a massive energy and cost saving, as well to a reduction on the CO_2 emissions equivalent to take off the road 900000 cars for 12 months.

Up to now, the only closed loop recycling process is the one for usage beverage cans (UBC): used cans are collected, molten together, and used again to create new cans without the addition of any other material. When it comes to the automotive industry things are a bit more complicated. There are two main ways, adopted by industries, to recycle Al alloys depending on their composition. Wrought alloys are recycled remelting the scrap with primary Al, and cast alloys are obtained remelting wrought alloys and adjusting their composition for the different purposes. Although these two methods meet the requirement so far, they will lead to a non-recyclable scrap surplus in the near future, consequently, new possibilities are being explored.

In this work, a method to recycle aluminium alloys based on fractional solidification is proposed. The technology developed is based on an idea proposed by A.L Lux and M.C Flemings in which a semisolid alloy is isothermally squeezed towards a filter. Lux and Flemings tested their method on Sn-Pb alloys and on a small scale (500 g). The technology developed in this thesis, has been tested first on model aluminium alloys, and once the optimised procedure was established, on real aluminium scrap alloys, and on a bigger scale (up to 3 kg). The effect of several parameters (temperature, squeezing procedure, ultrasound, and grain refinement) on the purification efficiency was investigated and a 60% purification efficiency was achieved. Along with the technology development, a more fundamental study was carried out focusing on the investigation of the semisolid deformation, the liquid migration through the mush and the role of morphology on the permeability of the semisolid alloy. Finally, through the use of a numerical model, the feasibility of the Scheil-Gulliver approach to our case study, was investigated.

Preface

I hereby declare that I am the sole author of this thesis, and this thesis is the outcome of the work performed at BCAST in Brunel University London from November 2016 to October 2020. This is a true copy of the thesis, including any required final revisions, as accepted by my supervisor.

I understand that my thesis may be made electronically available to the public; therefore I authorise Brunel University London to make it available electronically to individuals or institutions for the purpose of scholarly research.

Conferences

- Poster presentation at National Student Conference in Metallic Material, Sheffield University, July 2017
- 6th Decennial Conference on Solidification Processing - SP17, Windsor (UK), July 2017
- Poster presentation at ICAA16 International Conference On Aluminium Alloys, Montreal (CA), June 2018
- 11th International Conference on Magnesium Alloys and Their Applications- Mg18, Windsor (UK), July 2018
- Oral presentation at TMS 2020 149th Annual Meeting & Exhibition, San Diego (USA), February-March 2020

Publication and Awards

- Fractional Solidification for Purification of Recycled Aluminium Alloys, S Venditti, D Eskin, A Jacot - Light Metals 2020, Springer
- Winner of the three minutes thesis (3MT) competition during the UK solidification workshop (October 2019)
- Winner of the engineering college PhD symposium held at Brunel University (June 2019)

Table of Content

Chapter 1

Introduction

Aluminium usage in the society and the need for recycling

Aluminium is the third most abundant element on Earth, comprising 8% of its crust. It was isolated for the first time in 1835 by Hans Christian Oersted and, initially, mostly utilised in jewellery due to the cost and the difficulties of extracting it from its ore. Al is extremely reactive, so it is usually found combined with other elements in minerals, making it difficult to isolate. It is usually obtained from alumina (Al_2O_3) that is extracted from the bauxite ore and separated from the red mud thought the Bayer process. The Hall-Heroult process [1] is used to refine aluminium from alumina by electrolysis. It was due to this process, discovered at the same time by Charles Martin Hall and Paul Héroult in 1886, that the metal's cost was lowered from $15 per pound in 1884 to $0.50 per pound in 1890 allowing the widespread use of this metal. Nowadays Al is the most used metal in the world after iron. In comparison to steel, it has low melting point, is rather soft and has a three-time lower density (2.7 g/cm). However, due to a relatively low strength, it is not commercially used in its pure form and is often alloyed with other elements to make it stronger. More than 450 alloy designations have been registered for Al alloys [2]. They can be classified as wrought alloys with a lower concentration of alloying elements (up to 10%) and cast alloys which have a higher concentration of elements (>8%). Both cast and wrought alloys are employed in many sectors of our daily life: transportation, construction, packaging, beverage cans. In the transportation sector, originally aluminium was employed in aircraft and some luxury cars, due its lightweight, but recently it is being used as well in cars, ships, trucks, lorries and bicycles. In 2007 more than 30% of the cast and wrought alloys in the market were used in this sector. In the automotive industry, especially, the use of Al alloys is gaining more and more interest as they can replace steel components in cars to make them lighter and safer, as well save CO_2 emissions. Aluminium alloys, in fact, are the main constituent of car structures, panels and wheels. The average use of aluminium in car industry is about 180 kg per passenger vehicle and the estimation is that this will raise to 250 kg per passenger vehicle in 2025 [3]. In buildings, Al is mostly used in windows, façade, doors, doors handlers, staircases, roller-shutter and sun-shading systems. Its characteristic formability, high strength to weight ratio, corrosion resistance, makes Al so suitable in building applications making possible intricate, stable and light-weight structures.

Aluminium is also an ideal material for packaging because of its unique properties. In fact, even in its thinnest form, it keeps food or liquids isolated and not contaminated by light, moisture, oxygen, microorganisms and unwanted aromas [4].

Due to this widespread use and good corrosion resistance, it is estimated that 75% of the 700 million tonnes of aluminium produced since commercial manufacturing began in the 1880s, is still being used as secondary raw material today [5]. A huge percentage of Al alloys used in society, in fact, comes from secondary aluminium (recycled from scrap). Aluminium is the material used in our daily lives that has the highest potential for recycling because its remelting does not modify the chemical and physical properties. What is even more important is that recycling Al only employs between 5 to 10% of the energy necessary to extract it from the bauxite ore, leading to considerable economic and environmental benefits. In fact, one tonne of recycled Al allows one to save up to 8 tonnes of bauxite, 14,000 kWh of energy, 40 barrels (6300 litres) of oil, 238 million Btu's of energy and 7.6 cubic metres of landfill [6]. It follows that there is an increasing interest from the manufacturing industry (and, in fact, society) to find suitable methods that could optimise the efficiency of the scrap recycling. In 1990 the total aluminium production was 28 million tonnes with 8 million tonnes recycled from the scrap. Today Al demand is close to 97 million with 31 million recycled from scrap. The main threshold in recycling Al into high-value materials, and applications, is the tolerance to the variation in chemical compositions of alloys. For this reason, both casting and wrought alloys can be obtained by recycling but the different percentage of alloying elements in these alloys implies the use of different recycling routes for these two groups of alloys [7]. Moreover, different alloying elements can be separated from aluminium in different ways. The challenge is to decrease the amount of unwanted impurities in the processed and recycled scrap. Such impurities find their way into the scarp through indiscriminate sorting, and collection of scrap, as well as due to still unavoidable mixing of different alloy grades. Also, scrap alloys may combine with other materials like rubber, plastic, glass, fasteners, paint etc. To improve the quality of the scrap material and to optimise the recycling process, different preliminary treatments are applied. The sorting process consists of different separating methods to clean Al alloys prior to melting. Magnetic contaminants are removed by placing the scrap in a conveyor belt that passes near a permanent NdFeB magnet so that the magnetic field generated by it attracts the ferromagnetic material [8]. This technique is widely used for recycled beverage cans (UBCs) to separate aluminium and steel cans. Light-weight materials like plastic and foams are separated by vertical air separation system [9]. The scrap material is inserted in a column with air flow blowing upwards so that the heavy metals are collected at the bottom and the lighter material are driven up. Some light-weight material can be lost in the process, and this is the drawback of the method. The most common way to separate non-ferrous materials in the scrap is the dense media separator [10]. It consists of three baths in which the specific gravity (SG) is gradually increased. The first bath has SG=1 and separates foam, wood, and low-density plastic. The specific gravity is then increased to 2.5 with addition of magnetite or ferrosilicon powder. In this way Mg, and high-density plastic, are separated.

The last bath, SG=3.5, separates Al cast and wrought alloys from heavier metals like Zn, Cu and Pb. Even though this method is very much used, it implies high cost of maintenance. Finally, to separate cast scrap from wrought alloys scrap, the hot crush method is applied [11]. Usually cast alloy, due to the higher number of elements, have a lower solidus temperature than wrought alloys so the process consists in heating up the mixture of alloys to temperatures below the eutectic one, and crush them. Cast alloys are easily crushed while pieces of wrought alloys are merely deformed. Sometimes spectroscopic techniques are applied as well to identify and separate different alloys. Among these, laser induced breakdown spectroscopy (LIBS) [12], has shown great potential. A high energy laser beam hits the surface of the metal scrap that absorbs the energy and produce excited atoms and ions in the emission spectrum. This spectrum is read by a polychromator and photodiode detector, which sends the signal to the computer. Finally, a robotic arm sends the piece to the appropriate bin.

Table 1 lists the most common impurities and their concentrations in presorted cast and wrought alloys scrap [13]. Some alloying elements are really difficult to separate from Al and they tend to remain entrapped even after re-melting and diluting. Among them, iron and silicon are harmful tramp elements for aerospace and automotive applications because the formation of intermetallic phases with Fe and Si, impacts the fracture toughness and ductility of these alloys. Usually Mg and Zn can be removed from Al alloys by adding a chemical compound known as flux (usually an inorganic salt) to the melt leading to the formation of chlorides or fluorides that can be removed from the melt by sedimentation or dross formation. Fluxes are particularly used for secondary Al but the amount necessary to make the reaction efficient is quite high, which makes it a drawback to the process. Moreover, fluorides and chlorides produce toxic gases that need to be filtered from emissions. Zn is removed by distillation [14] but the process is still in the development stage. It consists in holding the melt at a certain controlled temperature and controlled vapour pressure. The melt is brought above the boiling point of Zn. Vapour condensation collection results in a final purified Al alloy.

Si and Fe can both be removed by adding manganese to the melt under an electromagnetic field [15]. Alternatively, Fe can be removed with the formation of primary Fe rich intermetallics followed by holding the melt at the sludge temperature formation for a short time and then removing the particles by filtration, gravity separation, electromagnetic separation, or centrifugation. A technology based on the formation of primary intermetallics and High Shear Melt Conditioning [16], has been developed at BCAST, Brunel University London to remove Fe from Al scrap, but the methodology has not been utilised yet in industry.

Table 1: Impurity concentrations in common presorted wrought and cast scrap [13].

	Al	Cu	Fe	Mg	Mn	Si	Zn	Others
Wrought 1	97.1	0.11	0.59	0.82	0.21	0.51	0.45	0.19
Wrought 2	96.7	0.30	0.60	0.60	0.20	0.90	0.50	0.10
Wrought 3	93.1	0.95	1.01	0.89	0.12	2.41	1.25	0.27
Wrought 4	93.1	1.20	0.70	0.70	0.30	2.60	1.20	0.20
Cast 1	83.5	4.40	0.40	0.40	0.30	8.0	1.90	0.40
Cast 2	86.0	3.90	0.10	0.10	0.20	6.30	2.30	0.30
Cast 3	88.4	2.50	0.75	0.58	0.26	5.18	1.27	1.19
Mixed wrought and cast	90.1	2.30	0.80	0.50	0.20	4.50	1.20	0.30

All the methods just described above are still in the development stage and even if they have been proven successful, the automotive industry is still using primary Al to maintain the quality of the alloys. Remelting of scrap with the addition primary Al is by far the most used way to recycle wrought alloys. This is rather expensive process as it requires the use of primary aluminium. Recycled casting alloys are obtained by scrapping high-value alloys to produce lower-value grades allowing for a larger concentration of impurities. Although these strategies are widely applied, they lead to a non-recyclable scrap surplus and are not economical and environment-friendly; therefore, new methods need to be found. It is then necessary to find new suitable ways to recycle alloys that could meet the interest of the industry based on the knowledge and research interests of the academia.

1.2 Outline of the thesis

This chapter is introductory.

The second chapter provides a survey of the state-of-the art in purification techniques and lays a fundamental and technological base of this thesis. It starts with thermodynamics of phase diagrams, which is essential for understanding the fractional solidification technology. An overview of fundamentals of solidification and solidification processing is given to support the analysis of microstructure and to illustrate solute partitioning in order to improve the purification achievable with the technology developed in this thesis. A quick description of semisolid processing is also given to highlight that, although semisolid technologies are available, this work differs from those. A review of known purification techniques including fractional solidification methods is given.

The third chapter is focused on the methodology, describing the technology that has been developed and the alloying systems tested, along with the characterisation techniques that were used to explain the mechanisms of the partitioning and to prove the purification achievable.

The fourth chapter describes and analyses the semisolid structure, its modification during the squeezing and how this deformation impacts the liquid migration. The effect of the ultrasonic vibrations and the grain refinement of the alloy are evaluated as parameters influencing the migration of liquid in the mush.

The fifth chapter is a theoretical investigation of the role of back diffusion of the purification efficiency. A description of the models currently available is initially given. The focus is then shifted on a model developed by Prof. Alain Jacot that describes in a simplified way the squeezing process, and the role of back diffusion for different alloying elements in Al.

The sixth chapter is focused on the evaluation of the purification efficiency. The results of the purification process are discussed for the initial set-up developed and for the upscaled optimised set-up. Different parameters that play a role in the purification efficiency and their effects are evaluated.

The final chapter comprises the conclusions and the outlook for future research and development.

CHAPTER 2

Fundamentals and approaches in alloy purification

Secondary aluminium alloys obtained from the end of life scrap of cars, aerospace, or transportation sector in general, are contaminated with different type of impurities. Not only alloying elements, but also fasteners, coatings, rubber components, and other contaminants picked up during the shredding process which contribute to the scrap composition. In order to be recycled and used, secondary Al alloys need to meet some requirements, therefore purification processes are necessary, even if the recovery of pure Al is almost impossible from a thermodynamic point of view. In this chapter, we discuss the principle of fractional solidification and the technologies available so far in literature with their drawbacks. We start with phase diagrams as they constitute the foundation of fractional solidification. This is followed by fundamentals of solidification because this is the key aspect. Finally, an overview of semisolid processing, its applicability to purification and its drawbacks, will be presented.

2.1 Thermodynamics of solidification

Solidification is a process of transforming a liquid (metal, alloy, organic mixture) into a solid phase and involves changes in concentration and energy as well as structure formation (dendrites, constitutive phases, porosity). Solidification is crucial in several fields of knowledge and application: ice formation, food chemistry, volcanology, and metallurgy. Metal solidification, especially, has a key role in many industrial processes. Before getting into discussion of the solidification principles and solutes redistribution at the liquid/solid interface, it is important to have an insight into the thermodynamic principles that are essential to understand solidification processing.

Thermodynamics is the study of the behaviour of system under the effect of a physical alteration like pressure or temperature [17], [18]. A system is defined as a body of matter within boundaries that separate it from the surrounding. A system is made of components, chemically distinct entities, and contains phases which are portions of the system with uniform physical and chemical properties separated by boundaries from other parts of the system. Three variables (temperature, pressure, and volume) define the state of the system. Therefore, the system is described by a state variable which can be written as a function of thermodynamic variables. State variables are the Gibbs free energy (G), enthalpy (H), internal energy (E), entropy (S). The free energy describes if the system, at certain fixed values of composition, temperature, and pressure, is at equilibrium. This equilibrium is reached when G is at a

minimum value. This means that the system is stable, and it remains in this way unless there is a variation of temperature and pressure and/or composition. Gibbs free energy is defined according to Equation 1

$$G = H - TS. \quad (1)$$

The simplest thermodynamic system is the one component system. Below an example of one component system: water, is shown.

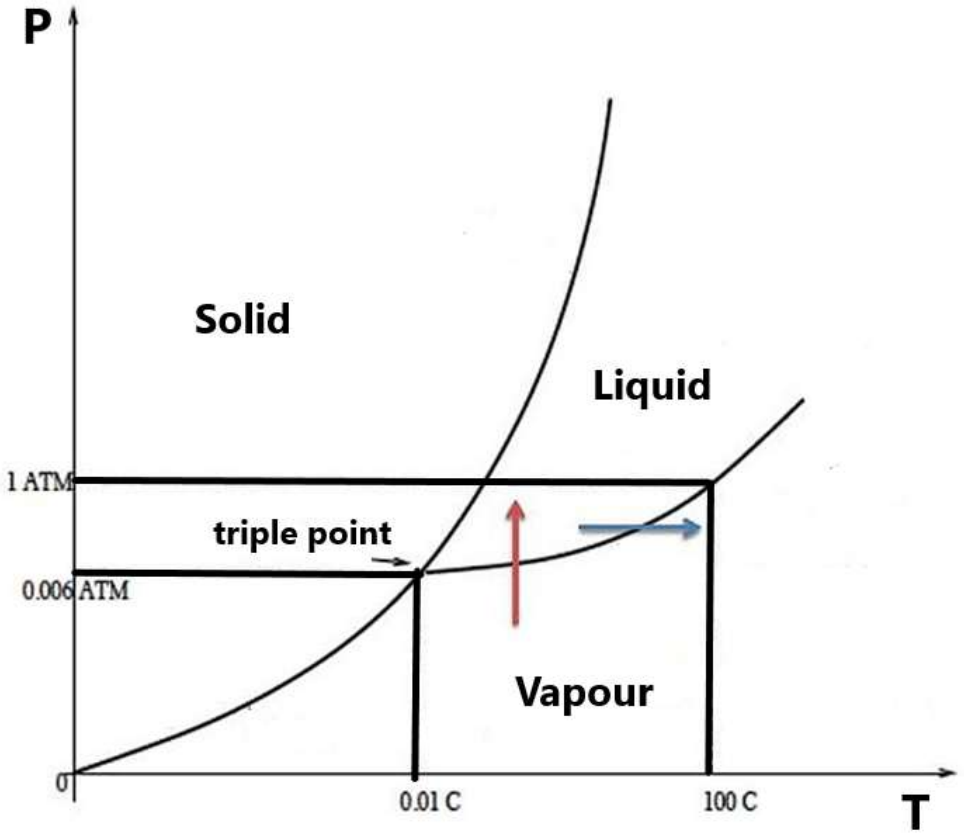

Figure 1. Phase diagram of water adapted from [19].

The phase diagram is made of three regions corresponding to three different phases separated by three lines that are merging in the single point defined as the triple point. This point is defined only by a certain value of T and P when all the three phases are in equilibrium. In this phase diagram composition is considered a constant, and the variables changing are pressure and temperature. Although this phase diagram is very common, for example in physical chemistry, there is another type of phase diagram in which the pressure is considered constant and the variables changing on the axis are temperature and composition. Phase diagrams like this last one, find wide application and use in metallurgy, as the properties of metals, as the condensed matter, do not vary much with pressure within normal range of variation. Therefore, these phase diagrams are a valid tool to understand the change in composition, and phases

of the components. For aluminium alloys, phase diagrams are important to understand the change that the system is undergoing depending on the different treatment. A -ne-component phase diagram represents the simplest example of phase diagrams, however multi-component phase diagrams are more used in metallurgy to explain the alloys thermodynamics. In this work, phase diagrams represent the basis for understanding and controlling the fractional solidification process.

Figure 2 shows a binary Al-Si phase diagram. Three different phases can be identified: liquid (L), and two solid phases (α) and (β). One case sees the regions where these phases co-exist, i.e., semi-solid region α+L within certain values of temperature and composition, and the eutectic mixture α+β. The α phase identifies the solid solution based on Al, meanwhile β identifies the solid solution based on Si. Both solid phases have a solubility limited to a certain range of temperature and composition.

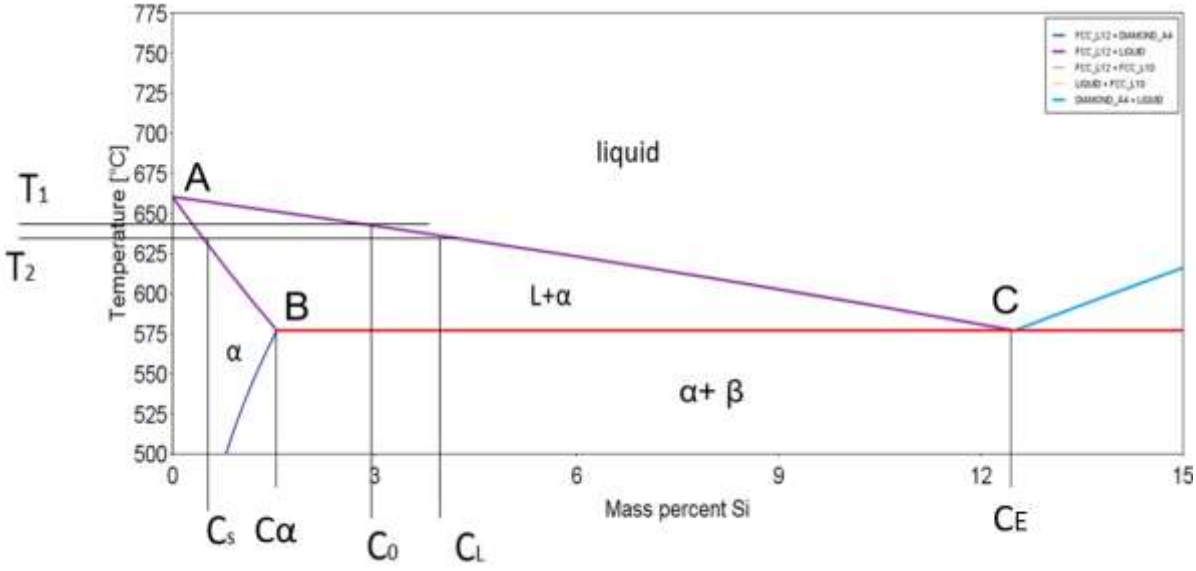

Figure 2. Al-Si phase diagram obtained by Thermocalc software

The line AC is called the liquidus curve and below this line, at certain values of temperature and composition, the formation of the solid phase is starting. The line shows how the solidification temperature of the alloy decreases according to the increasing amount of Si until the point C. This point is identified by specific values of temperature and concentration and is called the eutectic point and it is related to the eutectic transformation

$$L \rightarrow \alpha+\beta \qquad (2)$$

The ABC line defines the solidus, below this line there is no liquid phase. Along the line AB there are two phases in the equilibrium, along the eutectic line BC – there are three phases in

the equilibrium. In general, identification of phases in the phase diagram is quite simple, what is less immediate is the identification of the composition of a phase and its quantification inside a two-phase (or any multi-phase) region. For this reason, the lever rule is applied [18]. For a certain alloy composition, a horizontal line (tie line or canode) is drawn along the temperature chosen, connecting the points on the respective lines where the phases are in equilibrium. The ends of the tie line show the compositions of the phases in equilibrium. In order to quantify the amount of a phase in the two-phase mixture, for example the solid phase, we must take the length of the horizontal line that goes from the intersection with the C_0 (which is the original composition of the alloy) to the intersection with the liquidus line AC and divide it by the entire length of the conjugated line. In Equation 3 it becomes [18]

$$\frac{C_0 - C_L}{C_L - C_S} \tag{3}$$

Similar calculation for the quantification of the liquid phase (Equation 4)

$$\frac{C_0 - C_s}{C_L - C_s} \tag{4}$$

Usually the composition of an alloy is defined as mass fraction (mass.% or wt%). Sometimes, it is preferred to use the volume fraction because its value can be calculated from the microstructure. The volume fraction can be converted using the weight fraction and the value of the density according to Equation 5 [18]

$$V_\alpha = \frac{\frac{W_\alpha}{\rho_\alpha}}{\frac{W_\alpha}{\rho_\alpha} + \frac{W_\beta}{\rho_\beta}} \tag{5}$$

Where Wα is the mass fraction of the component α (pure aluminium in this case) and ρα is its density. Same for component β (silicon in this case), Wβ is the mass fraction and ρβ is its density.

The foundation of the phase diagrams lays on the thermodynamic laws. Among these laws, the Gibbs rule [18] defines the phases that exist in a phase diagram at equilibrium conditions, according to equation 6.

$$P + F = C + N \tag{6}$$

Where P is the number of phases, F is the degree of freedom (number of variable that can be changed without changing the number of phases coexisting in equilibrium), C is the numbers of components, N is the number of physical quantities usually two (pressure and temperature). So, in a region in which there is only one phase, for example at temperature higher than 660 °C (Fig.2), the number of degrees of freedom are two, and two parameters are necessary to identify the position of the alloy in the phase diagram. In the semisolid region, instead, where the solid and the liquid phase coexist, the value of F is equal to one. It means that, for example, the composition of the alloy can be in any position of the along the line T_2. Vice versa, if the composition of the solid phase along T_2 is fixed and known, it is possible to know the composition of C_L and the temperature.

The phase diagram also allows us to understand how solutes redistribute during solidification, and this is particularly important for the development of the topic of this thesis.

2.2 Fundamentals of solidification

As Boettinger and Banerjee mention, solidification is a general phenomenon that occurs in various processes, e.g. explaining ice damage on crops and chocolate processing, but it gets particular relevance when it is applied to metals and alloys, including aluminium alloys [20]. Casting based on solidification is, in fact, one of the oldest manufacturing processes and one of the main metal processing technology [21]. Solidification is a phase transformation from the liquid to the solid and in every phase transformation, a new phase forms with different physical and chemical properties. The phase transformation typically requires two stages: nucleation and growth. Nucleation is the formation of small particles of the new phase which, in this case, are small solid particles. Growth is the process by which the new phase grows in size propagating and consuming the liquid phase. Nucleation requires a certain activation energy to proceed to the growth stage [18]. This activation energy is a function of temperature and of the latent heat of fusion released during the solidification process. In the case of equiaxed solidification, the process is driven by the heat transfer from the liquid through the solid that is forming and through the wall of the mould into the surrounding, to compensate for the released heat of fusion. There are of course several factors influencing solidification (energy, species, transportation phenomena) and they are not going to be discussed in this chapter, but it is important, for the scope of this thesis, to give a general and basic overview of solidification [22]. When a material solidifies, the solid phase acquires a certain morphology depending on the condition of the solidification and this morphology can be characterised by different orientation or geometry. In the case of alloys, the most common solidification structure is the dendritic one (Figure 3) characterized by a tree like shape. The name dendrite comes from the

ancient Greek word *dendros* that means tree. Depending on the direction of solidification, the dendrites can grow in one direction preferentially, developing columnar grains, or in all the directions, forming equiaxed grains. Usually, consequently to dendritic formation, there are developments of phenomena like: coarsening and dendritic fragmentation that depends on solidification conditions. The study of the microstructure, then, is a valid way to understand and trace back which phenomena took place during the process.

When the solidification starts, a redistribution of solutes at the interface happens, under the condition that limited (or local) thermodynamic equilibrium prevails. Usually the redistribution of solutes is aided by transport processes happening primarily in the liquid phase. The tie line (see Figure 2) connects the solid composition at equilibrium with the respective liquid phase composition, showing the difference of the compositions of the solid and the liquid phases at the interface between them.

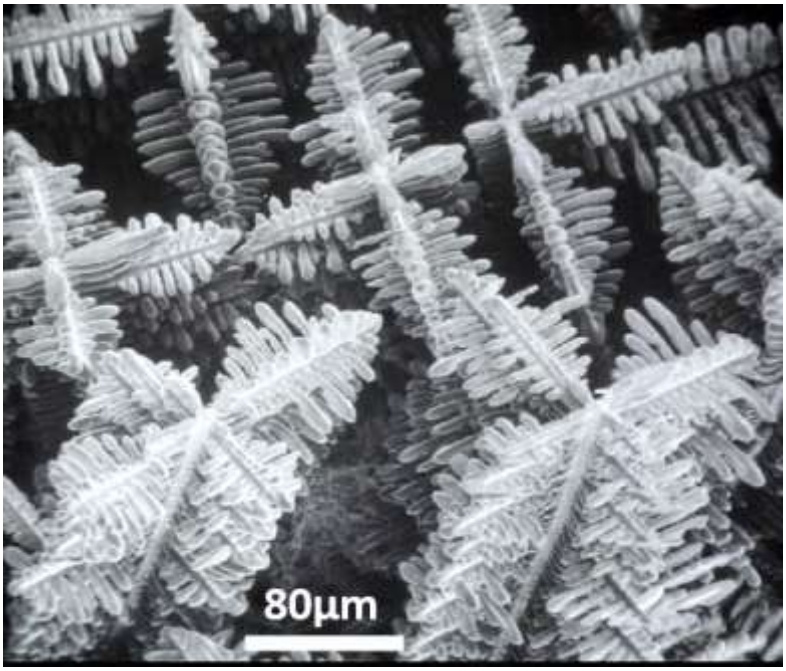

Figure 3: SEM image of dendrites in a cobalt-samarium-copper alloy adapted from [23].

The tie line represents graphically the concentration jump that is expected between conjugated phases in dependence on the temperature. The condition of equilibrium is intended to be only local and not global. During local equilibrium three conditions must be satisfied [22]:

1. Thermal equilibrium $T_s = T_l$
2. Mechanical equilibrium $P_s = P_l$
3. Chemical equilibrium $\mu_s = \mu_l$

Where T is the temperature, P is the pressure and μ is the chemical potential. Meanwhile the first two conditions are of immediate understanding, the third condition implies that the components on both sides of the tie lines in different concentrations, maintain the same chemical potential exchanging short diffusive fluctuations. The equality of chemical potential is limited to the small region where the two phases are in molecular contact to each other.

This redistribution of solutes at the interface is a key concept for fractional solidification because its extent defines the purification achievable. The partition of solutes can be defined by a partition coefficient according to Equation 7 as the ratio between the concentration of solutes in the solid and the concentration of solutes in the liquid at a certain temperature.

$$K = \frac{C_s*}{C_L*} \tag{7}$$

Where C_s* is the concentration of solutes in solid and C_L* is the concentration of solutes in the liquid.

Partition coefficient is determined from the phase diagram of the alloy. It can be calculated from the liquidus and solidus line since it depends on the solute solubility in the liquid and solid phases (Figure 4) [17]. The partition coefficient depends only on the interface temperature and the pressure under the condition that the interface remains quiescent.

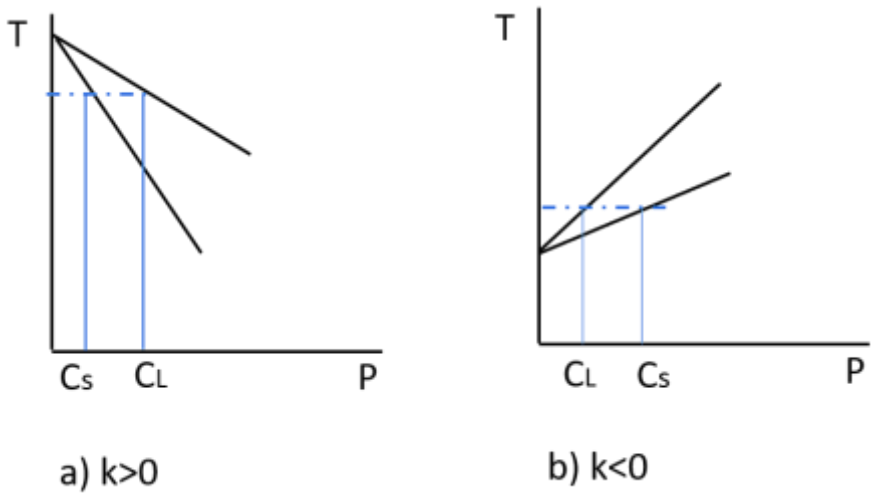

Figure 4. Schematic phase diagram showing solidus ad liquidus lines a) k<1 and b) k>1 adapted from [24].

This redistribution of solutes at the interface, controls the microstructure and the fraction of eutectic or other phases that form. In many solidification models, it is assumed that the partition coefficient is constant through the solidification process. This is valid only if the liquidus and solidus slope are considered straight lines, so the slopes are independent of temperature and

composition. This assumption cannot be valid for every phase diagram, so it can be considered as an approximation for solidus and liquidus lines bordering eutectic (k<0) or peritectic reaction (k>0) (Figure 4). Note that for having rejection of solutes from solid to liquid, k has to be less than one. In this case, the lower the partition coefficient, the bigger the partitioning, i.e. the difference between the solute concentrations in liquid and solid phases.

The partition coefficient appears is several mathematical expressions, such as the solid fraction forming during solidification. There are two equations describing the solid redistribution during solidification. The one shown below is the lever rule equation

$$f_s = \frac{1}{1-k_0}\left(\frac{T-T_{liq}}{T-T_f}\right) \tag{8}$$

where T_{liq} is the liquidus temperature, T_f is the solidification temperature and k_0 is the partition coefficient mentioned earlier.

Equation 8 implies local equilibrium at the interface and infinite diffusion is present in the solid and in the liquid. These conditions are never achievable. Instead, the solid fraction evaluation according to the Scheil Gulliver mode, consider equilibrium being local but assumes that diffusion in the solid can be neglected. In fact, the diffusion in the liquid state is few orders of magnitude faster than the one happening in the solid so the solid diffusion can be neglected. This assumption leads to the second equation that represent the forming solid fraction during solidification

$$f_s = 1-\left(\frac{T-T_f}{T_{liq}-T_f}\right)^{\frac{1}{k_{0-1}}} \tag{9}$$

The estimation of the solid fraction according to Scheil-Gulliver approximation is less that the one according to lever rule.

There are modifications of the Scheil-Gulliver equation that take into account diffusion in the solid phase. All these models are characterised by the Fourier number (or dimensionless diffusion) that is defined as

$$F = \frac{Dt_f}{X^2} \tag{10}$$

Where D is the diffusion coefficient, X is the length scale that is usually the secondary dendrites arm spacing, and t_f is the local solidification time. In general, it is not correct to assume that the length scale is always fixed, as it is necessary to also consider the coarsening of the

microstructure. In fact, the Beckerman-Voller [25] model adds in the Fourier number a parameter (called α again) that takes into account this coarsening effect.

2.3 Semisolid processing and microstructure

The concept of semisolid processing was initiated, by chance, in 1971 at MIT when a PhD student stirring continuously a Sn-15 wt% Pb alloy during cooling, found out that the alloy showed a thixotropic behaviour, meaning that when it is sheared it flows but when left to stand it gets thick [26]. This student, together with his supervisor Prof. M.C Flemings, discovered that stirring a semi-solid material during cooling, would result in less shear resistance of the material than when it is cooled to the semisolid state and then stirred isothermally. The study of the microstructure showed that when the material was constantly stirred during cooling, the solid phase was formed as spheroids in the liquid matrix, while the one that was cooled to the semisolid state was made of dendrites [26]. Hence, shearing during cooling changes the solid structure, breaks the dendrites arms, and results in a more rosette like structure that, finally, becomes spheroidal. For hydrodynamic reasons, the movement of these spheroidal particles in the liquid matrix is much easier than the ones that have a more dendritic structure. This behaviour is due to the formation of clusters of solid particles when the shearing is stopped, and the consequent break of the same cluster as soon as shearing is started.

In general, the microstructure of a semi-solid metal slurry can be categorized as: “liquid like” slurry, containing dispersed solid particles behaving like a fluid under external forces, or as a “solid like” mush made of clusters of solid particles with a certain yield strength. The deformation mechanism of these two structures is completely different. For thixoforming application, the structure needs to be fluid slurry where the solid fraction is less than 0.6 [27]. This specification is important because the two different types of structure behave differently upon deformation. To characterize the microstructure of a semi-solid slurry, at a fixed composition, it is necessary to define or calculate the volume fraction of the solid particles, their size, shape, and distribution. The volume fraction can be calculated from the equilibrium phase diagram or from the Scheil–Gulliver Equation 9, and it is fixed at a fixed temperature. Particle shape can be obtained from image analysing software and is calculated applying the following equation [27]

$$F = \frac{4\Pi A}{P^2} \tag{11}$$

Where F is the shape factor, P and A are the perimeter and the area of the object. Particle distribution can be calculated from the 2D optical images using the number of particles in

agglomerates. The particle distribution and the particles sizes can also be obtained using conventional metallographic techniques from microscope images [27].

Different mechanisms can be found in literature to explain the spheroidization phenomena observed during semisolid metal processing and up to now there is not yet a unified theory [28]–[30]. These mechanisms consider dendrite fragmentation, dendrite arm root remelting, and growth-controlled mechanism. Vogel et al. [31] proposed the dendrite arm fragmentation mechanism suggesting that the dendrite arms bend plastically under the shear force created by the stirring. The plastic deformation induces misorientation in the dendrites arm that leads to geometric dislocations. At high temperatures these dislocations rearrange themselves to generate high angle grain boundaries through re-crystallization. Any grain boundaries, having an energy twice greater than the solid liquid interfacial energy, are wetted by the liquid metals resulting in a detachment of the dendrite arm. Han and Hellawell [32] suggested dendrite arm remelting due to the solute enrichment and thermosolutal convection because the vigorous stirring prevents the formation of a stable diffusion field for continue dendrite evolution. Recently some mechanisms have been proposed that consider the spheroidization as a result of a growth phenomenon where the dendrite bending could give rise to a rosette formation without any mechanical effect [33]. Qin and Fan [34] attribute the rosette formation to a growth phenomenon. According to their work, the penetration of the liquid into the interdendritic region lead to a growth change rate. In fact, with increasing turbulent flow, caused by high shear rate, the growth rate increases laterally and at the root of the dendrite arm resulting in the rosette formation, or even spheres when the intensity of the turbulence is enough to allow it.

The mechanisms briefly described here are just a fraction of the material available in literature. Despite all the mechanisms proposed, the process of spheroidization remains still unclear. More studies need to be done to understand the effect of factors like alloy composition, temperature intensity of the melt flow on the morphology of the particles.

The scope of this brief excursus is to illustrate that the mechanisms happening during semisolid processing are quite complicated, and to focus, also, the attention on the morphology and the structure of a semisolid material. Although this thesis is not related to semi-solid processing as intended in recent industrial applications (thixoforming and thixoforging), there are similarities in the structure and morphology with the samples obtained at the end of our purification process, especially for the spheroidization phenomena, coarsening and liquid migration.

2.4 Fractional Solidification

Fractional solidification is a separating technique in which a material is processed in a semisolid state with solutes partitioned between the solid and the liquid phase [35]. Fractional solidification has been widely applied in metallurgy specially to obtain high purity aluminium (known as zone melting) and nowadays the research is ongoing on applying the method to aluminium scrap. This separating technique is also used in food chemistry to obtain purified fatty acids [36], or in geochemistry to study the composition of magma [37], [38]. The basic principle of the separation lays in partitioning. While the solidification happens, and if the solubility of the solutes in the liquid is higher than in the solid, the growing primary solid phase rejects the solute elements at the interface enriching the liquid phase. This situation happens for all alloys in which the partition coefficient (C_s/C_l) is less than one. The theoretic principle can be easily illustrated in the phase diagram (Figure 2). The initial composition of the alloy is represented by C_0. When that alloy is cooled down until the temperature in which the solid and the liquid phase coexists, the composition of the alloying element (Si in this case) in the solid fraction, depicted by C_s, is lower than the composition of Si in the liquid fraction (C_l). Eliminating the liquid fraction at this temperature, in the semi-solid range, will result in a solid fraction purer than the initial composition of the processed alloy. The major issue with the fractional solidification is to what extent the secondary constituents can be taken out of the semi-solid alloy. Sillekens et al. [39] gave a theoretical evaluation of the performance of the purification process assuming that the solid and the liquid fraction are completely separated and that the refining process happens in one step only. So, they defined the efficiency as (equation 12):

$$\eta = (1 - \frac{C_s}{C_0}) \tag{12}$$

where C_s and C_0 have been defined previously. When η= 1 it means that the alloying element, or solute, or Si in this particular case, is completely removed. Instead η= 0 means that no purification happened.

Another useful parameter is the yield (P) indicating the quantity of refined product, compared to the one of the unrefined product [39]:

$$P = \frac{C_l - C_0}{C_l - C_s} \tag{13}$$

Here, P=1 (100% product, no residue), P= 0 (100 residue, no product). The efficiency can also be expressed as a function of P as follows:

$$\eta = \frac{(1-P)(\,C_E - C_\alpha)}{C_E - P(C_E - C_\alpha)} \tag{14}$$

where C_E is the composition of the liquid fraction at the eutectic temperature and C_α is the composition of primary α aluminium at the eutectic temperature. When P=0 than η_0 is the maximum purification efficiency in a single purification step defined as

$$\eta_0 = \frac{C_E - C_\alpha}{C_E} \tag{15}$$

According to the previous equation, Table 2 shows the possible purification efficiency for the major alloying elements in Al alloys. It is worth to note that the results are purely theoretical, and the solidification process is considered to happen at the equilibrium so, in the real situation, the results could be quite different. Moreover C_α and C_E are the compositions of the solid and liquid fraction at the eutectic temperature but, in in reality, it is essential to work in the semisolid range, at temperatures higher than the eutectic because processing the material at the eutectic temperature is not possible, due to the very high viscosity of the mushy materials and well developed solid-phase structure. Nevertheless η_0 gives a general indication to what extent an element can be theoretically purged out from the alloy. The results are very good for Si, Fe and Cu, fairly good for Mg, and marginal for Mn.

Table 2: Theoretical efficiency evaluation from phase diagrams of Al binary alloys [39].

	T_E	C_α	C_E	Maximum temperature range	η_0
Silicon	577	1.6	12.6	83	87
Iron	655	0.06	1.8	5.5	97
Copper	548.2	5.65	32.7	112	83
Magnesium	450	17.1	36	2.5	55
Manganese	658	1.25	2.0	210	38

Historically speaking the origin of the fractional solidification process can be dated back to the invention of the Pattinson process [40] to separate silver from lead, but a wider application arrived in the second half of the 20th Century with the invention of a zone melting technique

[41]. The zone melting technique consists of pulling slowly a solid ingot through a thin section of a furnace. This implies that only a small region of the ingot is molten at any time. By moving the sample through the heater, this molten zone travels through the sample from the head to the end, leaving the growing solid fraction purer. However, zone melting is a slow and energy-consuming process that aims at receiving very high-purity metals, e.g. aluminium or gold. As commercial alloys (target of recycling) allow for some impurity concentration, e.g. 0.1-0.2% of each element, the use of zone melting would be not economically viable.

Over the years a number of methods and setups have been developed to achieve fractional solidification. The main distinction in the fractional solidification techniques is whether the crystallization is enhanced by a surface (Layer based process) or, it does not involve any surfaces and solid crystals grow in the melt (suspension process) [39]. Further, the layer-based process can be divided into a static process or a dynamic process, depending how the mechanism of the mass transfer happens. Even though some works have been developed using the layer-based process, they were concerning mainly high purity Al or, when applied to Al alloys, further purification steps were needed to increase the purification. A suspension process can be categorized as continuous type or batch-wise type, depending on whether the purification takes place by steps or in a continuous loop. In the following section all the different categories are considered describing their feasibility as well their drawbacks. The review on the fractional solidification apparatus will then follow with the description of different filtration methods developed starting from the idea of M.C Flemings and A.L. Lux.

2.4.1 Suspension process

Batch-wise type

As a first example of suspension process in a batch mode, we are going to consider the patent developed by M.C. Flemings, R. Mehrabian, and R. Geiger [42]. The method can be applied for the purification of Al alloys and Sn-Pb alloys.

As we can see from Figure 5, the setup consists of an electric resistance furnace (7) in which a container is inserted. Inside the container a semi-solid slurry, made by liquid (2) and solid crystals (4), is present. This slurry is agitated by a rotating blade represented by (8). Once the semi-solid material has reached a desired temperature, two separating process are possible.

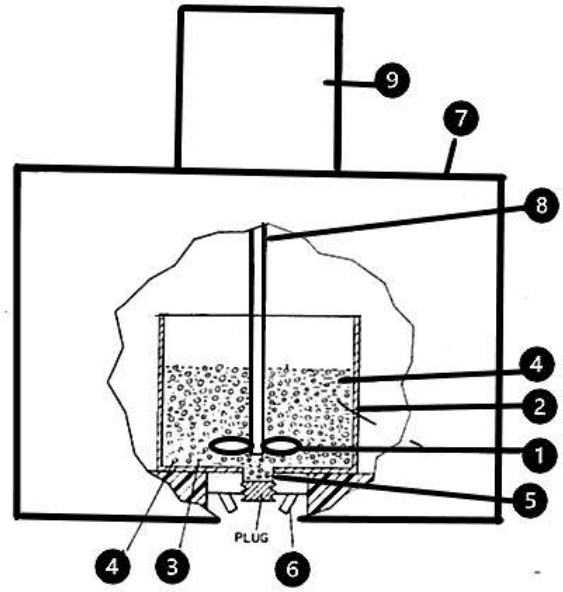

Figure 5. Experimental set-up of the invention for suspension process, adapted from [42]: (9) is an electric motor, (8) is a shaft that drives a rotating blade (1), (7) is an electric resistance furnace, (6) are nozzles, (5) is the tap hole, (4) are solid pieces suspended in in the liquid (3), mixture of solid and liquid is indicated by (2).

In the first one, the agitation of the blade is maintained, especially in the vicinity of the tap hole, to allow the slurry to pass through the hole (5) where nozzles (6) with gas jets “atomise” the fully liquid particles to very fine particles that consequently solidify. The existing solid crystals cannot be atomised, and they are larger in diameter then the finer liquid ones. The refining process consists in separating the larger particles from the smaller ones. In the other variety of this separating process, once the slurry is formed, the speed of the blade is lowered, so that it does not agitate vigorously the metal close the hole. The purpose of this is to give to the slurry a “thixotropic” behaviour so that the solid particles are hold back and do not fall into the hole. A ceramic foam filter can be eventually employed to aid the separating process. The invention has been applied on Sn-15 wt% Pb and Al-30 wt% Si-6 wt% Fe-1 wt% Ti alloys. For the lead-tin alloy, two types of experiments were executed, varying respectively the semisolid fraction and the rotation speed of the blade. According to what is described in the patent, in order to be successful, the purification process should produce particles formed from a solid fraction expected to contain 2 wt% or 3 wt% Pb but they only managed to achieve particles with 12 wt% Pb. As it is also stated in the paper, further improvements are needed. For the Al-30 wt% Si-6 wt% Fe-1 wt% Ti alloy there was a significant decreasing in the weight percentage of all alloying elements: 56% purification for Si, 71% for Fe, 84% for Ti. Despite some good results, building up such set-up remains not feasible for industrial application because it would require tight control of the different components, and it is quite complicated to reproduce as

lab-scale device. Moreover, the way the separation of particles happens, through atomisation, seems not easy to handle in a real experiment. Nevertheless, a variation and improvement of this approach is represented by an Alcoa crystallizer [43]. As in the previous case the solidification happens in the melt bulk without a separating surface or layer. So, the method is classified as a suspended process or batch type.

Figure 6 is a representation of this invention. There is a container (1) with an aluminium alloy. This container has three inner walls made of

1. an insulating material which may be heated (2)
2. alumina powder (3) to avoid molten metal to flow out of the container
3. a refractory material (4) to avoid heat loss.

The solidification happens at the top of the container by taking out the heat gradually and causes the formation of Al crystals that are floating in the liquid phase enriched in impurities (6,8). Due to the gravity force, the crystals start to fall down to the bottom of the container. A tamper (7) is employed to compact the crystals at the bottom and to allow the liquid part to exit from the container by 14. The bottom of the container is heated to prevent any encrustation of the crystal and to allow some liquid entrapped in the solid, to melt and get out by outlet 13. Once the crystallization process is ended and all the liquid is taken out, the purer crystals are melted and collected by 13.

This method has been tested on an Al-Si alloy with a composition of Si less than the eutectic one. The example shows that the liquid metal removed by the upper hole (14) has a higher content of Si than the crystals melted and discharged by hole (13). The idea of squeezing the material to help the liquid to move out of the semisolid mush is interesting. Nevertheless, there might be a strong possibility that the piston compacts together at the bottom, the liquid and the solid fraction already formed, unless the outlet 14 is big enough to give the liquid time to flow out before the piston reaches the bottom.

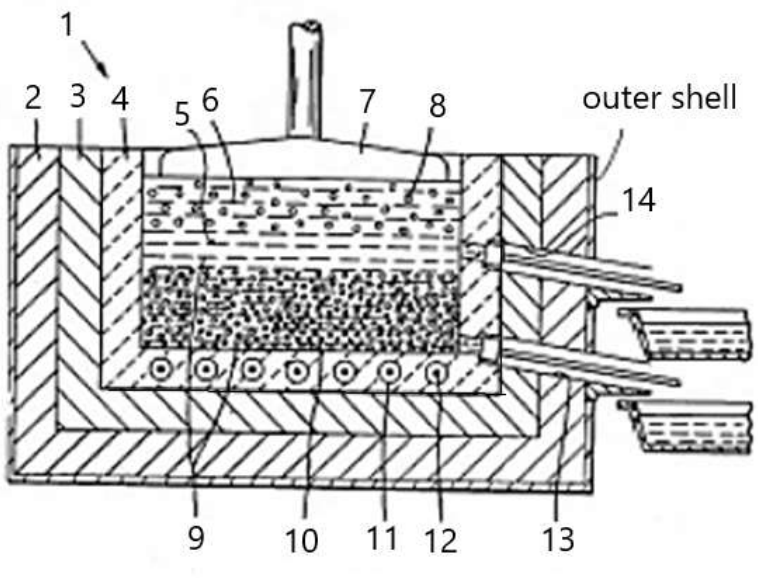

Figure 6. Alcoa crystallizer apparatus, adapted from [43]: (2) (3) (4) walls, (7) tamper, (6) liquid enriched in impurities, (8) crystals, (11) and (12) heating systems, (10) bed of packed crystals formed by the action of the tamper, (13) the upper hole where liquid is discharged, (14) hole where pure crystals are discharged.

Continuous type

There are different patents and technologies suggested in literature, for pursuing continuous suspension fractional crystallization process. We will discuss them following a chronological order beginning with the Yunnan crystallizer suggested in 1975 [44].

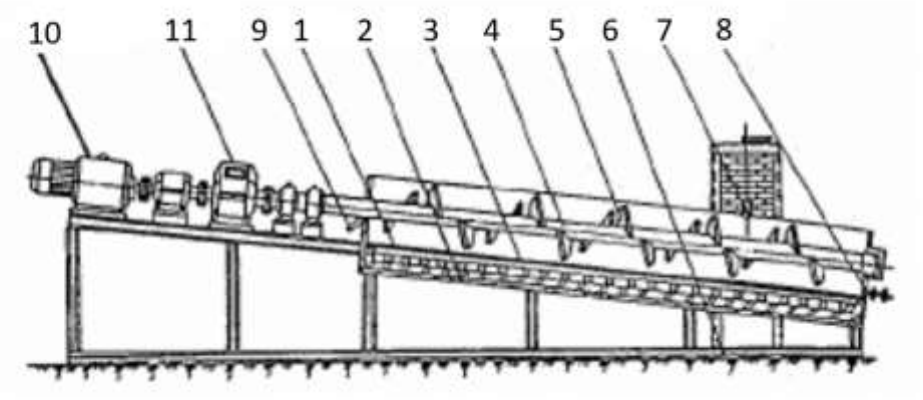

Figure 7. Yunnan crystallizer, adapted from [44]: (1) inner troughs, (2) outer troughs, (3) electric heaters, (4) screw axis, (5) spiral blade, (6) base, (7) charge pot, (8) outlet for liquid phase, (9) outlet for crystals, (10) motor, (11) gearbox.

The setup (Figure 7) consists of a spiral agitator, inside an inner trough, made by a screw axis (4) and spiral blades (5). Electric heaters are placed between an inner (1) and an outer trough (2). A motor (10) drives the spiral agitator and the speed can be settled by a gearbox (11). The inclination of the crystallizer towards the flat surface can be regulated (6). The crystallizer is heated up till the melting point of the feed material that has to be refined. The feed material is inserted in an amount necessary to submerge the screw axis. At that point, the motor is started, and water is sprayed on the surface of the melt causing the formation of some crystals. The crystals, stirred by the spiral, are moved upwards to outlet 9 meanwhile the liquid enriched in impurities is moved downwards to outlet 8, due to the gravity force and the inclination of the crystallizer. In this way a counter current flow is achieved. During the process the temperature of the heaters is adjusted to have, in the bottom of the crystallizer, a melt temperature close to the eutectic temperature of the material, and, in the upper part of the crystallizer, a melt temperature close to the melting point of pure crystals. The process is considered continuous because, as soon as pure crystals and liquid material are taken out of the crystallizer, new feeding material is inserted.

This process gives good results in removing Pb from Sn. The main issue with this method is that it cannot be applied to all metals especially not to those with high melting point. Moreover, some alloys have very small difference between the crystallization temperature of the molten alloy and the crystallization of the pure metal making it very difficult to establish a temperature gradient along the crystallizer. Moreover, the way crystals are moved to the outlet by the screw seems quite intricate, as well that there could be some issues on how to prevent crystals to stick on the spiral screw.

We are now going to describe a process for continuous refining of metals that consist in a column that has a hot zone at the base, and a cool zone at the top and a continuous temperature gradient between the two zones (Figure 8) [45]. The column contains slurry made by metal crystals and liquid metal. Crystals are formed in the cool zone and transported down to the hot region where they are melted and collected as pure liquid. The temperature in the cold zone is settled to allow the co-existence of the crystals and the impure liquid. In the hot zone the temperature is settled to permit the melting of crystals. Crystals are produced in the cooler zone of the apparatus by adding ingots of feed material. This ingot causes the chilling of the liquid that is in contact with it producing a mass of crystals that remains adhered to the metal body. The maximum benefit from the process can be attained if the crystals are smaller than the diameter of the column. Figure 8 shows how generally the apparatus works. The continuous ingot casting machine is indicated by zone 31. Above the line A-A there is the part of the apparatus associated with the ingot production, the melting and the withdrawn of liquid

from section 22 of vessel 21. Zone 23 is the melting zone and heaters 26 are placed at the bottom of the column. Liquid metal is then discharged by 27.

The ingot of metal, once it leaves zone 31, it passes through channel 32 above vessel 21 that contained the liquid slurry. Here the cold ingot chills the crystals and allows them to stick on it forming a thick layer. The ingot then moves down towards the hotter zone of the column where crystals melt and come off it. At the bottom of the column the ingot partially melts releasing more crystals and liquid.

The method is mostly applied for purification of zinc and tin from bismuth and cadmium, and for purification of Al containing small amount (0.2 wt%) of Si and Fe. The apparatus seems not suitable to process commercial Al scrap alloys with high percentage of impurities. It also needs the presence of feed material to help the formation of the crystals and this implies that it is not suitable for recycling. Moreover, the description of the setup itself remains a bit unclear. It is not well explained how the liquid is going to be discharged without remaining entrapped in the solid or how the ingot moves along the column.

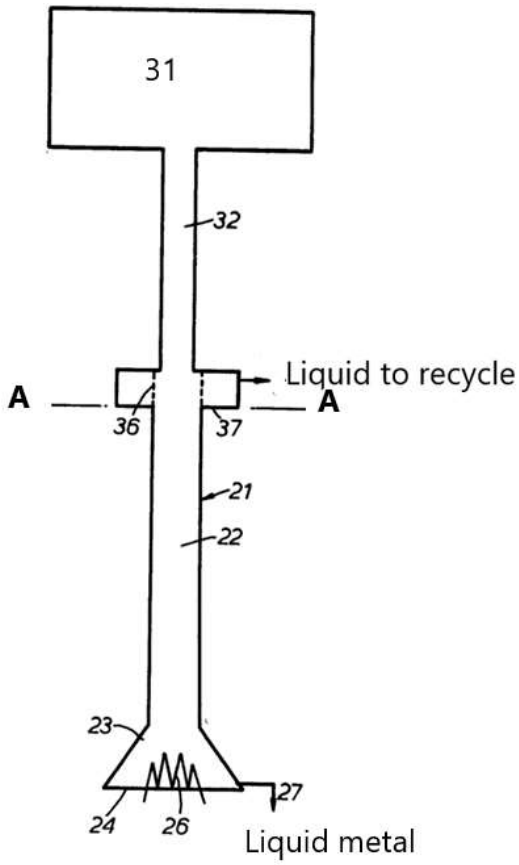

Figure 8: Apparatus for continuous refluxing involving continuous ingot formation, adapted from [45]: (31) ingot casting machine, (32) conduit, (36) and (37) heated gallery, (21) vessel, (22) refining section, (23) melting section, (26) heating element, (27) outlet for liquid metal.

A more recent technology is the Pechiney crystallizer [46]. The device allows a continuous fractional purification of metals on a rotary drum. As is shown in Figure 9 the drum is placed inside a channel where it forms, with the channel itself, a restricted space (5) that has a shape of half of a ring. This space divides the channel into an upstream zone (6) and a downstream zone (7). The drum is rotated along its axes by the direction indicated by the arrow. The solidification happens due to a cooling material (10), and the crystals that form (8) are settled in the space created by the channel and the drum. The channel in the upstream region is heated (9) to help the bath to be kept in the liquid state. The portion of the drum indicated as (11) is heated to help the crystals to melt and be discharged. The mother liquid instead is discharged from outlet (15).

When molten metal is inserted (13) the crystals start to form due to the cooling material and then settle in the space created by the channel and the drum (8). The drum rotates the crystals progressively melt because the portion (11) of the drum is heated, and they get collected in (14) as purer material. The mother liquid enriched in impurities is drawn off from (15).

This process is thought to be employed for high purity Al, where a single stage can be repeated several times to ensure a better purification. Moreover, additional cylinders parallel to each other can be inserted to create a kind of cascade recycling. Despite these benefits, there can be some issues on how the mother liquor is discharged and how to keep the upstream zone and downstream zone separated to avoid the back contamination of the solid phase with the liquid. Moreover, the patent does not show any results of the method leading to the conclusion that the description is purely theoretical and that the method has not been applied to real alloys.

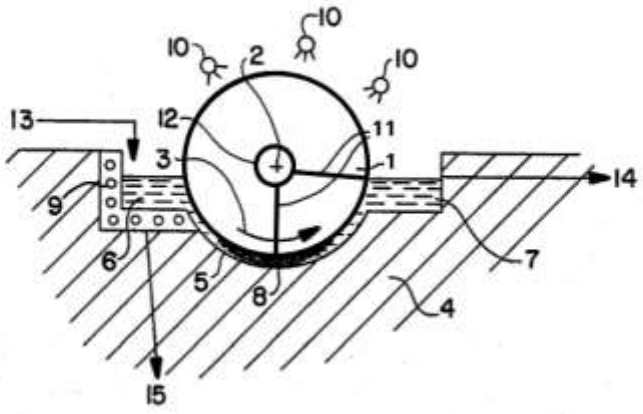

Figure 9. vertical section along the circle of the drum of Pechiney crystallizer, adapted from [46]: (1) drum, (2) axis, (3) direction of rotation, (4) channel, (5) crystallization space, (6) upstream zone, (7) downstream zone, (8) crystals, (9) heaters, (10) cooling material, (11)

sector of the drum, (13) door to introduce metal to purify, (14) point where pure liquid is take out, (15) point where mother liquor with impurities is drawn off.

The most recent method for continuous fractional solidification process is shown in Figure 10 [47]. It can be considered a different version of the Yunnan crystallizer, because the solidification is enhanced by a cooling liquid in which a counter current flow is established. The cooling liquid can be a salt of NaCl and KCl or/and NaF and KF containing $BaCl_2$ and BaF_2.

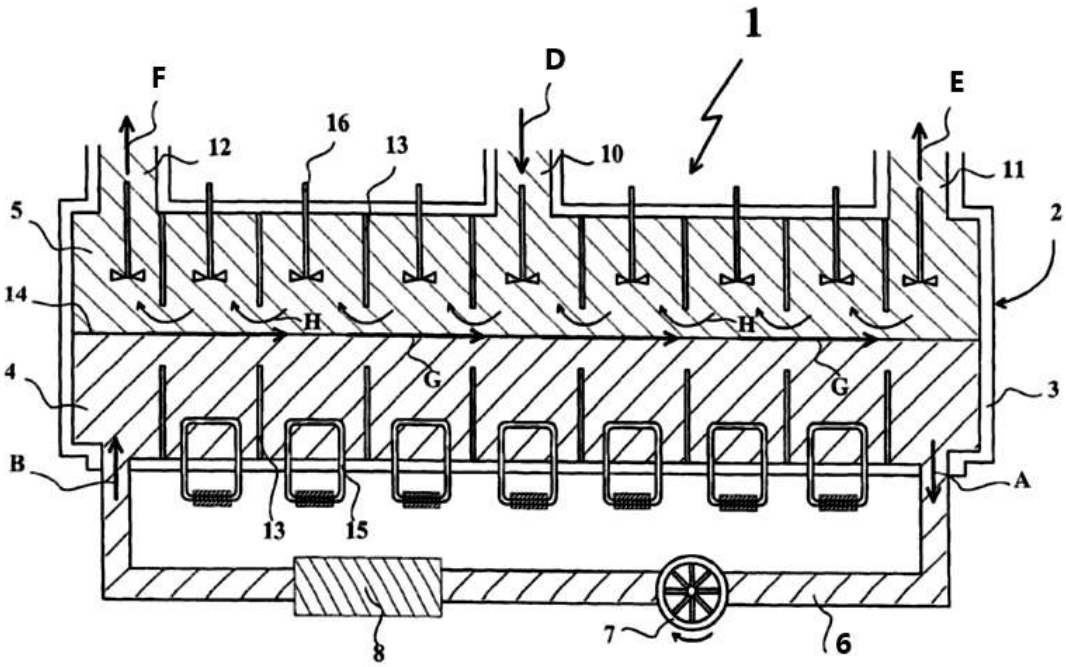

Figure 10. Experimental set up of continuous fractional solidification, adapted from [47]. (1) apparatus, (2) and (3) chamber, (4) cooling liquid, (5) layer of molten metal, (6) recirculation pipe, (7) pump, (8) cooling device, (10) supplier for molten metal without crystals, (11) outlet for discharging molten metal with crystals, (12) outlet for molten metal containing impurities, (13) compartment walls, (14) contact surface, (15) cooling elements, (16) mixing elements.

The device is made by a chamber (2) with thick walls (3). Inside the chamber there is a cooling liquid (4) and a semisolid alloy in which metal crystals are floating inside the liquid phase. The chamber is then divided into compartments (13). Each compartment in the zone of the partially molten metal has a blade to stir the material thus helping the crystals to remain in suspension. In each compartment, in the zone of the cooling liquid, there are additional cooling elements (15). The molten metal without crystals is introduced in the chamber through the door 10. At the contact surface between the molten metal and the cooling liquid (14), some crystals start to form. The liquid enriched in impurities is discharged through door 12 while the crystals are discharged by outlet 11. But it is not specified how the liquid, or the metal with crystals, are taken out from the chamber. A liquid aluminium alloy is inserted at a temperature close to the

melting temperature of pure Al. The contact between the layer of the molten Al alloy and the layer of molten salt, that is at lower temperature, allows the formation of crystals. The cooling liquid is transported through the chamber 2 and recirculated through the pump 6 and is cooled by the cooling device 8. During the process, the molten salt takes energy from the molten alloy so the cooling salt is gradually heated up going from the left side of the chamber to right side. As a result, there is an opposite gradient in the temperature of the molten metal between the left side and the right side. The crystals in the compartment on the left are forming at a temperature different from the ones in the right. This seems to be the key aspect of this method. In fact, when the crystals reach the right end of the chamber, they partially re-melt allowing some solutes to be eventually entrapped in the melt. This mechanism happens in all the compartments of the chamber and brings a final refined product that is purer than the one that was initially introduced. The apparatus seems very well thought, but some part of its mechanism remains unclear and intricate. The crystals forming during the process might adhere on the wall of the chamber instead of floating as nicely as described. Moreover, there is no description of the amount of liquid salt that is necessary to add in order to form the right amount of crystals. As well there is no description of the amount of material inserted in the systems and the amount purified from it. It is indicated that the apparatus can be used preferably for removal of Cu, Fe, Ga, Mg, Mn, B, Si, Sn, Zn, or Ni from molten aluminium, but no results are shown. This probably means that the invention has not been tested yet. It is suggested that the method could be employed for the production of high purity aluminium from Al alloys with Si and Fe content less than 0.20 wt%. It is clear that is not suitable for recycled Al scrap with high percentage of impurities, so it is out of the scope of this PhD project.

2.4.2 Layer-based process

As previously stated, in the layer crystallization the crystal growth takes place in contact with a surface. This should make easier to separate the solid from the liquid phase. One of the major issues in fractional solidification, in fact, is the inclusion of liquid in the purified fraction. Depending on how the mass transfer happens, the process can be further classified as static, if it occurs by diffusion, or dynamic, if is enhanced by turbulence.

Dynamic Process

The first method that we are going to describe is an Alcan patent for the production of high purity Al from aluminium alloys containing eutectic impurities [48]. The apparatus consists of a cylindrical crystallizer vessel (10) that has an open bottom. The vessel is settled on a support (14) on top of an induction furnace (11). The vessel has an inner channel (12) and a cylindrical

cooling jacket (13) that contains an air/water mist cooling flow. Both the crystallizer and the furnace are made by silicon carbide refractory material. An impeller (17) with radial vanes is inserted inside the channel.

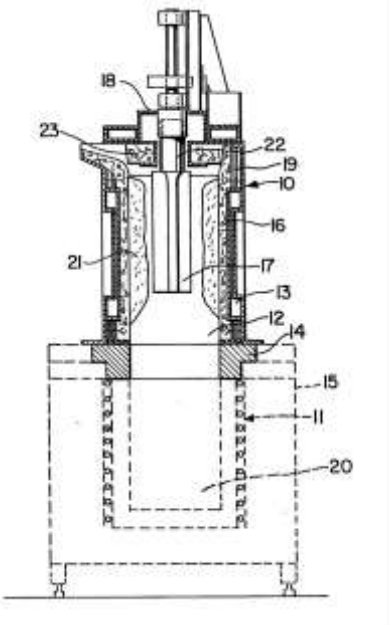

Figure 11. An experimental apparatus for production of high purity Al by dynamic layer process, adapted from [48]: (10) vessel, (11) electromagnetic furnace, (12) inner channel, (13) cooling jacket, (14) support, (15) cabinet, (17) impeller, (18) motor assembly, (19) insulating material, (20) cavity of the furnace, (21) solidified aluminium, (22) shaft, (23) insulating top.

During the process, part of an aluminium alloy that is going to be purified, is placed inside the furnace to be melted and the rest of the aluminium alloy is added gradually until the molten metal reaches the height of the cooling jacket. The molten metal is cooled by the water/air mist flow that passes through the cooling jacket and in the meantime is stirred by the impeller. The purified crystals solidify on the wall of the inner channel (21) and the liquid metal is poured out by simply tilting the crystallizer by a hydraulic mechanism. The stirring action is one of the key aspects of this process. As we have previously discussed, during fractional solidification solutes are rejected at the interface by the growing crystals. The stirring action increases the rate of mass transfer of the impurities from the solid/liquid interface to the melt. In this way the contamination of the crystals by the solutes is reduced. Moreover, the rate of building up impurities at the interface is influenced by the rate of solidification that is controlled by the flow rate of the cooling liquid. So, when the flow rate decreases, the crystallization rate decreases, and this results in a greater separation of crystals from solutes.

The present method allows one to process a large amount of material, having a crystallizer capacity of 200 kg, but it is employed only to obtain high purity Al from Al with an impurity

concentration less than 0.05 wt%. Considering that the recycled scrap has much higher concentrations of impurities, the present method seems not suitable for recycling

Static process

One interesting technology for static layer crystallization applied to aluminium scrap recycling, was developed by a research group at Delft University of Technology [49].

The experimental set-up is shown in Figure 12 below.

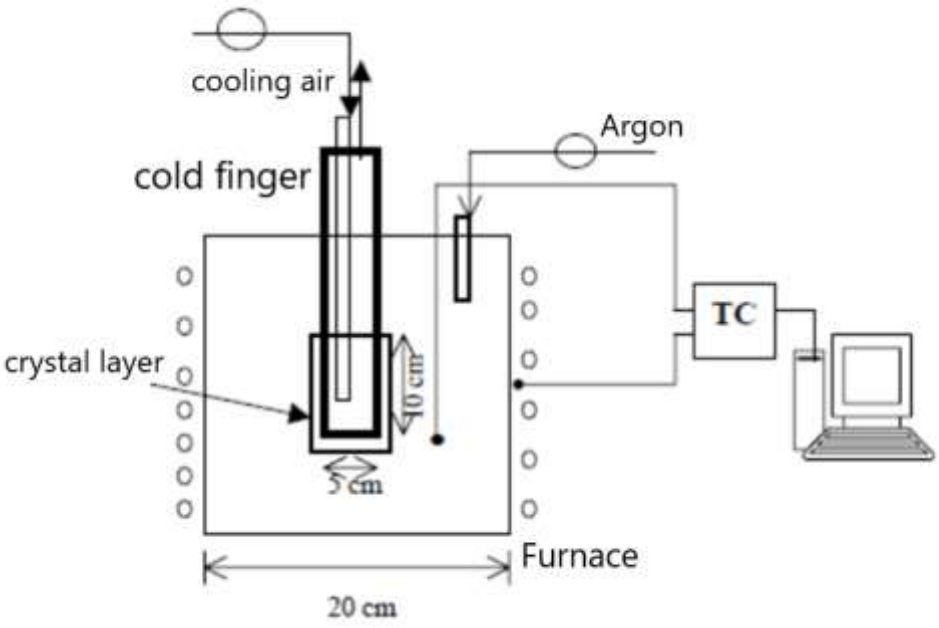

Figure 12. An experimental setup for static layer crystallization, adapted from [49]: A graphite crucible (50mm X 100mm) is inside a tilting furnace (200 mm length). A cylindrical ceramic cold finger is inserted in the crucible. Air is blowing inside the cold finger.

The apparatus consists of a titling furnace 20 cm wide. Inside the furnace an ISO-graphite crucible with dimensions 50 mm x 100 mm is placed. Once the alloy is completely molten, a ceramic cylinder, the cold finger, is made cold by air blowing inside it, is inserted in the melt. The cold finger is the rectangular shape, outlined in black, showed in Figure 12. The temperature is lowered until the melting temperature of the alloy. The cooling rate is adjusted by the air flow to achieve a certain growth rate. After a crystal layer of 2 or 3 cm is grown, the cold finger is taken out and is placed inside an oven to be subjected to the sweating process. During the melting stage of the alloy the temperature is controlled by a thermocouple attached

to the external wall of the crucible, while during the solidification stage the thermocouple is placed in contact with the melt.

This method seems easy to reproduce, and its engineering does not require complex machining or controls as other patents previously described. It gives good results in term of purification and has been applied on hypoeutectic Al-Si, Al-Si-Fe, Al-Cu-Mg alloys. The major issue with this invention is that some liquid fraction remains entrapped in the solid, so the final product, as stated in the paper, needs to be submitted to a sweating process to achieve better results. There are no reproducible details about how the sweating process is carried on.

2.4.3 Filtration based methods

A separate section deserves to be dedicated to the filtration experiments. We will consider first the work done by M.C. Fleming and A.L Lux [50] to build up an experimental set-up to pursue the fractional solidification using filtration. This setup has been the starting point for many others experimental works [51]–[53] on fraction solidification, including this PhD project.

Most of the apparatus that have been described previously are patents and they, unfortunately, come with some drawbacks. Some of them are not suitable for laboratory scale, some are not easy to reproduce or cannot be applied to aluminium alloys. Instead the experimental set-up that it is going to be presented in this section has key aspects that can be reproduced inside a laboratory without the use of a complex technology.

The experiment consists in an isothermal compression of a semisolid alloy against a filter through the use of a piston. Figure 13 is a schematic representation of the apparatus. It consists of a compressing system and a furnace. The compressing chamber is made by a stainless-steel crucible in which an alumina filter is inserted. The crucible is inside a brass cylinder. Two thermocouples are inserted in the wall of the crucible and one is inserted in the plunger that is machined to have the same diameter of the filter. The temperature is controlled to assure the minimum temperature difference across the sample. Before starting the experiment, the sample is placed in the crucible and the crucible is settled inside the brass cylinder that is positioned inside the furnace. As the sample is been heated, Ar gas is introduced at the top, meanwhile He gas is channelled through the quenching system to prevent the oxidation. The sample is heated up for about 20 minutes until the right temperature in the semi-solid range is reached. At this point, the plunger compresses the alloy towards the filter. The material that is been filtrated is collected in the quenching tank. The solid that

remains in the crucible behind the filter (the cake) is the purified fraction and it is removed and analysed.

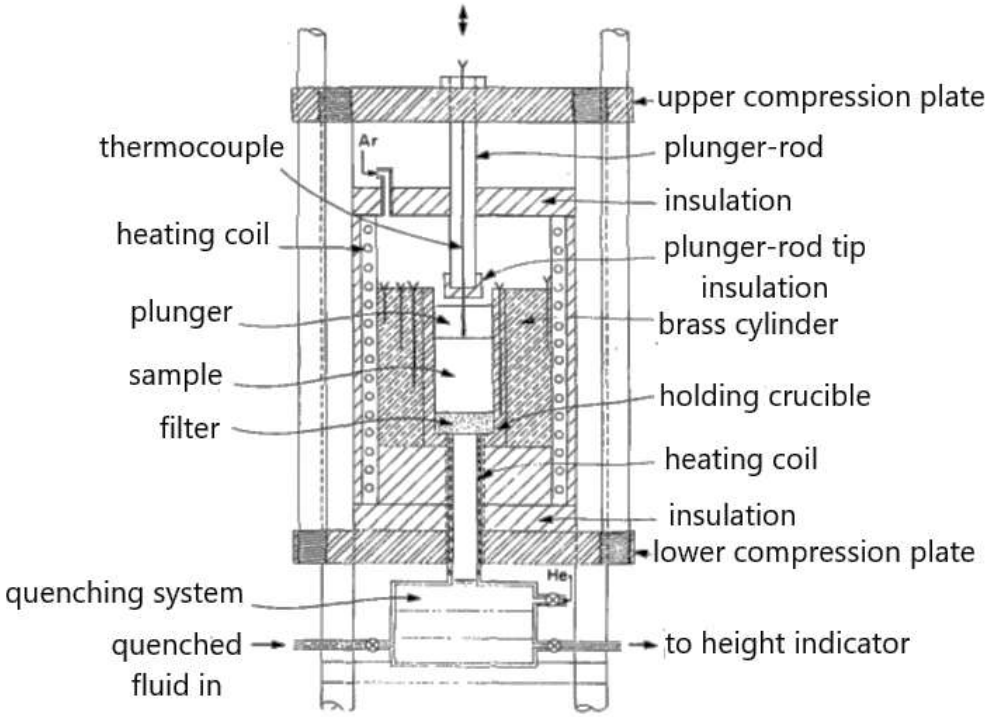

Figure 13. Controlled speed compression apparatus, adapted from [50]. A stainless-steel mould is inside a brass cylinder. A filter is placed at the bottom of the mould. A channel connects the mould to a quenching system. A plunger is used to compress the sample towards the filer.

This method gives good level of purification but was applied only for Pb-Sn alloys and only for very small quantities (500 g).

Following the idea developed by Flemings, A.T Ali et al. [52] designed a set-up (Figure 14) for the purification of Al-Si binary alloys. A small amount of material (5-10 g) is molten at 800°C and then gradually cooled down until the semisolid state is reached and hold at that prescribed temperature for a fixed time. Then, the squeezing is performed using a hydraulic jack positioned at the base of the furnace with the graphite seals moving toward the top surface of the sample. The total squeezing operation was carried on for 10-15 minutes. The work shows good results in terms of purification and a correlation is also established between the efficiency of refining and the holding time in the semisolid state. However, the method was applied only on a small scale which makes the entire process more controllable than a situation in which more material is processed. Moreover, the analysis was carried on a single alloying system only. It could be interesting to test if the same purification efficiency can be reached in different

alloying systems with different partition coefficients. The partition coefficient, in fact, influences the purification achievable.

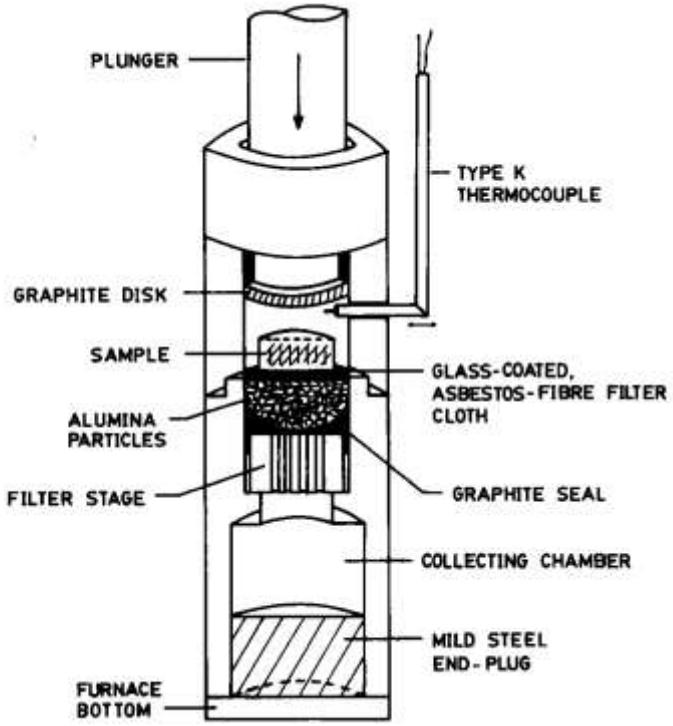

Figure 14. Schematic drawing of compression apparatus, adapted from [52]: the sample is molten and then kept at the semisolid state. The filter system is made by four parts: filter cloth made by asbestos fibre, graphite seals, a bed of alumina particles and a filter stage. Underneath the filter stage there is a chamber to collect the liquid squeezed out by a plunger. A thermocouple is inserted 50 mm from the top of the apparatus and connected to a controller to keep the temperature constant.

A more recent work on filtration, as a way to perform the fractional solidification, was done by T. Sotome and M. Ohtaki [53]. Their procedure as well, is based on the initial idea developed by Flemings et al. [50]. Figure 15 shows a schematic of the experimental set-up.

The set-up has been applied to an Al-3 wt% Si alloy, real car scrap, sash scrap and radiator scrap. In the experiment 8 kg of material are molten at 850°C and then poured onto the vessel and cooled down until the semisolid temperature. Once the temperature was reached the material was squeezed by the plunger. The weight and the composition of the refined material have been measured.

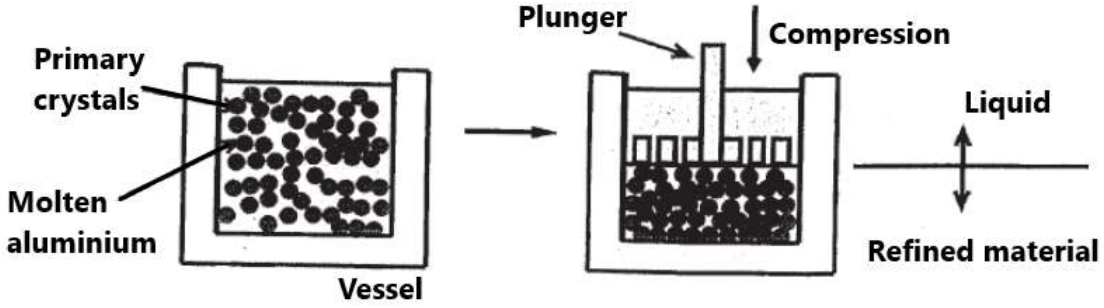

Figure 15. Experimental set-up made by two major parts, adapted from [53]: A vessel to hold and cool down the material to the semisolid temperature and a plunger to compress and separate the crystals from the liquid metal.

There is no indication on how the solid crystals and the liquid fraction are taken out from the set-up. The experimental results indicate that there was a considerable reduction in most of the alloying elements in all the scrap analysed but neither the measured sections nor the techniques used were specified. It is reasonable to think that some segregation may have occurred and probably it affected different areas of the purified fraction differently. It was also underlined that the Si removal increased with the compressing pressure, but a more systematic analysis would probably be needed. Moreover, it would be interesting to analyse, as well, the microstructure of the purified final product, to confirm the hypothesis of the formation of intermetallic phases pointed out in the paper.

K. Ichikawa et al. [54] have applied the squeezing process to obtain high purity Al from Al-Sn and Al-Ni alloys through the fractional solidification. Their experimental set-up showed in Fig. 16 is a clear reference to the Flemings'. idea.

The molten specimen is placed in the upper mould (60 mm inner diameter, 15 mm thickness). The specimen is heated and kept at the semisolid temperature. At this point pressure is applied to the surface of the specimen by the plunger. The purified fraction solidified on top of the filter and the squeezed-out liquid passed through the filter and solidified in the lower mould. The process brings very good results in purification of Al-50 wt% Sn, Al-1 wt% Ni and Al-2 wt% Ni alloys. The final level of purification is achieved by submitting the sample to further purification steps. There is also a correlation between the purification achieved, and the speed and the load applied during the pressuring phase.

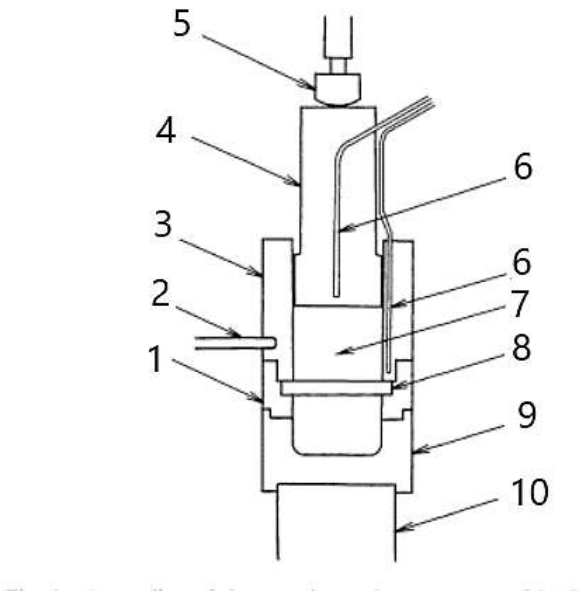

Figure 16. Schematic of the experimental set-up, adapted from [54]: 1) mould, 2) thermocouple,3) upper mould, 4) plunger, 5) motor driven rod, 6) thermocouple, 7) specimen, 8) filter, 9) lower mould,10) support

The apparatus is well designed, but it processes only 500 g of material. Even if the purification achieved is interesting, Al-Sn and A-Ni binary alloys are not typical alloying systems in the automotive wrought and cast alloys scrap which is more in the scope of this PhD project. In our experimental work, in fact, the model alloys tested have a composition similar to the most common wrought and cast alloys in the automotive industry.

2.5 Parameters influencing solidification

Among all the methods and technology to perform fractional solidification, the idea developed by A.L Lux and M.C Flemings is the one most suitable for our purposes. In fact, the idea of performing an isothermal squeezing of a semisolid alloy towards a filter does not involves the use of complex machinery and it can be easily upscaled. It also allows freedom in terms of designing of the experimental procedure, because it does not imply, or need, a specific geometry (the filter can be round or square, the piston can be machined according to the size of the filter, the force can be applied from the top or from the bottom).

The set-up described in 3.3.2 and 3.3.3 has been built and developed taking inspiration from Lux and Flemings performing an isothermal squeezing of a semisolid alloys towards a filter. However, there are several factors to consider performing the fractional solidification, that could affect and/ or enhance the final purification achievable. Below is given a description.

2.5.1 Time

The rate of solidification is influenced by the heat extraction rate and the rate of solute removal from the solid/liquid interface by diffusion in the solid, and by diffusion and convection in the liquid. Therefore, the solute redistribution at the interface, which is crucial in the fractional solidification process, is related to the diffusion of the solutes that is time and temperature dependent. On the other hand, the cooling rate gives the window of opportunity for realising the partitioning and separation of the liquid and solid phases. In this work, temperature will be set at a specific value in order to have a nearly isothermal process, so the operational window will be fixed in term of temperature. Time, however, is a variable during the course of experiments. Especially with the upscaled set-up developed in the second part of this work (3.3.3) the effect of time on the efficiency of the process needs to be evaluated.

In Section 2.2, the evolution of the solid fraction during solidification was considered only for two extreme cases: infinite diffusion in the solid and in the liquid (lever rule), and negligible diffusion in the solid (Scheil-Gulliver). It is true that for rapid solidification processes the solid diffusion can be neglected because the solid diffusivity is several order or magnitude lower than the liquid one. However, it is important to remember that this is just an approximation and that, in fact, the extent of solute redistribution in the solid phase depends on the time and length scale.

Diffusion is defined as the movement of atoms from one reticular position to another reticular position [55], [56]. This movement can only happen if the next reticular position is available and the moving atom has enough vibrational energy to win the bonding energy with the nearest atoms. This vibrational energy is temperature dependent. In the case of metal there are two mechanisms for diffusion: vacant diffusion and interstitial diffusion. In the first case an atom occupies an adjacent position left free from another atom. In the second case, atoms in interstitial position move to other free interstitial position. Diffusion is time dependent and this relation is often identified by the diffusion flux which represents the number of atoms that diffuses perpendicularly on a unitary section of a solid at a certain time.

$$J = \frac{M}{At} \tag{16}$$

Where M is the mass of the diffusing atoms, A is the area where the diffusion is happening, and t is time. In the differential form, becomes

$$J = \frac{1}{A}\frac{dM}{Dt} \qquad \text{J[kg/m}^2\text{s]} \tag{17}$$

The dependence of diffusion on time is expressed through the second Fick's law [17] as:

$$\frac{\delta C}{\delta t} = D\frac{\delta^2 C}{\delta x^2} \quad (18)$$

Resolving the differential equation applying boundaries conditions, the second Fick's law becomes [17]

$$\frac{C_x - C_0}{C_s - C_0} = 1 - \mathrm{erf}\,(\frac{x}{2\sqrt{Dt}}) \quad (19)$$

C_x represents the concentration at the distance x at a certain time t.

The diffusion coefficient is temperature dependent according to [17]:

$$D = D_0 \exp\,(-\frac{Q_d}{RT}) \quad (20)$$

Q_d is the activation energy (J/mol) and it can be considered the energy necessary to initiate the movement of the atoms. For big values of Q_d diffusion coefficient is small. D_0 is a constant and is independent from the temperature T, and R is the gas constant.

So, solutes redistribution is related to the diffusion of atoms at the solid/liquid interface. From equations 20, it clear that diffusion is time dependent. In fact, solid diffusion has effect in the solidification cracking susceptibility [57] and it can influence the microsegregation and the morphology of the alloy enhancing the coalescence of grains [58]. In general, it is important to consider the effect of back diffusion because it gives a more precise estimation of the different solid phases during the solidification especially in complex systems [59]. Sometimes, depending on the time scale of the solidification process, solid diffusion can be neglected but it needs to be remembered that this is an approximation.

2.5.2 Type of alloy

Section 2.2 introduced the partition coefficient and its role during solidification. Partition coefficient is crucial for fractional solidification because the rejection of solutes in the liquid phase, i.e. having the liquid enriched and a purer solid fraction, happens only when k<1. Contrarily, when k>1, the solid phase is the one containing the solutes and the liquid phase is purer (fractional melting technique [60]). The value of the partition coefficient has important implications regarding the propensity of an alloy to be purified.

Table 3 shows the partition coefficients for some common alloying elements for Al. For example, elements like titanium, vanadium and chromium cannot be eliminated from the solid solution by fractional solidification as they have k>1. This needs to be considered when

submitting an alloy to the fractional solidification technique since it might be a drawback of the purification process. Even in cases when the partition coefficient is less than one, like for Mg, a value of 0.51 means that the solutes tend to be stay in the liquid phase as much as in the solid one having consequences on the purification efficiency, as will be discussed in Chapter 6. Manganese has k very close to unity, which means that solute Mn does not partition much between the solid and liquid phases and, therefore, cannot be efficiently extracted. The value of the partition coefficient has an influence on the purification efficiency and gives, also, a threshold from which aluminium can be purified of the alloying elements.

Table 3: Typical alloying elements for aluminium alloys and the value of partition coefficient [61].

Element	k	Element	k
Ni	0.007	**Mn**	0.94
Fe	0.02	**Nb**	1.5
Si	0.13	**Cr**	2
Cu	0.17	**Zr**	2.5
2Zn	0.4	**V**	4
Mg	0.51	**Ti**	9

2.5.3 Temperature

Fractional solidification consists of processing the alloy in its semisolid state so to have the solutes partitioned between the solid and the liquid phase. It is important to select a specific temperature in the semisolid range, to process the alloy. Depending on the alloy, the solidification range is always different. Also, each temperature in the solidification range corresponds to a certain mass ratio between liquid and solid phases. It is logical that, in order to have the same processing conditions for every alloy, the mass fraction of the solid phase has to be the same. There are different ways to calculate the mass fraction of solid:

1. Calculation by Thermocalc using the Scheil equation or the lever rule (2.2).

2. Experiment by quenching a semisolid alloy and analysing its structure with a microscope.

Although the second method usually overestimates the solid fraction [62], In this work the mass fraction (or sometimes the volume fraction of solid) is calculated in both ways depending on the requirements. Choosing the right solid fraction is important because it influences the purification achievable. A higher solid fraction means more partitioning of solutes so more chance to enhance the purification. However higher solid fraction has implications for the behaviour of the semisolid material [27]. In order to achieve the separation of liquid and solid phases, the permeability of the semi-solid material should be sufficiently high, which implies a lower solid fraction. Also, in some alloys, going to higher solid fraction means working at semisolid temperatures in which the formation of some intermetallic starts, affecting the purification. So, to choose the right solid fraction means to combine the different features in order to get the best purification achievable. In fact, in this work, the experiments were executed at solid fraction equal to 25% in order to operate below the coherency point having enough solid fraction to enhance the partitioning of solutes.

2.5.4 Grain Refinement

Grain refinement is widely used in casting applications because small and more globular grains enhance feeding, decrease the hot tearing tendency, assure uniform dispersion of porosity and intermetallic [63]. In light metal industry, grain refinement is achieved adding small quantities of special master alloy to the melt. The master alloy produces microscopic crystals of a higher melting point compound and these crystals catalyse the formation of primary phase nuclei [22]. Typical Al-TiB_2-Ti master alloys also contain traces of solutes, for example titanium. It is accepted that Ti atoms segregate at the solid–liquid interface of the catalytic particles, e.g. TiB2, forming a thin layer resembling Al_3Ti compound enhancing the nucleation of Al onto TiB_2 particles as well as segregate to the solid Al–melt interface creating an region of growth restriction, limiting the grain growth [64].

There are other methods and technologies to obtain refined grains with different mechanisms acting (dendrite fragmentation, enhanced heterogenous nucleation, dendrite arm remelting etc.). Several works concern the use of ultrasonic field [65], [66]. Some others involve the use of the melt shearing technology developed at BCAST [67], [68].

The purpose of grain refining in this work is to obtain a more rounded structure that could facilitate the melt percolation in the semisolid alloy. We used the standard grain refinement technique using an Al-Ti-B master alloy.

2.5.5 Ultrasound

Ultrasound is an elastic oscillation with frequency above 16000 Hz. Specifically, the classification of acoustic sound, based on the frequency, is as follows: infrasound up to 16 Hz, audio sound from 16 Hz to 16 10^3 Hz, ultrasound from 16 10^3 Hz to 10^{10} Hz, hypersound above 10^{10} Hz.

Ultrasonic melt processing [69] is a physical process used to influence the solidification with the purpose of creating a better quality of the melt. Ultrasonic processing has gained considerable attention for its advantages in grain refining the melt without the addition of inoculants [70] eliminating the drawback associated with it. Ultrasonic processing benefits also the degassing of melt, refines primary phases (Al_3Zr, Al_3Ti, Al-Fe-Si and primary Si), and produces non dendritic structure [71], [72]. Due to the benefit that ultrasonic processing brings to the melt structure, it is often applied on a cooling melt just a few degrees above the liquidus temperature, in order to produce a fine non dendritic microstructure suitable for thixoforming applications. The mechanism that bring to the formation of this non dendritic structure are related to cavitation and acoustic streaming. Frequently in literature in topics related to degassing, filtration, and solidification of the melt, low-frequency vibration and ultrasonic sonication are considered the same treatment even though they differ physically and in the laws that govern the processing. Ultrasonication produces phenomena known as acoustic cavitation. Cavitation is a physical phenomenon in which a rapid change of pressure, in a liquid, creates a vapour-filled bubble in places where the pressure is low. Consequently, subjected to high pressure, these bubbles (or cavities, or voids) collapse and generate a shock wave. The formation of an acoustic streaming in the melt, allow the propagation of a high intensity vibration. Related to the cavitation phenomenon is the sonocapillary effect that is crucial for melt treatment like filtering and wetting/activation of solid inclusions. The sonocapillary [73] effect appears when a high- intensity ultrasonic field is applied close to a narrow space like a capillaries or small channels and an abnormal rise of the liquid is observed in the channels. When ultrasound is applied to melt in filtration procedure, the sonocapillary effect can facilitate the filtration enhancing the liquid to pass through the filter and the impurities to be filtered out of the melt.

In this thesis the ultrasonic vibrations are applied to a semisolid material. The fraction of solid is 25% so the structure should be identified as solid grains immersed in the liquid. In this situation the sonocapillary effect can still facilitate the movement of the liquid in the channels that are created between the grains. There might also be a competitive effect of coarsening of the solid matrix due to the energy that is being given to the system as a result of the ultrasonic treatment. This extra energy can cause re-heating and coarsening the solid grains [72].

2.6 Summary

- Fractional solidification is a well-known separating technique in different research fields. When it comes to metallurgy, it has been used mostly to produce high purity metals and only few works are focused on Al alloys, let alone recycled alloys.
- Most of the technology developed to perform fractional solidification is described patents and in some of them the technology has hardly been tested.
- The set-up developed by A. L. Lux and M.C. Flemings applies fractional solidification by isothermal squeezing on Sn-Pb alloy and is simple in operation and promising for recycling alloys.
- Phase diagram is an important tool to understand fractional solidification.
- Different parameters (time, temperature, type of alloy, grain size and morphology) influence the solidification, partitioning and, consequently, the purification.

2.7 Objectives of the thesis

The main objectives of this study are

- Apply the principle of fractional solidification for purification of aluminium from the most common and harmful impurities (or alloying elements).
- Develop a technology able to perform fractional solidification and upscale said technology.
- Evaluate the effect of solidification parameters on the purification efficiency.
- Investigate the role of the morphology and the deformation on the liquid migration inside the mushy zone.
- Evaluate the effect of solid diffusion on the purification efficiency using modelling calculation and experimental results.
- Test the developed technology on practically important alloying systems

Chapter 3

Methods and Materials

3.1 Selection of the model alloys and the real scrap

Factional solidification is a purification method based on partitioning of solutes between the solid and the liquid phases. The condition necessary for fractional solidification to happen, is to have a partition coefficient (k) less than one, so the solutes are rejected in the liquid phase leaving a purer solid fraction. For value of k higher than one, the solutes enrich the solid fraction leaving a purer liquid fraction. The separation technique that is based on this principle is known as fractional melting.

Table 3 in Chapter 2 lists the most common alloying elements for Al and the partition coefficients in relevant systems. Among these elements, we selected some typical compositions to prepare model alloys for testing an experimental set-up. The model alloys chosen, represent a compromise between the composition of typical cast and wrought aluminium alloys used in automotive industry and the purposes of this scientific investigation (different values of partition coefficient). The model alloys chosen are presented in Table 4.

Table 4. composition of the model alloys prepared and tested in the lab.

	Al	**Si**	**Fe**	**Cu**	**Ni**	**Mg**
Model alloy 1	97 wt%	3wt%	-	-	-	-
Model alloy 2	93 wt%	7 wt%	-	-	-	-
Model alloy 3	98 wt%	1 wt%	1 wt%	-	-	-
Model alloy 4	96 wt%	2 wt%	2 wt%	-	-	-
Model alloy 5	95 wt%	-	-	5 wt%	-	-
Model alloy 6	97 wt%	-	-	-	3 wt%	-
Model alloy 7	97 wt%-	-	-	-	-	3 wt%

Once the methodology was established and successfully tested, the investigation moved to test a real scrap alloy. The real end of life (EOL) scrap was supplied by Jaguar Land Rover as obtained from automotive industry. Average composition of the real scrap is shown in Table 5.

Table 5. Chemical composition of cast real scrap from EOL.

	Al	Si	Fe	Cu	Mn	Mg	Zn
Wt%	m.b.	6.82	0.80	2.34	0.21	0.55	0.89

3.2 Alloy preparation

In this work, Al-Si, Al-Fe-Si, Al-Cu, Al-Mg and Al-Ni has been chosen as model alloys. These model alloys were specifically prepared in the lab for the purpose of being tested with the experimental set-ups. Commercially pure (CP) Al (99.98 %), supplied by Norton Aluminium in ingot bars, was cut in pieces in order to fit inside a clay graphite A16 crucible (top diameter 184 mm, bottom diameter 130 mm, height 232 mm), coated with boron nitride, and placed in an electric resistance furnace at 700 °C until fully molten. Depending on the desired composition of the alloy, different amount of master alloys was added to the melt. To obtain Al-7 wt% Si and Al-3 wt% Si alloys, a certain amount of Al-20 wt% Si master alloy was added to the melt for one hour before casting it. For an Al-4 wt% Mg, commercially pure Mg was added to the Al melt. For Al-1 wt% Fe- 1 wt% Si and Al-2 wt% Fe- 2 wt% Si alloys, an Al-45 wt% Fe master alloy was added to molten Al and the temperature of the furnace increased until 800 °C for two hours to facilitate the melting. The temperature was lowered back to 700 °C to add an Al-20 wt% Si master alloy. For an Al-5 wt% Cu, Al- 50 wt% Cu master alloy was added to the melt. Al- 3 wt% Ni was obtained adding rods of Al- 12 wt% Ni master alloy to molten aluminium at 700 °C. Once the model alloy was fully molten, it was cast into ingots bars. The ingots moulds were coated with boron nitride to prevent sticking and were pre heated in a furnace at 200 °C for at least one hour before the casting. For every batch approximately 12 kg of each model alloy were produced.

Real scrap was supplied by Jaguar Land Rover as end-of-life (EOL) shredded pieces. These pieces were manually sorted and then placed inside a coated graphite crucible (top diameter 197 mm, bottom diameter 145 mm, height 260 mm) into an electric resistance furnace at 850 °C. The molten scrap was cleaned from the dross and then cast into ingot bars of 2 kg each. The ingot moulds were coated with boron nitride and preheated inside the oven before every casting.

3.3 Set-up description

Chapter 2 gave an overview of the fraction solidification methods available in literature. All the technologies described in the chapter are very well designed, but their reproducibility in a university laboratory can be quite challenging. For some technologies, even if a simplified design could have been built up, the results described in the patents, or in the papers, were not encouraging. However, a paper published by A.L. Lux and M.C. Flemings [50], reports fractional solidification performed by isothermal squeezing of a semisolid Sn-Pb alloy towards a filter. The isothermal squeezing seemed a feasible methodology to be used in our study to prove the fractional solidification principle on aluminium alloys and on a bigger scale. Nevertheless, some other approaches have been tested and are described below. Based on these preliminary experiments we have chosen a methodology that has been further implemented in a series of prototypes.

3.3.1 Preliminary trials

A cold finger experiment was designed following the idea of the static layer crystallization developed by Delft University of Technology [49]. The idea was to induce the solidification in the melt using a cold cylinder. To do so, 500 g of a model alloy was placed in a crucible inside a furnace. As soon as the alloy was molten, it was taken out from the furnace and a steel cylinder at room temperature was inserted in the crucible. A fraction of material solidified along this cold cylinder forming a shell while the rest of the sample remained liquid (Figure 17). The temperature was measured through a thermocouple inserted in the melt next to the cylinder. When the temperature reached the temperature at which the primary aluminium phase was 50% solid, the cold cylinder with the solidified alloy around it, was taken out of the melt.

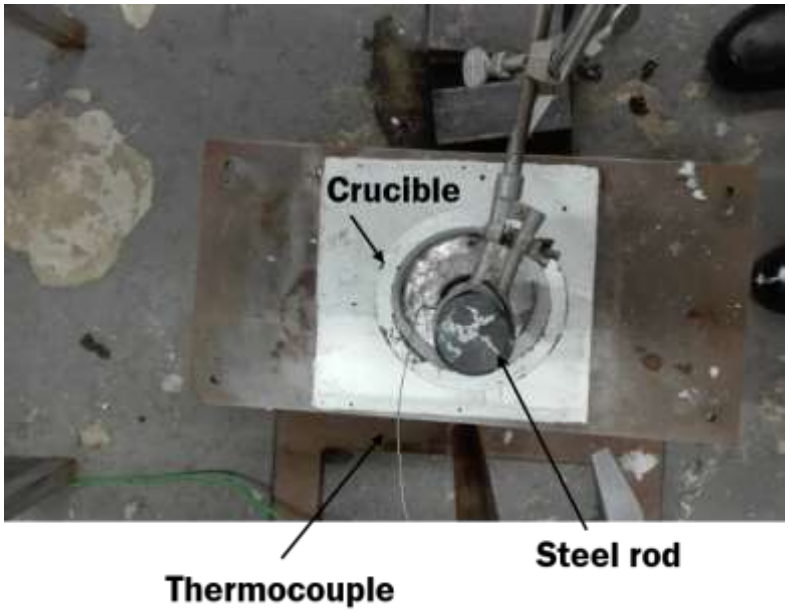

Figure 17: Cold finger experiment. A cylindrical steel rod is inserted inside a crucible in contact with the melt. A thermocouple is inside the melt to record the temperature.

Following the idea developed by Flemings [50], a filtration experiment was designed with its components shown in Figure 18. An amount, equal to 500 g, of a model alloy was placed inside a crucible into a furnace and left to melt. Once molten, the crucible was then taken out and left to cool in air until it reached a calculated temperature at which the primary α aluminium was 50% solid. At that point, the semisolid slurry was poured onto a filter through a sleeve and squeezed by a piston through it. The liquid fraction enriched in impurities passed through the filter, while the purer solid fraction solidified on the top of the filter.

Figure 18: Filtration experiment components: a crucible is used to melt the alloy. A sleeve is inserted in the crucible and a filter is placed inside the sleeve. The piston is used to squeeze the semisolid alloy to the filter through the sleeve.

In the cooling plate set-up (Figure 19), the idea was to induce the partial solidification of a continuous flow of molten alloy. A cold copper plate was placed at the centre of a refractory launder (Figure 19). The launder was sloped from the floor. The alloy, once fully molten, was poured in the launder and let to flow along. Once this flow passed onto the cold plate a fraction of melt solidified on it, while the rest of the liquid flowed into a crucible. A thermocouple was placed in contact with the plate to record the temperature of the melt during the flow.

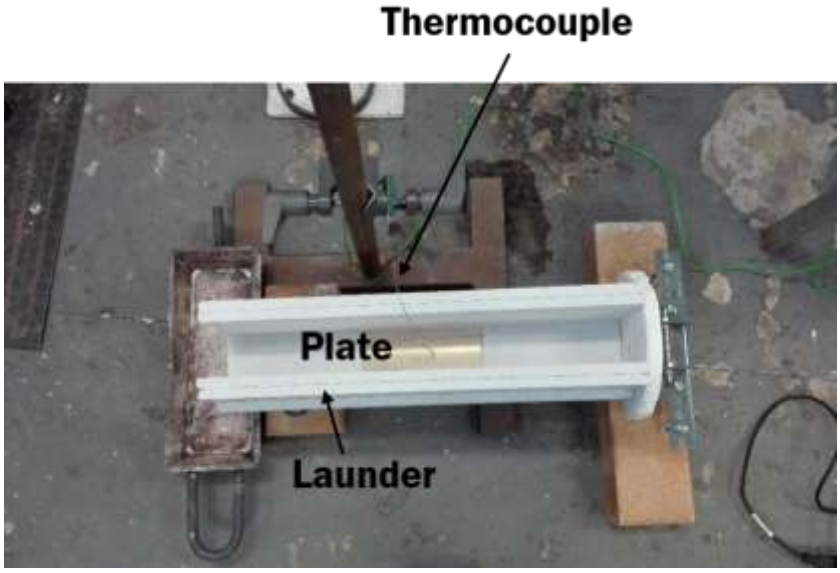

Figure 19: cooling plate set-up: A launder is made by refractory white board. Inside the lauder is a copper plate. A thermocouple is in contact with the plate to record the temperature of the alloy during the experiment.

The results obtained from the initial trials are shown in Table 6. These results gave us a foundation for the selection of the filtration experiment as starting point for the experimental work. The other two set-up did not give encouraging results and they were not investigated any further. So, following Flemings' idea, the isothermal squeezing of a semisolid alloy towards the filter became the technology that has been developed through this thesis. The developing of the set-up was a proper work in process, adjustment in the parameters control, as well in the geometry of the set-up, were constantly made in order to accommodate the issues being faced during the different experiments, and the optimisation of the parameters.

Table 6: Chemical composition of an Al-1.3 wt% Si- 1 wt% Fe before undergoing the preliminary trails and after the trials.

	Al	Si	Fe
Starting alloy	97.5 ±0.1	1.34±0.08	1.01±0.08
Cooling plate experiment	97.5±0.1	1.4±0.1	1.07±0.08
Cold finger experiment	97.6±0.1	1.32±0.09	0.99±0.07
Filtration experiment	97.9±0.1	1.16±0.08	0.83±0.08

3.3.2 Initial set-up

Figure 20 shows the components of the initial set-up. A ceramic foam filter was placed inside a cylindrical graphite sleeve (height 156 mm, bottom diameter 63.5 mm, top diameter 82.5mm). In order to have a sleeve with the same diameter of the piston, so to avoid any overflowing material, a channel was made using mouldable mastic. At the top, inside the wall of the sleeve, a thermocouple was inserted to control the temperature at the calculated value for a given fraction solid. This sleeve was then placed over a graphite crucible (height 141 mm, bottom diameter 76 mm, top diameter 114 mm). The sleeve and the crucible were surrounded by two electric heaters connected to a control box to control the desired semisolid temperature. The entire setup was surrounded by insulating wool to avoid temperature losses.

A cylindrical ceramic piston was used to squeeze the mushy alloy toward the filter. Since it was not possible to perform the squeeze manually, by hands, when the alloy was becoming too mushy, a hydraulic jack and a metallic frame were added to the set-up. Both the sleeve and the crucible were fixed on the hydraulic jack that can be lifted up and down. The hydraulic jack was placed at the bottom of the frame (Fig.20). After pouring a semi-solid alloy into the sleeve, the set-up was lifted up towards the top of the frame. In this way it was possible to exert a pressure on the semisolid material.

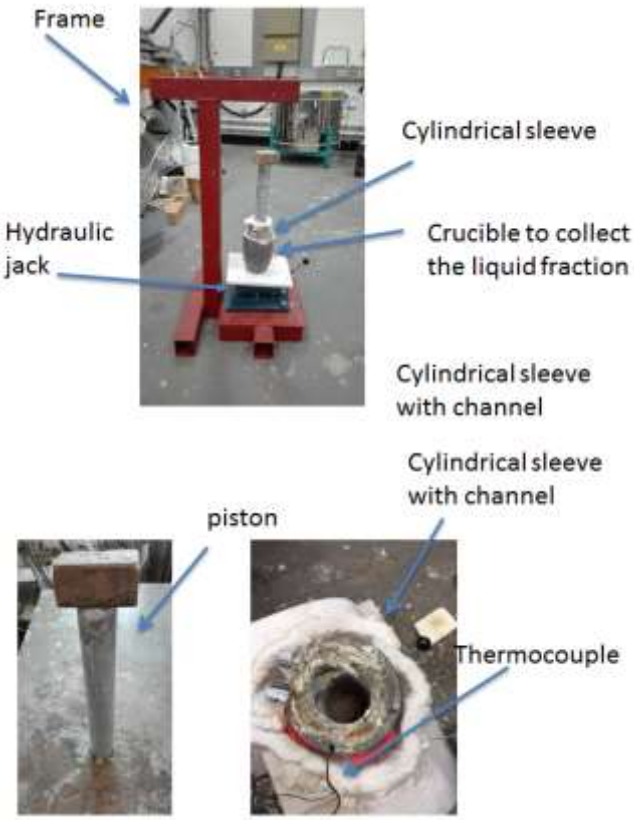

Figure 20: Components of the initial set-up.

Every experiment was run placing 500 g of an alloy inside a crucible into a furnace at 720°C. When the alloy was fully molten, the crucible was taken from the furnace and left to cool in air until the melt reached a semisolid state with a prescribed fraction solid. Once the right temperature was achieved, the mushy alloy was poured into the sleeve on the top of a refractory filter and the slurry was squeezed by the piston through the filter. The liquid enriched with impurities passes through it while the purer fraction solidified on the filter (Figure 21).

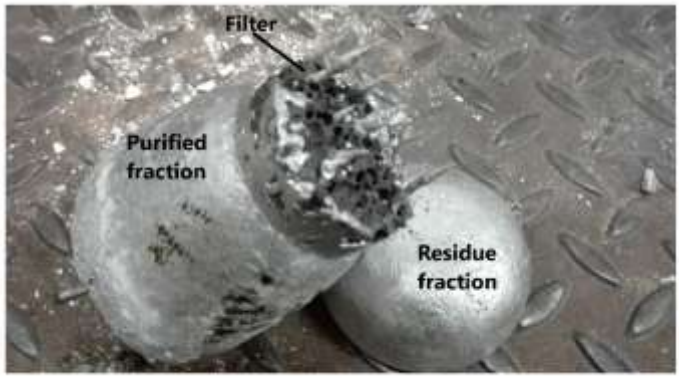

Figure 21. photo of an example of the purified fraction that solidified on top of the filter, and the enriched liquid fraction (residue) that passes through the filter and solidified in the reservoir.

This first set-up was tested on Al-Si and Al-Fe-Si alloys giving good results in terms of purification efficiency (see Section 6.2). Despite the good results, this set-up lacked proper controls and gave inaccurate results. Considering that every component was made of graphite or clay, the set-up was too fragile and happened to crack sometimes during the experiments because of the pressure exerted by the piston. Consequently, a new more robust set-up, in which the components were made of steel, was designed, and built. With this second set-up, it was possible to process up to 3 kg of a semisolid material.

3.3.3 The second and upscaled set-up

A coarse SiC filter (30 ppi) with a diameter of 84 mm was fixed at the centre of a squared plate (Figure 22 b) that has a hole specifically machined to accommodate it. Initially the plate was not heated, as we can see in Figure 22 b, but later it was decided to make four holes (3 mm dia) in the plate to insert four cylindrical cartridge heaters. The reason was to avoid that the filter, being colder than the melt, could induce solidification preventing discharge of the melt, and consequently the purification. This squared plate was placed on top of a reservoir (steel cylinder with refractory lining). The purpose of the reservoir was to collect the liquid fraction that passed through the filter during the squeezing process. The reservoir was surrounded by electric heaters and insulating wool in order to minimise temperature gradient between the two sides of the filter.

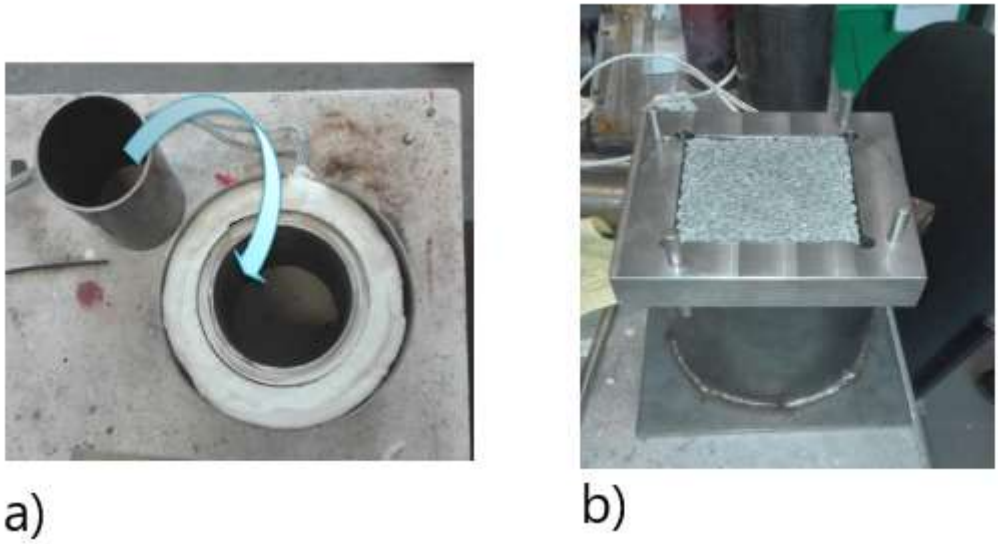

Figure 22. a) cylindrical furnace and sleeve. b) squared plate with ceramic filter on top of a reservoir.

On top of the plate containing the filter, was placed a cylindrical electric furnace with an inner steel channel (84 mm in dia.) able to hold up to 3 kg of a slurry and open on both sides (Figure 22 a). The channel is positioned on top of the filter. The entire set-up was placed, as the previous one, on a hydraulic jack that can be moved up and down.

A stainless steel sonotrode connected to a magnetostrictive transducer (17.5 kHz), with a diameter of 82 mm to fit in the channel inside the cylindrical furnace, was used as a piston to squeeze the slurry through the filter. Ultrasonic vibrations were either switched on when the experiments required that, or the piston was used without vibration applied. Every component of the set-up was coated with boron nitride to avoid the molten metal to stick to the parts. Figure 23 shows the assembled setup and its scheme.

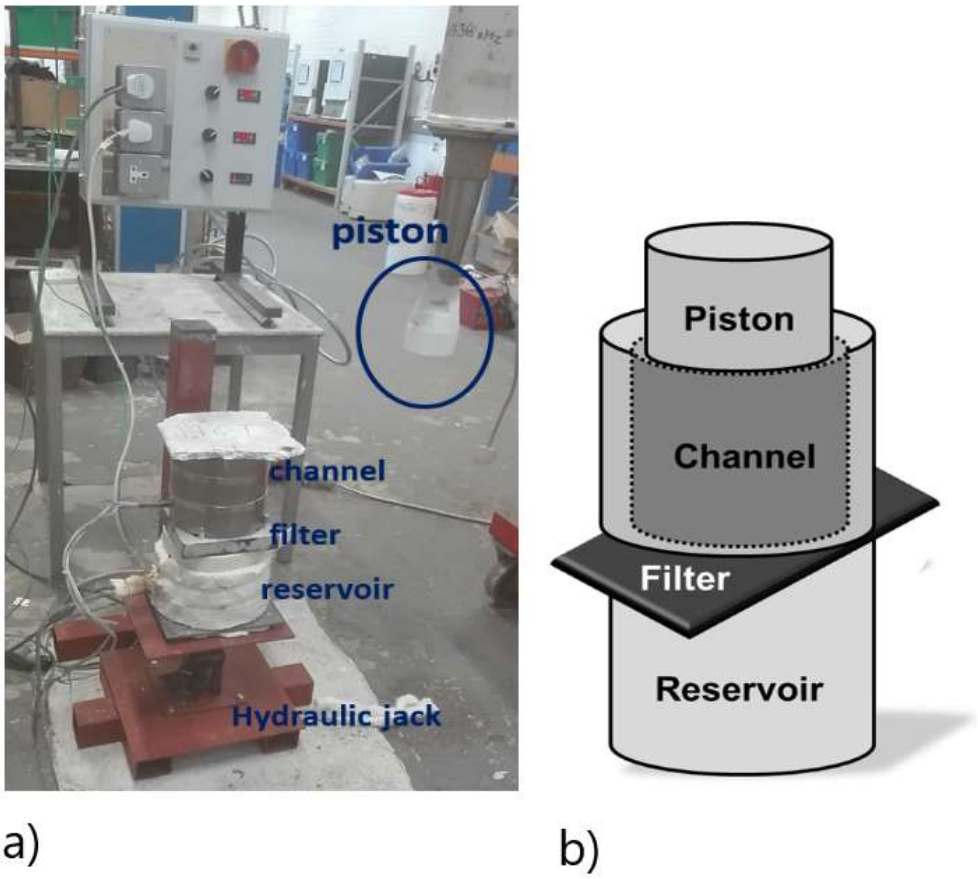

Figure 23. a) photo of the set-up b) scheme

3.4 Experimental procedure

Every standard experiment was done using 2000 g of model alloy ingots, or real scrap alloys, and placing the charge in a clay-graphite crucible inside the furnace at 720 °C. In some cases, the alloy was superheated to 820°C to dissolve master alloys or a grain refiner (Al5Ti1B 4 kg/t) was added to the molten alloy some minutes before taking it out from the furnace. Once the alloy was fully molten, it was taken out and let to cool at the air until the semisolid prescribed temperature was reached. This temperature was selected to be 30% of the primary Al solid fraction and was calculated by Thermocalc using the Scheil-Gulliver equation. While cooling down, the alloy was constantly stirred with a rod made of refractory material to make the composition homogenous. The semisolid slurry was then poured into the channel, on top of the filter. Although the calculated semisolid temperature of processing was the one for 30% solid fraction of Al, during the experiments the actual pouring temperature was few degrees higher the calculated one. In fact, during stirring, the solidification started from the wall of the crucibles moving towards the centre. It follows that some of the alloy remained attached to the wall making more challenging the pouring. Hence the need to pour the alloy few degrees before the calculated temperature. The piston/sonotrode was then lowered in contact with the slurry, and the hydraulic jack was lifted up. In some cases, a disk was placed between the sonotrode and the mushy alloy. The squeezing was performed by lifting up the entire set-up toward the piston. In some cases, while the squeezing was performed, ultrasonic vibrations were applied until the alloy was too solid to be squeezed any further. At an initial stage of the experimental practice, the squeezing procedure was performed lifting the set-up, by the hydraulic jack, towards the piston as quickly as possible until it was not possible to squeeze anymore. The main concern, in this situation, was to avoid the solidification of the slurry inside the channel, making difficult to perform the squeezing. The quick solidification was happening because the temperature was not very well controlled (initially there were no cartridge heaters in the steel plate holding the filter as described above). Also, the squeezing procedure was causing a compaction of the mush not giving the liquid enough time to move towards the filter, and leaving it entrapped at the grain boundaries. So, in a second stage of the experimental work, the experiments were done by squeezing in steps, lifting the set-up only a couple of centimetres and taking an interval of 2 minutes between the steps, for a total of the experiment equal to 13 minutes. Adopting this squeezing procedure, experiments were carried with the application of US (3 kW power) for the entire duration of the squeezing time, and without the application of US for a reference sample.

Sometimes, just before pouring the semisolid alloy inside the channel, a small portion of semisolid slurry was taken to quench it in water. A preheated ceramic tube (3 mm dia) was

used to collect the sample. The purpose of this was to observe the structure before the procedure. Also, small samples were taken from the liquid alloy to control the chemical composition and the initial structure.

The purified final product, 83 mm dia and aprox. 55 mm height, (Figure 24), obtained from the fractional solidification process was cut from the filter for further examination (Figure 25) and the liquid fraction collected under the filter was then remelted and cast into special composition moulds.

Figure 24. Cylindrical purified sample, cut from the filter, obtained at the end of the process.

3.5 Material Characterization

3.5.1 Chemical analysis

In optical emission spectroscopy (OES), samples need to be ground with sand paper (320 grit) to make the surface completely flat. For the purified cylindrical fraction, the measurements were taken along the vertical cross section (Figure 25 stage 2) of the purified cylindrical fraction, and also on the round flat surface that was previously in contact with the filter. The composition samples, obtained from the casting of the liquid faction collected under the filter, were ground on the round surface, and analysed as well with OES. The measurements were executed with Foundry Master Pro (Oxford Instruments), using software Waslab3. The resolution of the instrument is 0.1 wt% in the chemical composition. From the chemical analysis it is then possible to calculate the yield of the process and the purification efficiency. In this way, a quick evaluation of the performance of the set-up was possible with the conclusions if a modification was needed.

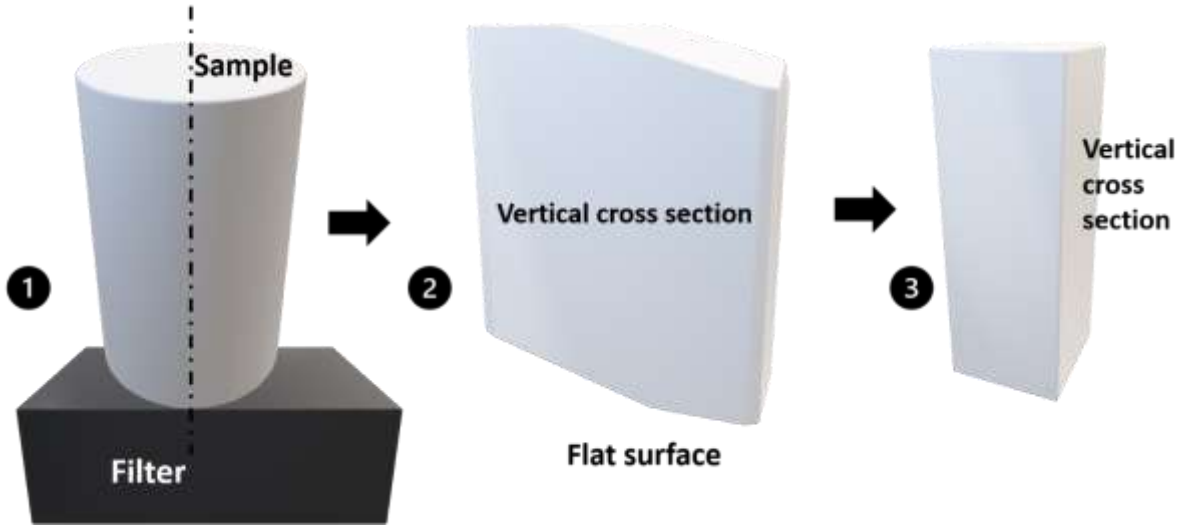

Figure 25. Scheme of how the purified sample is cut before being analysed with different techniques. Initially (stage 1) the sample is machined from the filter and the resulting cylinder cut into two halves (stage 2) that are analysed with the OES on the flat surface and on the vertical cross section. From a central area of one of the halves, a cuboid (5 mm x5 mm x5 mm) is cut to be used for CT measurements (stage 3). A second cuboid (stage 3) is cut from a central area of the second half, mounted with the hot press on a resin, and the analysed with optical microscope.

3.5.2 Structure analysis

Metallography

The samples were cut along the cross section in order to make small rectangular samples (2 mm × 3 mm). Metallographic microstructural analysis was done using an optical microscope (OM) Carl Zeiss Axioscope A1 equipped with an AxioCam MRm digital camera and software Zencore to process images. The analysis was done only on the purified fraction and the samples were analysed along the vertical cross section (Figure 26 stage 3). Samples were ground using 10N force for 5 minutes with each different grinding papers (320, 800 and 1200 grit). Once completely flat and without any scratches, the samples were polished using diamond suspension, first with 3 µm particles and then 1 µm particles. As the last stage, samples were polished with silica suspension. Between each polishing step, the samples were cleaned with ethanol, in an ultrasonic bath, to prevent any inclusions to remain entrapped in the pore.

In order to measure grain sizes, anodizing was performed dipping the polished samples in a 10% water solution of tetrafluoroboric acid at 20 VDC. The immersion time depended on the

type of alloy tested and the current measured. These samples were then observed under polarized light.

From the optical microscope analysis, it was possible to evaluate the grain sizes, the volume fraction of liquid entrapped at the grain boundaries, the shape factor, and the specific surface. All these parameters allowed then the calculation of the permeability of the sample.

Scanning electron microscopy

A scanning electron microscopy (SEM) JCM-6000PLUS BENCHTOP with max voltage 15kV with a JEOL EDS detector, was used to obtain the structure on a much smaller scale in order to measure the variation of composition of the elements inside the grains. This was done to verify if back diffusion phenomena might have affected the samples and consequently the purification. The analysis was done on the vertical cross section of the purified samples and these samples were prepared with the same procedure described in the previous paragraph.

Computed tomography

Purified fraction samples were cut along the cross section in order to have size 5 mm × 5 mm × 5 mm cuboid (Figure 25 stage 3) and analysed with Zeiss Xradia 410 Versa X ray microscope microcomputer tomography scan. Scan and Scout software were used to acquire data. XM Reconstructor to reconstruct the data and software VG studio Max 3.0 and ImageJ to analyse the images. All measurements were done at an optical magnification of 4 times. Depending on the type of sample, the beam energy used was within the range 80-100 kV with values of currents within 100-125 mA and a pixel size of 3.7 µm.

Through computed tomography was possible to visualise and analyse the liquid channels, or pockets, that remained entrapped in the sample, and to measure, as well, the porosity and voids that were present inside the sample. Nevertheless, it was not possible to obtain a good 3D reconstruction for every type of alloys because the resolution of the scans depends on the difference of density between the aluminium matrix and the alloying elements, that manifests in the black and grey contrast in the volume reconstruction.

A set of data obtained by Professor Peter D. Lee's research group in the University of Manchester was kindly given to us for the analysis [74]. This data set was obtained from by high speed X-ray tomography in synchrotron using a semi-solid Al-15 wt% Cu alloy and contains 7 tomograms, each of those containing 900 radiographs collected in 9 seconds. The

experiments were done using a 53-keV monochromatic X-rays on the 112 beamline at the Diamond Light Source. Figure 26 gives a scheme of the experimental set-up.

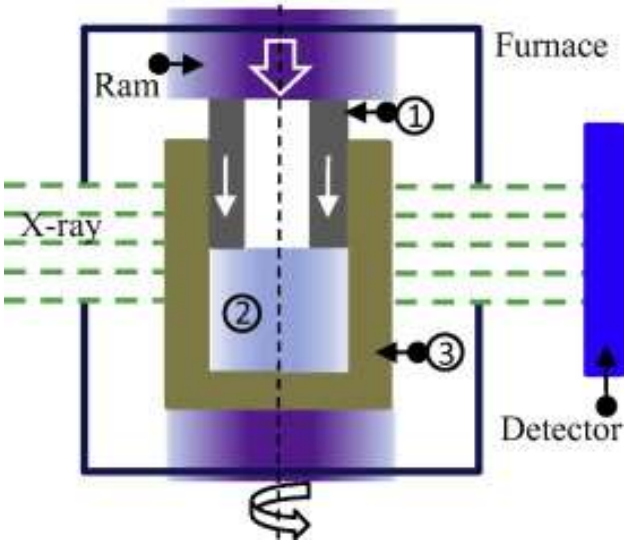

Figure 26: Schematic of the experimental set-up (72): 1) alumina tube; 2) semi-solid specimen; 3) boron nitride holder.

A cylindrical specimen 2 was placed inside holder 3 (Figure 26) and held at a precise semisolid temperature (approx. 27 wt% solid fraction formed). The experiment took place by pushing down alumina tube 1 onto specimen 2 that was extruded back with liquid phase exudation. The alumina tube was pushed down every 45 seconds and for every displacement originated from the push, a tomogram was recorded for the duration of 9 seconds. During the recording of the tomogram, the set-up was rotated by 360 °C. Liquid exudated from the mush on the top of specimen 2. This experiment resembles our process in deformation of the semi-solid alloys with liquid evacuated from a free surface.

3.5.3 Modelling

Thermocalc

Thermocalc 2019b is the software used, in this work, to obtain phase diagrams and fraction of solid according to the Scheil equation. This software allows, also, the calculation of the composition of a phase. The calculations were based on the data supplied from a wide database for different Al-based materials, i.e. TCAL4

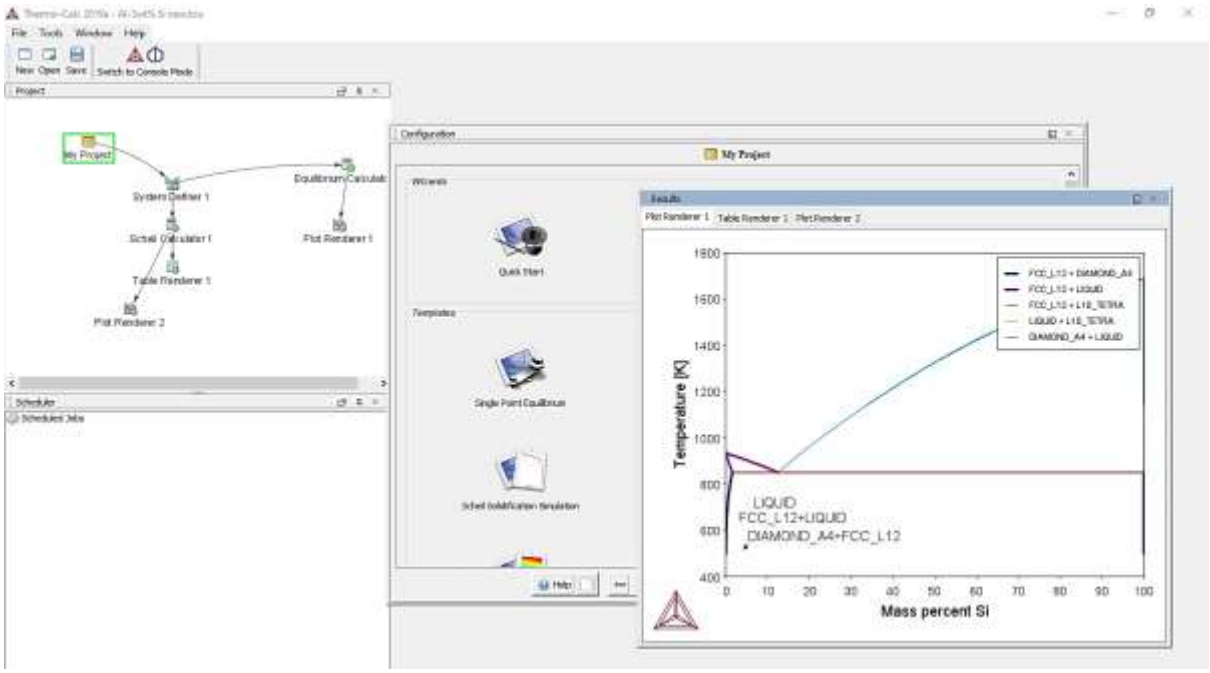

Figure 27. Thermocalc interface for calculation of an Al-Si phase diagram.

Diffusion model

The diffusion model was developed by Prof. Alain Jacot at Brunel University London. It is a numerical microsegregation model which simulates the drainage of liquid around a grain. The microstructure was represented in 1 dimension using spherical symmetry. The initial size of the calculation domain was selected from the experimentally determined average distance between two grain centres just before squeezing. Starting from a negligibly small solid seed surrounded by liquid of nominal composition, solidification prior and during squeezing was described by solving the solute diffusion equations in the solid and liquid subdomains. The position of the solid/liquid interface was updated at each time step from a local solute balance assuming local thermodynamic equilibrium at the interface. The effect of squeezing was simulated by eliminating progressively the liquid cells on the right-hand side of the finite volume grid, following some prescribed squeezing kinematics.

The calculation was run inserting specific values of parameters for each alloy. These values were:

- Size of domain
- Liquidus slope
- Nominal composition
- Partition coefficient

- Time of the experiment
- Semisolid holding temperature

The purpose of using a diffusion model was to find out if there could be some diffusion effect from the liquid to the solid (so-called back diffusion) during the twelve minutes in which the experiment takes place. Even though the model is a simplified description of the real experiment, it represents a good enough approximation to draw conclusions about the extent of diffusion.

Chapter 4

Effect of semisolid squeezing

4.1 Introduction

In this work, purification via fractional solidification is realised by isothermal squeezing of a semisolid alloy towards a filter. Working with a semisolid medium is very challenging and many factors need to be considered when studying such a system. First of all, the quantification of the solid fraction is crucial because the behaviour of the material is different depending on the amount of solid phase, changing from a liquid-like slurry to a solid-like mush (Section 2.3). In this thesis the solid fraction has been quantified either by Thermocalc applying the Scheil-Gulliver equation, or by image processing of optical microscope images taken from samples quenched from liquid, or from the samples obtained at the end of the experimental procedure. What also needs to be remembered is that during the squeezing process, the semisolid sample is deformed during the time in which the experiment takes place. In fact, the alloy is mechanically pushed by the piston (sonotrode) towards the filter and this squeezing affects not only the configuration of the liquid channels inside the solid matrix, but also the matrix itself. The response of the semisolid alloy towards the squeezing and the liquid migration through the mush is very important for understanding the fundamental mechanism that lays behind the technology developed in this work.

The deformation of a semi-solid material was the subject of numerous works, in different research field, where the mechanical properties, liquid flow and microsegregation are scrutinised [74]–[78]. However, up to now, there was no technique that allowed one to observe the kinetic and the structural changes related to the semisolid deformation. The new technology that allow us to address this issue is *in situ* synchrotron tomography. Fortunately for us, a relevant study on semisolid structure and characterization upon deformation was done by a research group of Prof. Peter D. Lee in The University of Manchester. In a number of papers [74], [78], [79], they described an experiment on in-situ synchrotron tomography of a semisolid Al-Cu alloy subjected to deformation. They investigated the volume fraction of solid, the type of stress the material is subjected to (shear or compressive) and the response of the liquid channels to the deformation. The purpose was to explain the kinetics of liquid migration through a mushy alloy, which is much relevant to our work.

In this chapter, we initially discuss the work done by the Manchester group and the hypothesis they draw based on their results. This will be followed by our own analysis of the same dataset that was kindly given to us by Prof. P.D. Lee. The reason of analysing their data was to assist the interpretation and analysis of our own results. The experimental procedure explained in

Section 3.3.3 makes it clear that we cannot analyse the kinetics of structure changes and liquid flow through the mush during an experiment in our experimental setup. For understating the fundamental mechanisms in the alloy during the squeezing process, we need to rely on a model experiment like the one done by P.D. Lee et al.

In this Chapter we will also consider the effect of some parameters (ultrasound and grain refinement) on the semisolid structure and the liquid distribution. The mechanisms playing a role in the morphology of the semisolid structure will also be discussed. The effect of the deformation on the structure itself, and on the liquid flow, will be evaluated along with the calculation of the permeability prior and after the purification process.

4.2 In-situ synchrotron study of a semisolid Al-Cu alloy during deformation

Figure 28 shows, in different axes orientation, two radiography images of a semisolid Al-15 wt% Cu alloy, belonging to two tomograms recorded at different times and with different displacements (see Section 3.5.2 for experimental details). The light grey areas represent the liquid channels, and the dark grey areas the solid α-Al grains. Figures 28 a) and b) are images taken from the tomograms in which the displacement caused by the push of the alumina tube it is very small. Figures 28 c) and d) reflect a tomogram recorded at the end of the experiment when the alumina tube is lowered down until the end and the liquid has been back extruded. At the beginning of the experiment, the deformation caused by the alumina tube is very small and the amount of liquid exudate, represented by the dome in Figure 28 b), is considerably less than the one formed at the end of the experiment in Figure 28 d). So, in the final stage of the deformation most of the liquid has been ejected into the cavity and the orthogonal view xy (Figure 28c) displays the liquid exudate in the central part of the view. B. Cai et al. [74] reported in the paper, the volume of the expelled liquid (the dome) increased with the vertical displacement at a constant rate. Consequently, the liquid fraction in the remaining sample decreased resulting in densification of the mush and in closure of existing channels/porosity, especially in the regions in which the force, due to the deformation, was exerted vertically [74].

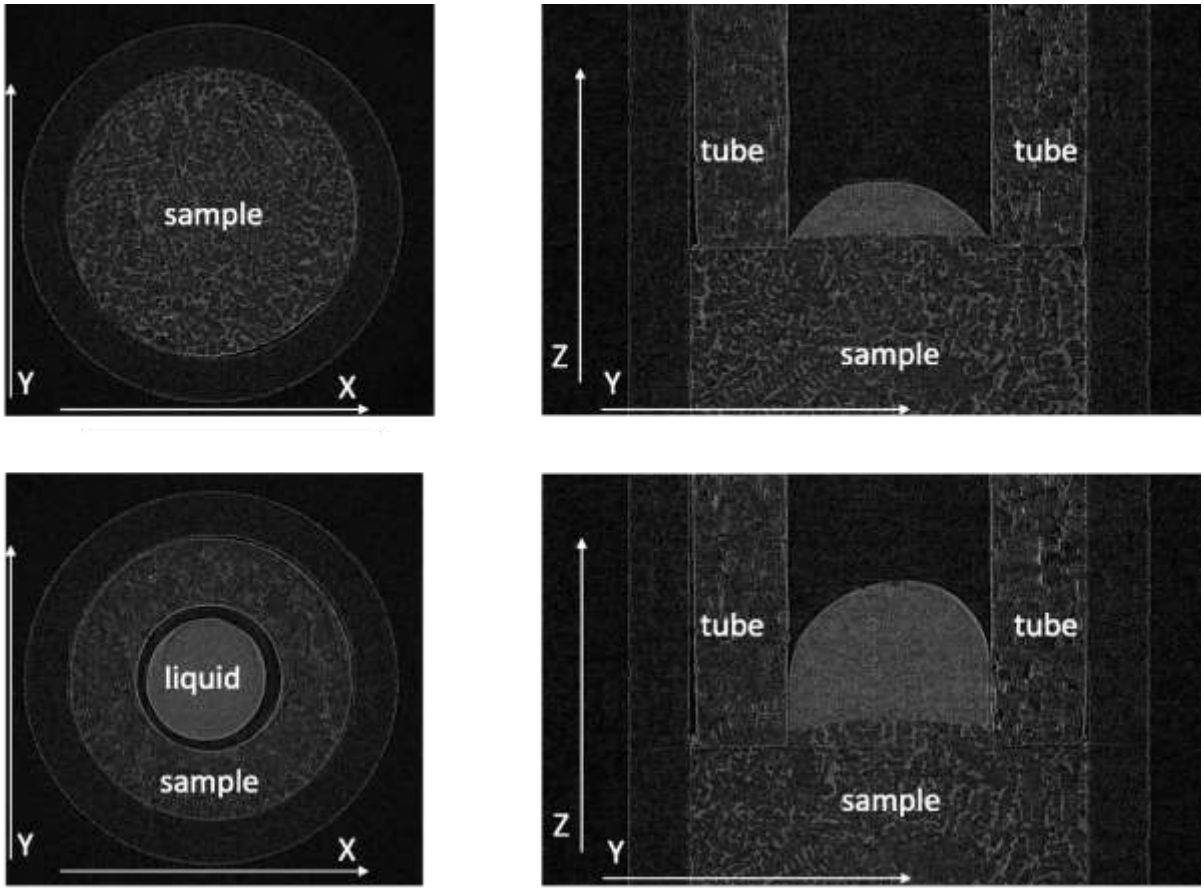

Figure 28: X-ray tomography slices in xy and yz planes: a) and b) beginning of the extrusion process; c) and d) end of the extrusion process. (Courtesy of P.D. Lee and B. Cai)

Moreover, the permeability, calculated for each time step of the process, seems to decrease monotonically, within the liquid fraction decreasing from 27% to 15% in the sample region, leading to the hypothesis that the deformation compresses the mush increasing the flow resistance and blocking the liquid flow inside the semisolid matrix [74]. Considering that the purpose of our research is to evacuate as much liquid as possible from the mush, it is important to understand how the densification happens, and also, if there are any preferential channels developing or closing during the deformation of the mush. Some reference data [78], [79] suggest that when the compression of a semisolid mush with globular or dendritic grains is axial, the liquid channels occasionally open instead of closing. For example, shear stresses may cause a dilation moving liquid from one location to another between grains. In the *in-situ* experiment, the compressive stress causes densification of the mush. In the case of our experimental set-up the scenario is somewhere between these two cases. The force exerted by the piston is axial, but the liquid migrates through the mush and is expelled through the filter. Nevertheless, the analysis of the literature and the data provided by Professor Peter D. Lee, help to single out important parameters required for understanding the response of a semisolid mixture to deformation, i.e., the volume fraction of solid, the microstructure and

specifically the shape and size of the grains, and the existing porosity in the sample. In fact, B. Cai at al. [74], conclude that the deformation is inhomogeneous because the propagation of the compression in a granular medium, is dependent on the microstructure and tend to follow percolation pathways [80].

Regarding the same data set we just discussed (experimental details in 3.5.2), we analysed the variation of the area of eutectic liquid entrapped at the grain boundaries, in several regions in the semisolid sample during the deformation process. In order to do so, the cross-section of the sample was divided in regions of interest (ROI) as shown in Figure 29. The purpose of this analysis was to have a general idea if there were preferential channels formed upon deformation of a semi-solid sample. Preferential channels would imply that the amount of eutectic volume fraction is small in certain regions, because the liquid migrating through the mush towards the exudate dome leaves less amount of liquid behind. On the other hand, there might be some regions of the sample where the migration of liquid does not happen, due to the closed channels, resulting in uneven composition across the whole sample.

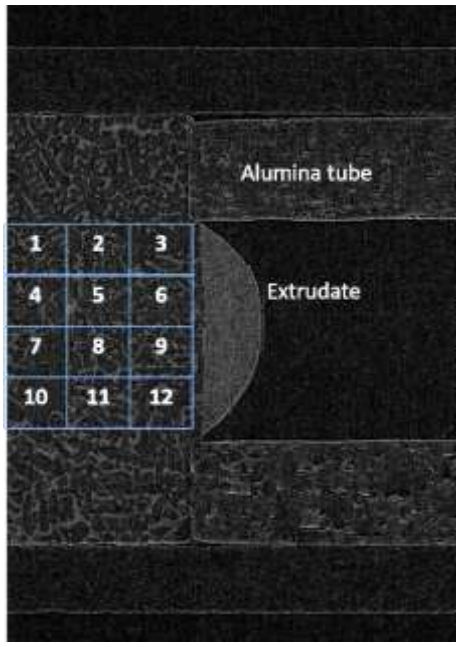

Figure 29: An orthogonal view on the xz plane of the tomography image in the last stage of the deformation. The cross-section was divided into 12 ROIs. (Courtesy of P.D. Lee and B. Cai)

Analysing the variation of the liquid channel thicknesses, is a good way to understand if the mush is undergoing densification uniformly or the liquid is having preferential paths or forming liquid pools in certain areas. Figure 30 illustrates the variation of intensity of light grey areas, which represents the thickness of the liquid channels entrapped in the solid aluminium matrix.

The analysis was done by processing the images using imageJ. The areas have been calculated every 10 radiography images inside a tomogram made of 900 radiography images. The experiment is made of 8 tomograms. The values showed on the x axis are the results of the values calculated every 10 radiograms but averaged for the eight tomograms. On the y axis is represented the intensity of the grey areas. The bigger the intensity, the thicker the channels are. It follows that thicker liquid channels represent a higher volume fraction of liquid. It would be expected that the volume fraction liquid would decrease from ROIs further from the dome of exudate liquid to ROIs closer to the dome. Hence, if the liquid is being pushed towards the dome, it means that thickness of the liquid channels is smaller and the intensity of the light grey areas in the graphs in Figure 29 is decreasing. This would also be in agreement with what stated by B. Cai et al. [74] that the volume fraction of liquid inside the sample is decreasing because of the compressive stress.

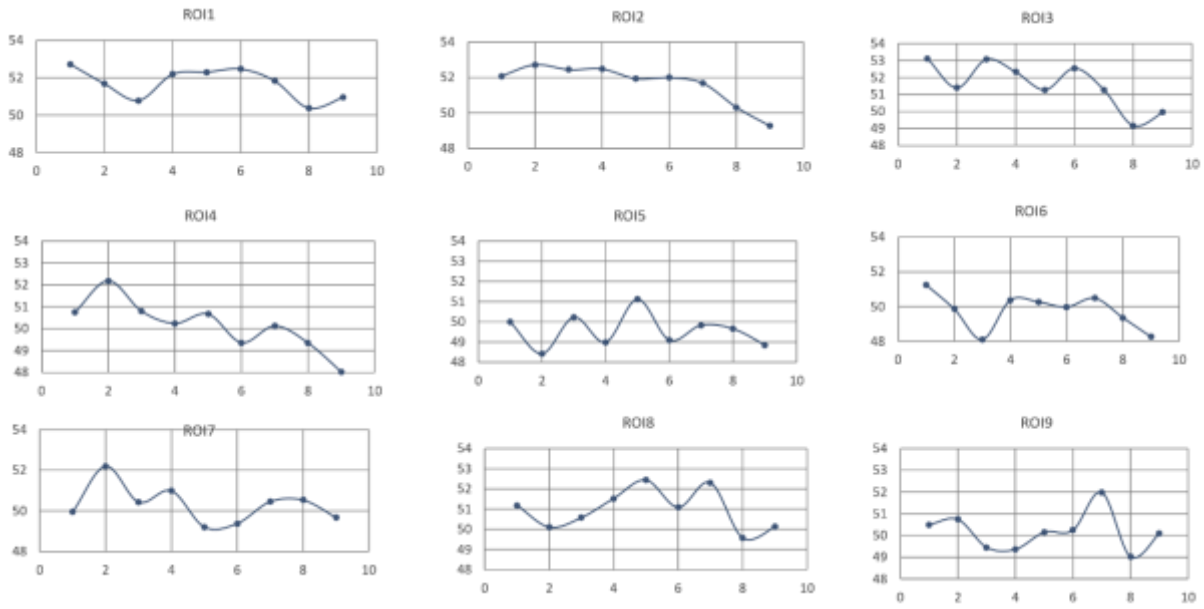

Figure 30: Representation of the variation of intensity of light grey areas for different ROIs. The y axis is the intensity of dark grey areas. The x-axis shows ROIs, see Fig. 29 for the numbers and location of ROIs

The liquid channels in fact are expected to be narrow and thin (low grey value) in the central area of the billet because of the densification of the mush due to the compression. But in the areas next to the dome, the intensity of the grey areas is expected to be higher in the graphs, because the liquid is being pushed towards this region, as it is proven by the increasing volume of the dome, and the decreasing permeability in the central area of the billet [78]. The volume fraction of the liquid channels, however, does not follow a linear trend and seems quite random as it is apparent from Fig. 30. Even if there is a fluctuation in the open area, is it mostly inside a single ROI and not related or translated to the next ROI. These data support the hypothesis

that the liquid channels open and close randomly inside the squeezed volume, and there is no linear relationship with the distance from the point of the force application, to the open end of the mush, where exudation of the liquid occurs. Having a random distribution of the volume fraction of liquid makes it more difficult to control the liquid flow. On the other hand, the absence of preferential channels makes the “processing” of the volume more uniform. In a separating technique it is crucial to understand, and to influence, the migration of the liquid in order to achieve a high purification efficiency. As the liquid flow inside a matrix is influenced by the microstructure, changes in the microstructure need to be investigated to understand the mechanism of the process, and this will be considered in the next Section.

4.3 Distribution of liquid fraction due to deformation

The squeezing procedure deforms the mush and forces the liquid channels to open or close depending the way the force is exerted. The response of the material to the deformation depends on the structure of the material itself (particle size and shape, solid and liquid fraction) [81].

Through the *in-situ* tomography characterisation described in the previous Section, we learned that the liquid channels do not form a preferential path inside the mush during the deformation. They open and close rather randomly. In this Section, we discuss the distribution of the liquid inside the mush as obtained from the purified fraction collected at the end of our fractional solidification experiments. Note that the scale of the samples in this study is much larger than in the in-situ experiments. From the analysis of the distribution of the eutectic fraction at the grain boundaries, it is possible to reconstruct the migration of the liquid fraction during the process. It helps that the tested alloys are simple binary alloys in which the liquid fraction solidifies as the eutectic mixture.

A sample tested, obtained at the end of the process, was first cut in two halves. One half was then sliced in three along the height (Figure 31). For every slice, a grid was drawn in which every spot had a precise x and y coordinate. The slices were then analysed, with optical emission spectroscopy, to get the composition of Cu in very spot. The composition and the location coordinates were then plotted to have a 3D plot. The purpose of knowing the distribution of the Cu inside the sample is to understand the migration of the liquid inside the sample, e.g., if there is a preferential region in the sample where the liquid concentrates.

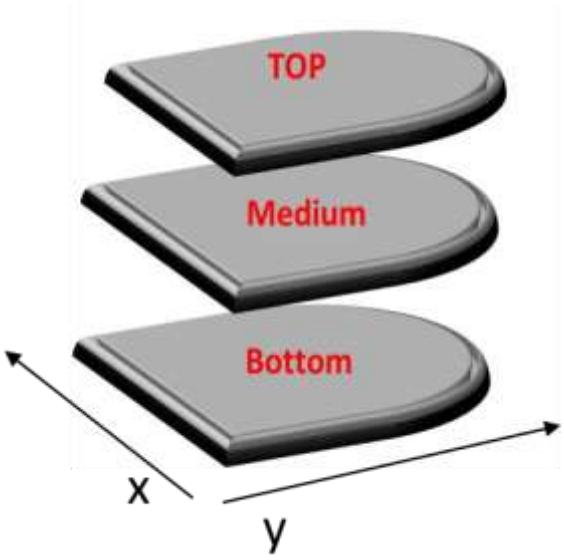

Figure 31: Schematic of how one half of a purified sample was sliced.

It would be expected that the area of the sample close to the filter, i.e., in the regions labelled as bottom in Figs. 32-33 had a higher concentration of Cu (hence, eutectic). It would also be expected that, since the force exerted by the piston is on the top part of the sample, the liquid should be forced to move inside the mush towards the filter so liquid channels should close at the top and open towards the bottom. However, Chen et al. [82] reported that, when a semisolid material had a high amount of liquid fraction, the axial deformation force push the liquid flow to move towards the side of the sample, leaving the central region depleted. In their experiments, a cylindrical sample (10 mm dia and 11 min length) was deformed according to the upsetting method using a Rastegave's specimen [83]. It follows that, in their work, the dimension of the sample was much smaller than in our work.

Figure 32 demonstrates the profile of the concentration of Cu inside the purified fraction of an Al-5 wt% Cu alloy that was squeezed in one step only and did not undergo any additional treatment. The areas in red, are the areas in which the composition of Cu is lower, so it means that in these areas there is less retained eutectic and, hence, the purification has been more efficient. In fact, during the purification process, the liquid is squeezed out of the mush and this changes the composition of the overall alloy. It follows that in those regions in which the composition of Cu is lower, the liquid was squeezed out changing the local composition of the alloy. Looking at these red areas, it seems that the liquid fraction does not decrease gradually moving from the top to the bottom, it actually decreases mostly at the side following a random path.

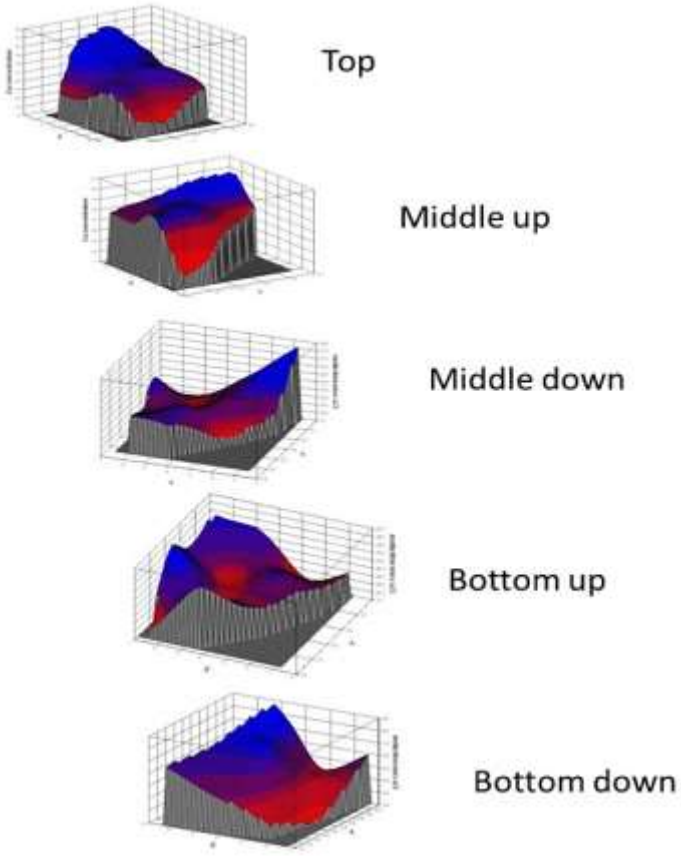

Figure 32: Profile of the concentration of Cu inside the purified fraction of an Al-5 wt% Cu alloy that underwent the procedure of squeezing by one continuous step and with no additional treatment. Blue region is where the concentration of Cu is higher, red region where it is lower.

When the sample undergoes superheating before the squeezing procedure (as it will be shown later it results in large dendritic grains), it seems that the migration of the liquid is rather random as shows Fig. 33a. The path the liquid flow follows, is tortuous and not uniform in every region of the sample. Very similar behaviour happens, when the sample has been previously grain refined (smaller and uniform dendritic grains), the profile of the concentration or the volume fraction of eutectics does not decrease in a homogenous way (Figure 33b). These results are in agreement with the analysis done on the data from the Manchester group. But, in all our tested three samples it is possible to identify a central area depleted of liquid, similar to the observation of Chen et al. [82]. A depleted central area is visible in both the middle regions in Fig. 33b, in the middle up region in Fig. 33a and the bottom up section in Fig. 32. There is, however, a big difference in the way how the mush has been deformed between our experiment and the experiment by Chen et al. In their case, the deformation was exerted on a cylindrical sample from the top and the bottom, while in our experiments, the force was applied only from the top. This could explain why, even if in our samples the central areas are depleted

in eutectic liquid, the interdendritic liquid, in general, still continues to flow randomly through the volume, until it reaches the filter.

Note that in all these purified samples, the squeezing (or deformation process) happened in one step only, so the mush is compacted and the liquid expelled in a relatively short amount of time that was not, probably, sufficient for the liquid to migrate fully though the mush.

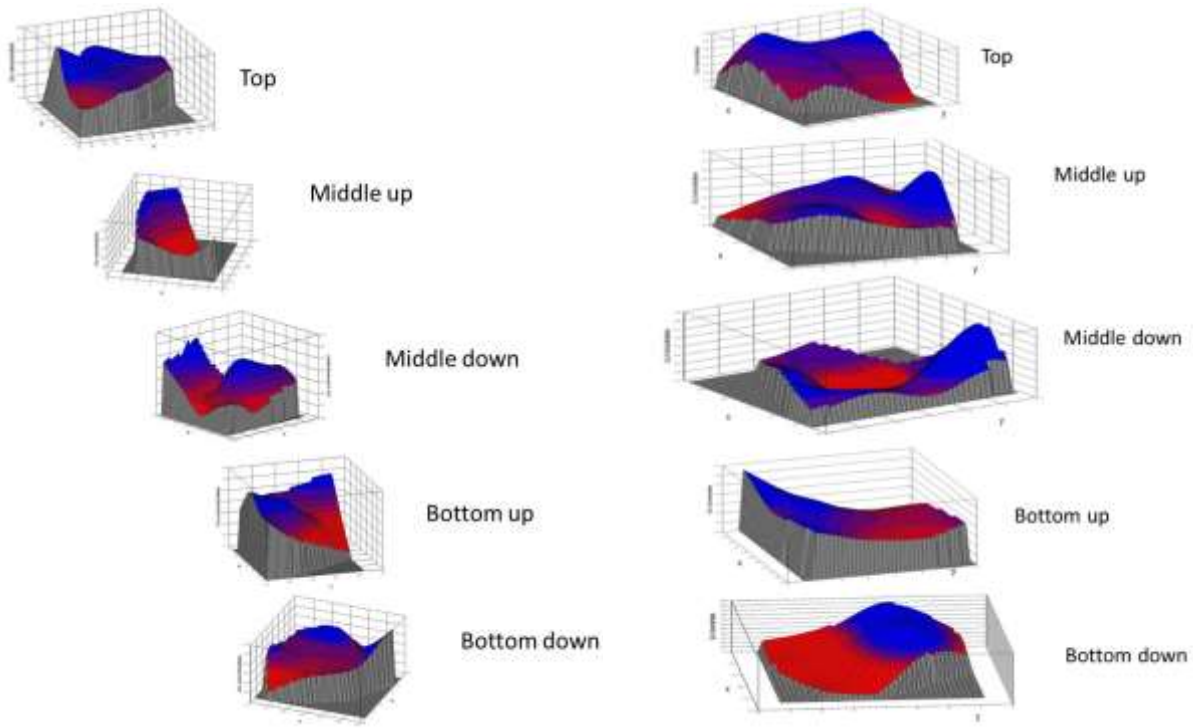

a) b)

Figure 33: Profile of the concentration of Cu inside the purified fraction of an Al-5 wt% Cu alloy that underwent the procedure of squeezing by one continuous step in two different conditions: a) superheated to 820 °C prior the squeezing and b) grain refined prior the squeezing.

In this work, as described in Section 3.3.3, the experiments were not always done in a single step. In the second stage of experimental campaign, the squeezing procedure was changed to a multi-step procedure in which each step was performed every two min for a total time of 13 min. Below we present some results about the evaluation of the liquid flow inside the mush for a multistep procedure, using computed tomography.

Figure 34 represents one slice (xy orientation) of a CT tomography scan of a region in the cross section of the purified fraction of an Al-5 wt% Cu alloy (see Fig. 25 for details). The dark

grey areas are α-Al grains and the narrow light grey channels are the liquid phase that remained entrapped at the grain boundaries solidifying as eutectics at the end of the process. Three purified Al-5 wt% Cu samples treated in different conditions were analysed with computed tomography. These sample underwent the purification with a squeezing procedure performed by steps (see details in Section 3.3.3). Additional treatments were also performed before or during the squeezing: grain refinement with Al5Ti1B and ultrasonic vibration, respectively. Figure 35 shows the volume fraction of the light grey channels measured from the 2D slices (Figure 34) taken in different areas of the cross section of the samples, i.e. areas close to the filter and areas far from the filter.

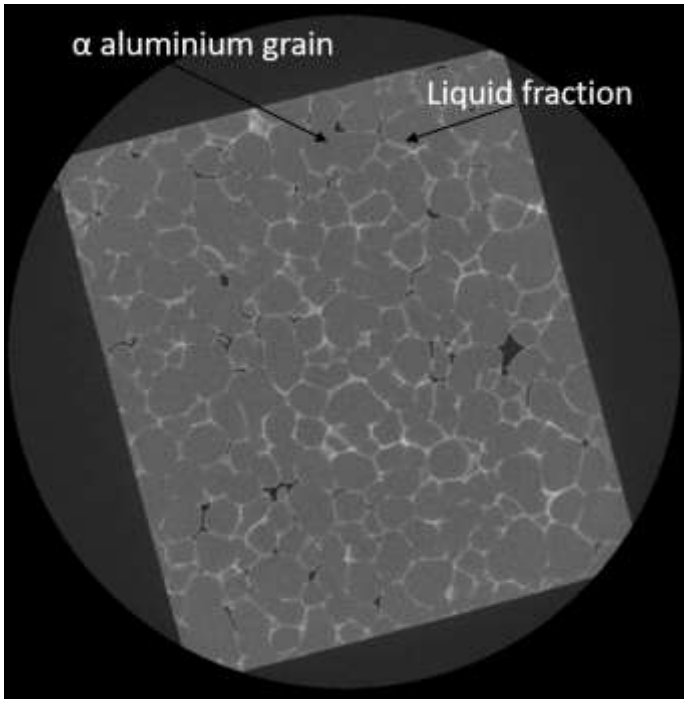

Figure 34: An xy view of one slice of the purified fraction of an Al-5 wt% Cu alloy obtained from CT scan. Dark grey area is α Al grains. Light grey area is the liquid fraction entrapped at the grain boundaries.

The distribution of the volume fraction, moving from a region far from the filter to a region close to the filter, is not gradual in any of the three samples. When the sample is treated with US only, the liquid fraction gradually decreases half-way through the sample, and then increases again. Probably the initial squeezing steps help the liquid to flow towards the filter, but the growing solid fraction originating after the first squeezing steps, might impede the flow to migrate easily towards the filter. For the two grain refined samples (Fig. 35 b) and c)) the volume fraction of the liquid repeatedly decreases and increases through the cross section of

the sample, with the sample additionally subjected to US showing large oscillations. We can conclude that in all three conditions, the distribution of the liquid does not show monotonic behaviour.

It seems that having additional treatment to the semisolid alloy during the squeezing procedure does not influence much the distribution of the liquid. The liquid migration due to the squeezing, remains inhomogeneous despite the additional treatment. However, the push exerted by the piston forces the liquid towards the filter, as demonstrated by the rise of the volume fraction of liquid in the lower section of the purified sample.

As stated at the beginning of this section, the morphology and the structure of the semisolid sample influences its response to the deformation. So, the next Section is dedicated to a deeper study of the effect of the microstructure on the volume fraction as a result of deformation.

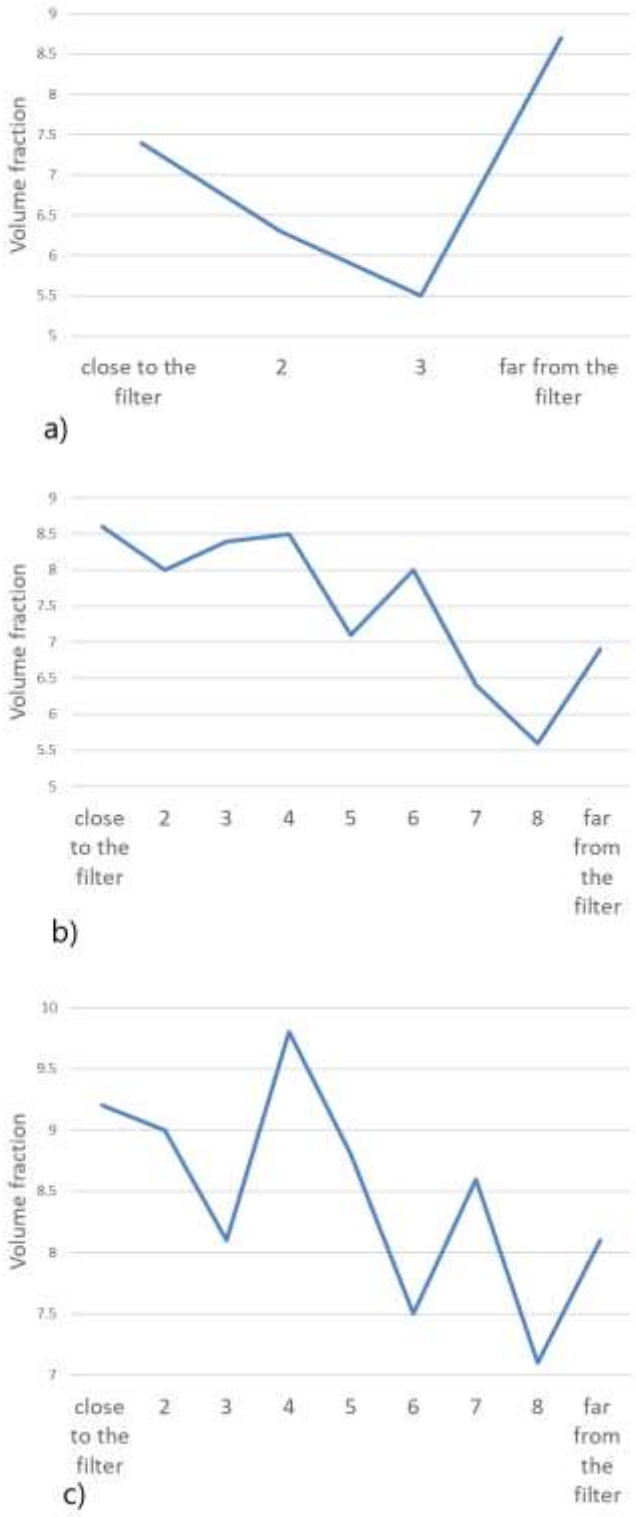

Figure 35: Volume fraction of light grey areas calculated in each section of the CT sample, from the region close to the filter to the region far from the filter for the purified fraction of an Al-5 wt% Cu alloy undergoing a squeezing procedure by steps in different conditions: a) US vibration applied during squeezing; b) grain refined prior to the squeezing; c) grain refined prior to the squeezing and US vibration applied during the squeezing.

4.4 Effect of microstructure on the liquid flow

The analysis of the effects of microstructure on the liquid flow was done using the post-mortem examination of the starting alloys and the purified fractions.

The first parameter that is going to be discussed is the grain size and morphology. Then the discussion will focus on the effects of the US vibration due to the sonocapillary effect. And finally, the effect of the squeezing procedure will also be taken into account.

Figure 36 shows six different structures of an Al-5 wt% Cu alloy. The alloy has been processed with the isothermal squeezing in a single continuous step. Before undergoing the purification process, the three alloy charges have been subjected to different starting treatment: melt superheated to 820 °C, superheated to 720 °C (standard condition), and superheated to 720 °C and grain refined with Al5Ti1B.

The grain size and morphology before the fractional solidification are quite different, and clearly depend on the melt processing as Fig. 36 a, c, e demonstrate, and Table 7 shows quantitatively. The purpose of this investigation was to analyse the effect of the three different grain sizes on the volume fraction of eutectic liquid that remained entrapped during the squeezing process.

The different solidification conditions (superheating and grain refining) are independent of the purification process. These conditions are applied to the alloy when it is still in the liquid phase, before undergoing the purification process. However, they may affect the purification process influencing liquid migration and the grains arrangements.

Before undergoing the purification process, the microstructure of the alloy is characterised by dendrites with big grain size for the sample superheated to 820 °C, and dendritic structure with smaller grains for the one superheated to 720 °C. When grain refiner is added (Fig 36 c)), the structure is finer and made of equiaxed grains. After the purification process, the features of the initial structures are completely lost. The dendritic shape has disappeared for a more globular and rounded structure due to the spheroidization process caused by the increase in the internal strain energy caused by the high isothermal temperature and the deformation [84].

In the sample superheated to 820 °C the grain size decreases after the purification process; while in the sample superheated to 720 °C and in the grain refined one, it increases at the end of the purification process (Tables 7 and 8). The decreasing of the grain size can be explained due to the fragmentation of the dendrites during the squeezing process. There can also be coarsening of the dendritic tips due to the flow of the interdendritic liquid, and the drive to decrease the surface energy of the interface [85], contributing to spheroidization. Breaking of

the dendrites and coarsening happens as well in the sample superheated to 720 °C, but here, a combined effect of coarsening and coalescence of smaller grains [84] is happening, increasing the grains sizes. Same processes occur, also, in the sample grain refined previous to the purification process, increasing the grain size. Coarsening is driven by lowering the solid liquid interfacial area (i.e. surface energy) and results in dissolution of small and sharp features and growing of the large ones. In fact, during coarsening, the dendritic structure changes to a more globular structure. Two main mechanisms of globularisation are: Ostwald ripening and coalescence of dendritic arms due to the preferential deposition of solid in the areas along the dendrite arms [85]. This deposition of solid is caused either because the tips of the dendrite arms join together entrapping the liquid, or because the growth of the root into the interdendritic liquid.

According to the literature, at a given starting solid fraction [85], 25% in this case, larger grains should have thicker liquid films around them in comparison to smaller grains, due to the lower specific surface area. If the liquid does not properly leave the semi-solid matrix, it is expected that the amount of liquid entrapped will be greater in a structure with larger dendritic grains, like the one when the sample is superheated to 820 °C. Consequently, a rounder structure, like the one with a circularity equal to 0.86 (Table 8), would ease the flow of the interdendritic liquid with lesser amount trapped between dendrites, increasing the efficiency of the squeezing process. Also, according to a series of studies available in literature [27], [86], [87] they suggest that the Ostwald ripening may lead to a loss of entrapped interdendritic liquid because the small particles dissolve and the entrapped interdendritic liquid would merge with the bulk liquid fraction that surround the solid grain; instead coalescence of complex shaped particles, results in liquid entrapment. This makes the evolution of entrapped liquid rather complex especially at short holding time [27], like happens in a squeezing procedure done in one step. From the data shown in Table 8, the amount of remaining liquid in the purified sample that was previously grain refined is the lowest one, confirming that the volume of ejected liquid is the highest in comparison to the other two samples. Contrarily, a coarser dendritic structure, like the one superheated to 820 °C has the largest volume fraction of the liquid entrapped, because, despite the mechanism of coarsening during the squeezing process, the liquid migration is facilitated less than in the situation in which the alloys is grain refined, acquiring a more rounded structure even before the squeezing procedure.

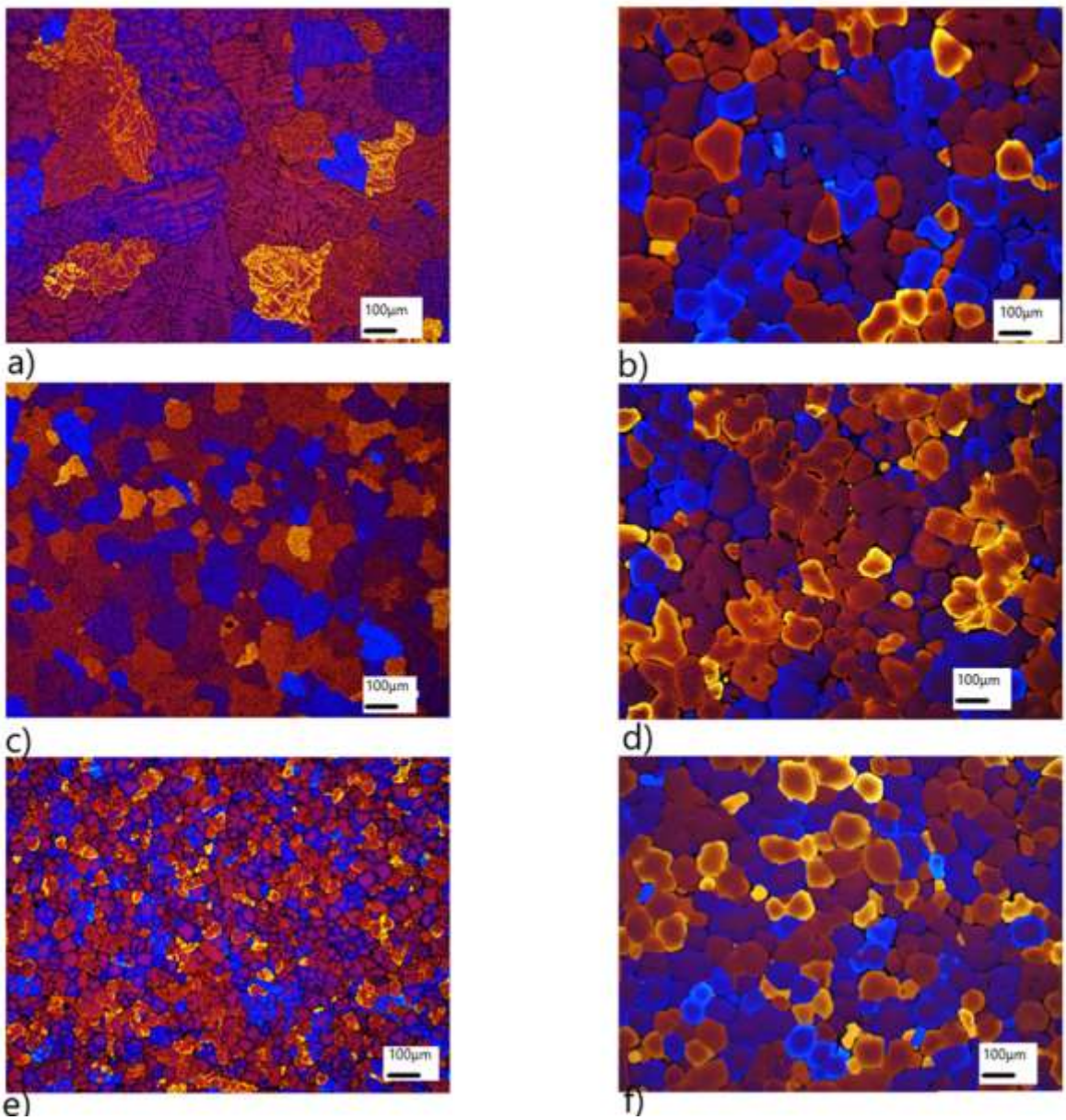

Figure 36: Microstructure of an Al-5 wt% Cu alloy with regard to the different starting conditions prior the purification process (a, c, e) (samples taken at 700 °C) and after the fractional solidification purification process (b, d, f): a), b) melt superheated to 820°C , c), d): melt superheated to 720 °C, e) f): same as (c, d) and grain refined.

Table 7: Grain size for three samples of an Al-5 wt% Cu alloy cast at 700°C

	Superheated 820 °C	**Superheated 720 °C**	**Grain refined**
Grain size, μm	586 ± 39	180 ± 15	130 ± 10

Table 8: Grain size, volume fraction of eutectics, and circularity of grains for the purified samples of an Al-5 wt% Cu alloy with three different starting conditions prior to the squeezing process (see Table 6).

	Superheated 820 °C	**Superheated 720 °C**	**Grain refined**
Grain size, μm	312±12	299±10	218±7
Volume fraction of eutectics, %	3.4±0.3	3.0±0.2	2.8±0.2
Circularity	0.786	0.77	0.83

In a globular structure where the shape of the grain is very close to a sphere (circularity very close to 1), the domain can be described by a parallelepiped containing spherical balls [88] and it can be represented as figure 37 shows: the spherical balls are the grains and the areas between the grains is the liquid fraction.

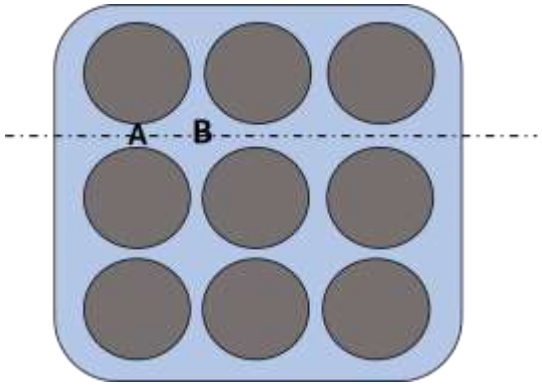

Figure 37: Generalised scheme of a sphere packing inside a domain. **A** represents the area between grains belonging to two different rows and **B** represents the area between two different layers of spheres.

Let us now measure the thickness of the liquid channels that remain entrapped in the matrix. The thickness has been calculated as the intensity of dark grey areas in the optical microscope images of the purified fractions of three Al-5 wt% Cu alloys that underwent different treatments before the purification process. A higher intensity value means a larger grey area, hence, more liquid volume. In Figure 38, the intensity of the grey areas is given versus the length of the vertical cross section of the sample (see Section 3.5 for more details about sample characterisation). If the grains exhibit a shape factor close to one, by approximation we can consider these grains like round spheres, and one possible arrangement of sphere is the one shown in Figure 37. If we assume that these spheres (or the rounded grains in a semisolid matrix) are packed like showed in Fig. 37, then, measuring the intensity of the grey areas along the dotted line in Fig 37, should results in an alternation of high peaks and low peak. The high intensity peaks (Fig.38) represent area B of Fig. 37, low peaks (Fig.38) represent area A of Fig. 37. Higher grey values mean more liquid volume, as it would be expected in area B. Having a look at the three graphs is Fig. 38, the graphs in which there is a regular alternation of higher peaks and lower peaks, are for the sample superheated to 720 °C and for the one grain refined.

In the sample superheated to 820 °C, seems that the thickness of the channels is more homogenous, without an alternation of A and B areas. Comparing this result with the amount of liquid volume entrapped at the grain boundaries (Table 8) that is the highest. In fact according to literature [77] [89] in semisolid materials that had an initial coarse and dendritic structure, even after processing, the solid particles are very irregular and still maintain an interconnected structure, leading to the hypothesis that the sample superheated to 820 °C may not have a grain packing as the one showed in Fig 37.

It seems that even if the features of the microstructure present in the alloys prior the purification process are not maintained after the fractional solidification, due to several mechanism playing a role, the initial structure still influences the amount of liquid volume that remains entrapped inside the mush effectively influencing the purification efficiency, as will be discussed in Chapter 6.

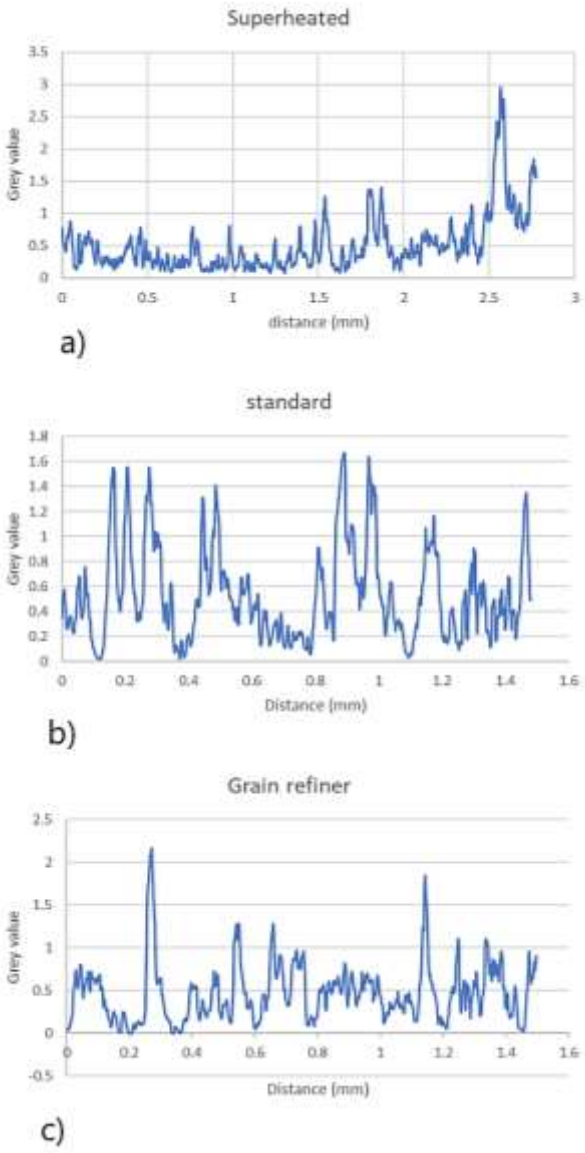

Figure 38: Distribution of the thickness of the liquid channels versus the cross section of the sample in the purified fraction of samples that were previously a) superheated to 820 °C b) standard condition c) grain refined. Note the different Y-axis scale.

As mentioned in Section 2.5, it is well known that ultrasonic vibrations ease the filtration process [69]. In a semisolid alloy, the solid skeleton can be considered as a filter and identified as a porous media, with the liquid fraction distributed inside in channels. Therefore, the application of vibrations upon the semi-solid material is expected to help the liquid to move in the mush. In the experimental set-up used in this work, the application of ultrasonic vibrations, through the sonotrode/piston on the mush, should help the liquid to open its path through the mush and reach the filter to be squeezed out. Moreover, the ultrasonic vibrations may assist in grain refining by fragmentation and accelerated diffusion [90], [91], so the application of

ultrasound may also influence the structure to facilitate the liquid migration. It is expected that the effect of the ultrasonic vibrations would be similar to the grain refinement.

The analysis of the grain sizes and morphology of the purified fraction (Figure 39) does not show any significant differences in the final structures irrespective of the starting condition and application of ultrasonic vibrations. Probably the isothermal holding in the semi-solid state and the deformation by squeezing (coarsening and globularisation of dendritic grains [85], [89]) overcomes all other factors in terms of changing the grain size and morphology.

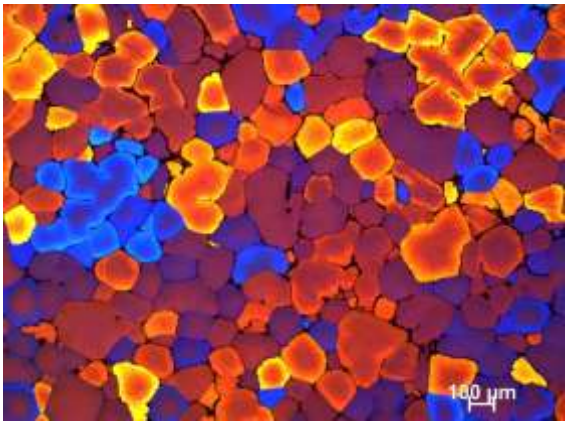

a) Grain size 267±11

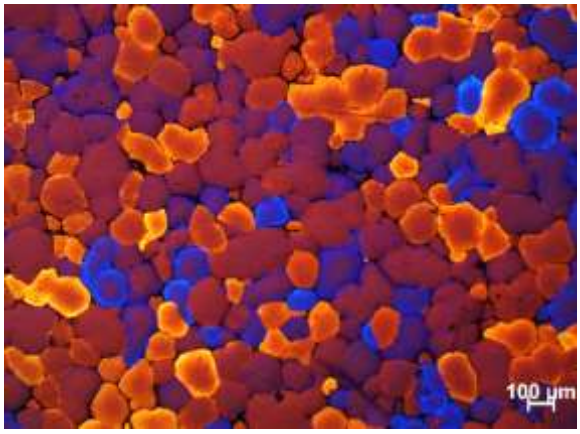

b) Grain size 252±12

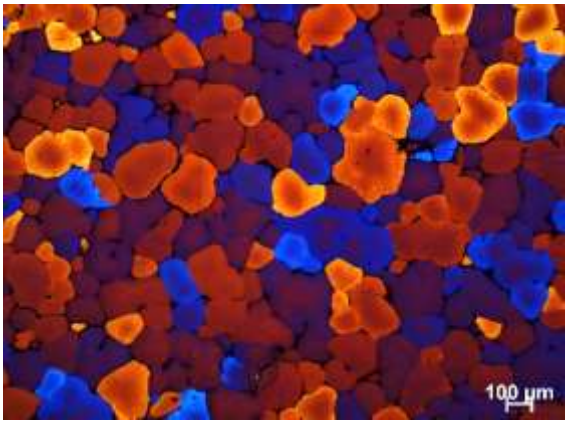

c) Grain size 270 ±13

Figure 39: Microstructure of the purified fraction of an Al-5 wt% C alloy: a) squeezing without ultrasound; b) ultrasonic vibration applied during squeezing no grain refiner; c) grain refined before the squeezing and no ultrasound.

On the other hand, Figure 40 shows that the distribution of porosity depends on the initial structure and conditions of squeezing. The porosity represents the areas that were previously occupied by liquid and that could not be refilled by the incoming liquid. In the procedure without grain refinement and ultrasonic processing, the large voids are distributed across the large sections of the sample, demonstrating poor feeding of the liquid throughout the sample,

expected for the sections close to the filter. When the structure was grain refined, i.e. made by round particles, the liquid moves uniformly through the mush, as demonstrated by the fact that the porosity is distributed evenly along the height of the sample (Fig. 40c). In the case when US was applied to the alloy that had not been grain refined (Fig. 40 b) the porosity is formed mostly in isolated upper areas, confirming the liquid had flown down towards the filter with relatively good feeding across the sample, except for the upper part where the liquid cannot be fed in. Note that a squeezing procedure was in these cases done in one quick step, which may not give enough time for the liquid to flow through the narrow channels.

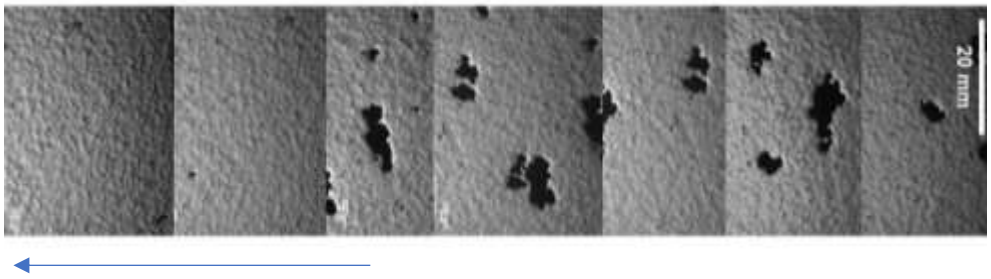

a)

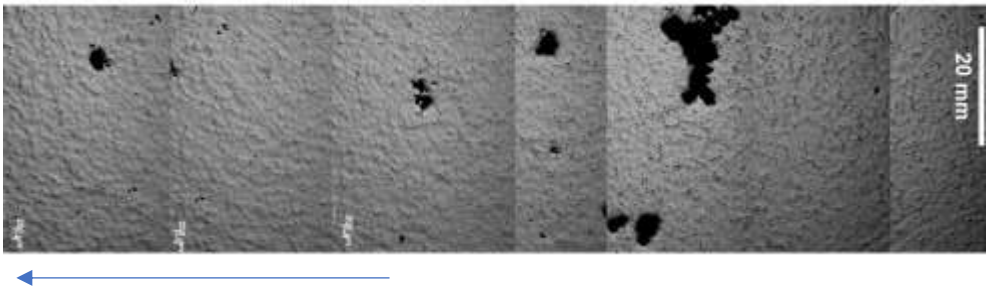

b)

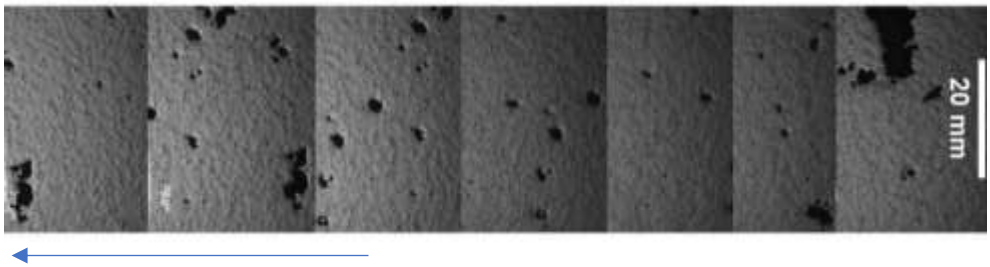

c)

Figure 40: Microstructure of the entire height of in the central section of the purified fraction of an Al- 5 wt% Cu alloy: a) squeezing without ultrasound; b) ultrasonic vibrations applied during squeezing no grain refiner; c) grain refined before the squeezing no ultrasound. The arrow

represents the direction of the filtration, so the region next to the tip of the arrow is the region close to the filter

In order to further investigate and relate the effect of ultrasound to the migration of the liquid through the mush (due to the sonocapillarity effect [92] (Section 2.5)), the squeezing procedure was changed and, instead of having one continuous step, the squeezing was performed in six steps, done every two minutes, to give time to the liquid to move through the mush.

The amount of liquid that remains entrapped at grain boundaries at the end of the purification process, is considerably higher when the squeezing process happens by one step only, as Figure 41 shows. The dark grey regions, representing the liquid fraction enriched in Cu, are very small and almost difficult to detect when they sample undergoes a multi-step squeezing procedure (Fig. 41b)).

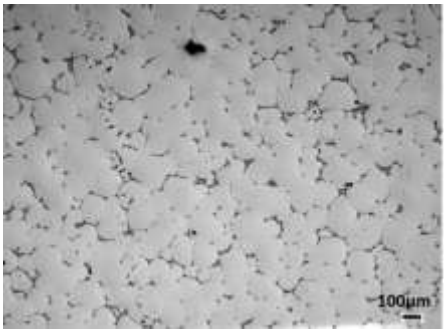

a) 4.2 vol.% liquid fraction

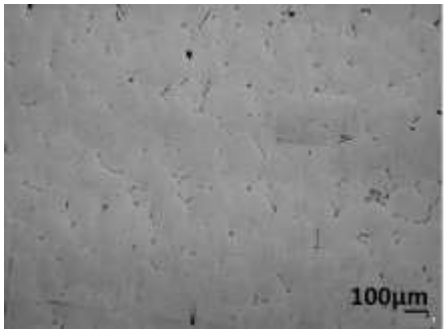

b) 1.1 vol.% liquid fraction

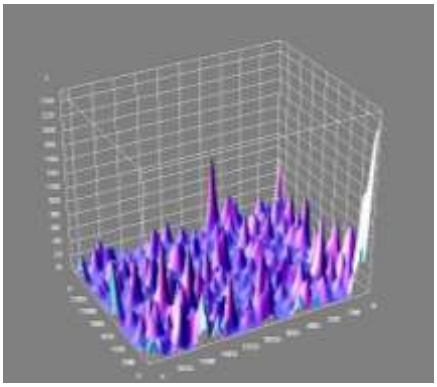

c)

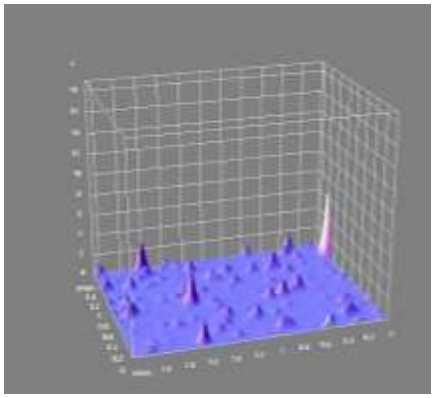

d)

Figure 41: a) Microstructure of a central area in the vertical cross section of the purified fraction of an Al-5 wt% Cu alloy after being squeezed in one step only with the application of ultrasound ; b) microstructure of purified Al-5 wt% Cu after being squeezed in 6 steps over 12 min with

the application of ultrasound; 3D surface plots showing the intensity of dark grey regions representing the liquid fraction for the purification process in which squeezing happened: (c) in one step only and (d) in 6 steps.

This is also confirmed by the 3D plots in Fig. 41 c) and d), where it is clearly seen that the intensity of peaks is almost negligible after multi-step procedure in comparison to the peaks in the surface plot of one step squeezing procedure. From the values of volume fraction of liquid that remains entrapped in the structure, it seems that performing a squeezing by steps considerably helps the migration of the liquid through the mush. We can expect that ultrasonic vibration may give additional effect in evacuating the liquid from the mush. In order to further understand what happens to the semisolid material during “stepped” deformation (or squeezing), four different samples were studied after being subjected for stepped squeezing for different periods of time, up to 14 min. The results of grain structure are shown in Figure 42 for an Al-5 wt% Cu alloy processed in the experimental set-up for 2, 6, 10 and 14 min of deformation. In this case ultrasonic vibrations were applied to the mush. Table 9 gives some quantitative information.

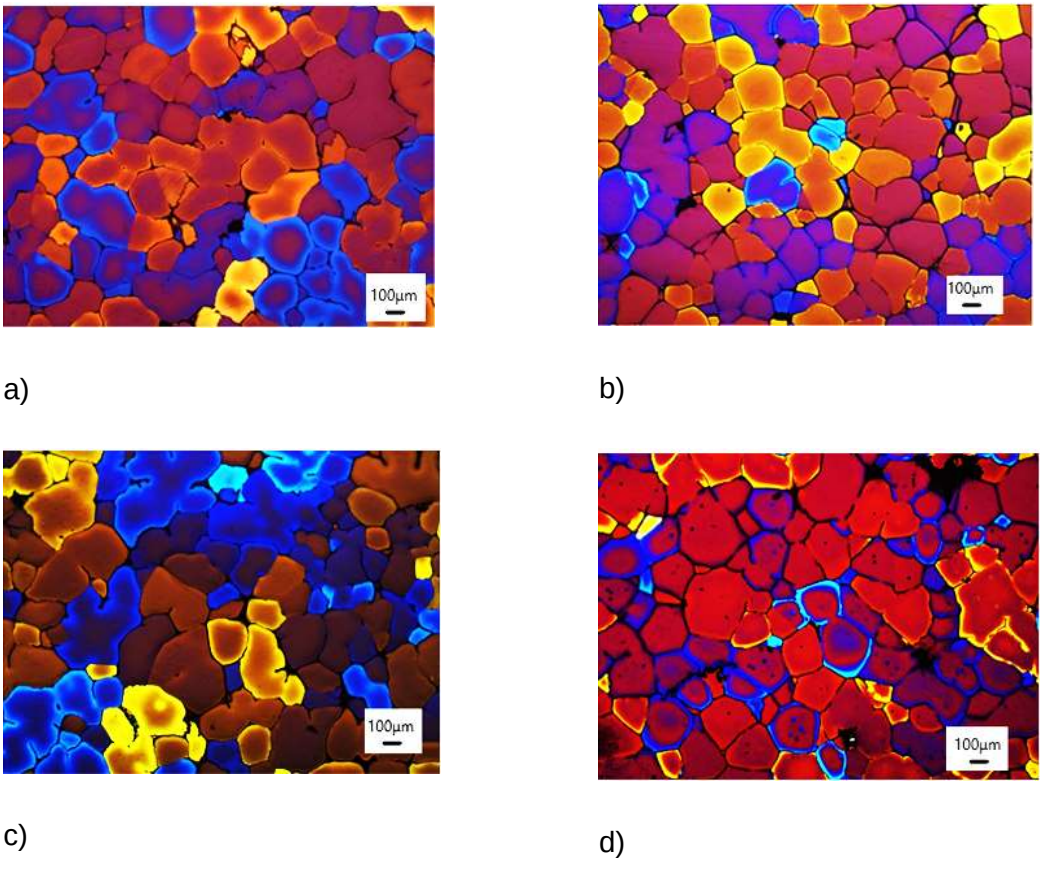

a) b)

c) d)

Figure 42: Microstructures of a central area of the cross section in the purified fractions of an Al-5 wt% Cu alloy processed by isothermal squeezing with the application of ultrasonic vibrations for a) 2 min, b) 6 min, c) 10 min, and d) 14 min.

Table 9: The average grain size and volume fraction of remained liquid for samples undergoing different squeezing time.

	2 minutes	**6 minutes**	**10 minutes**	**14 minutes**
Volume fraction liquid, %	2.0±0.3	4.7±0.4	4.7±0.2	2.38±0.3
Grain size, μm	321±12	297±7	326±9	342±8

Chen and Tsao [82], studied the semisolid deformation of an A356 alloy and they proposed four deformation mechanisms:

1. Liquid flow mechanism (LF)
2. Flow of liquid incorporating solid particles (LFS)
3. Sliding between solid particles mechanism (SS)
4. Plastic deformation of solid particles (PDS)

The first two mechanism are prevalent for high volume of liquid fraction when solid particles are surrounded by liquid phase, the other two mechanisms are dominant when the solid particles have contacted each other. Figure 43 shows schemes of the grain rearrangement in the four different scenarios before and after the deformation [82]. At the beginning of the deformation process, mechanism 1 and 2 are more likely to happen because of the higher liquid fraction. With the progressing of deformation, the solid particles start to have contact with each other and, mechanism 3 takes over initially, followed by mechanism 4 for increasing solid fraction.

Let us now come back to our samples to discuss how the results of Chen and Tsao can be applied to our work. The values reported in Table 10 are averaged for the entire cross section of the purified sample analysed. The optical microscope images obtained from the purified samples, do not show any differences if taken in a different region in the cross section. It was chosen then, to show images (Fig.44) taken from a central area in the vertical cross section of the samples.

Going back to the discussion, when the squeezing process happens for two minutes, the volume fraction that remains entrapped at the grain boundaries is only 2% (Table 9). In fact, at the beginning of the experiment, the alloy has a very large volume fraction of liquid, being only 25% solid. So initially, a great amount of liquid volume passes through the filter just by the separating of the liquid from the semisolid alloy while pouring the slurry into the channel (in

two minutes of experiment no squeezing is performed, the first squeezing step happens after 2 minutes). According to Chan and Tsao results, at this point of the experiment we should be in a situation of liquid flow mechanism.

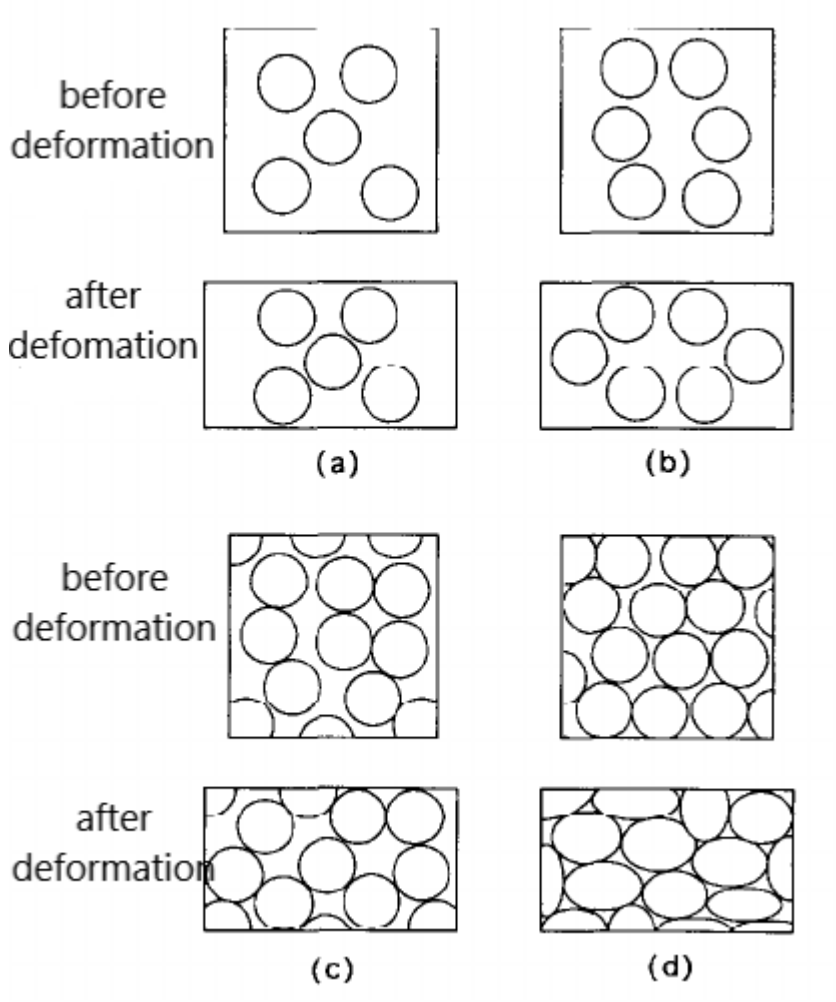

Figure 43. Four main deformation mechanisms a) liquid flow b) flow of liquid incorporating solid particles c) sliding of solid particles d) plastic deformation of solid particles, adopted from [82].

When the semisolid alloy is processed for 6 minutes, a higher volume fraction of liquid remains entrapped. In fact, in 6 minutes of processing there are two squeezing steps in which liquid fraction is ejected out of the mush, changing the average composition. The mechanism now dominating should be the second one (flow of liquid incorporating solid particles). Also, the solid fraction in the channel, is growing because the liquid is being ejected through the filter. This solid exerts resistance to the squeezing making the evacuation of the liquid more difficult. In fact, after 10 minutes of squeezing, the volume fraction is still 4.7%, because the solid fraction is growing, and the material is resisting the squeezing, and the mechanism dominating now is the sliding between solid particles. After 14 minutes, the mechanism taking over is the plastic deformation of solid particles. It is interesting to notice that after 14 minutes the volume

fraction of liquid entrapped is decreased in comparison to the two previous situations. In this configuration the solid particles are in contact with each other creating narrow channels of liquid between them, it is possible that is creating the condition for the sonocapillary effect to happens. The sonocapillary effect [92], [93] is the excessive pressure created close to a capillary entrance by the collapsing of cavitation bubbles. This results in a rapid rise of the liquid inside the capillary channel. Also, the ultrasonic vibrations cause an increase of temperature in the melt and semi-solid material [94], [95] and this could lead to some remelting at the level of the secondary dendrites arm spacing, contributing to broadening the channels, release of the liquid entrapped inside the dendrite envelope and easing the flow of the liquid towards the filter.

Note also that the grain size does not increase linearly with the deformation time. It needs to be considered that different mechanisms are in fact taking place during semisolid deformation, isothermal holding and ultrasonic treatment: Ostwald ripening dominating at low solid fraction [27], [96], [97], dendrites remelting, coarsening of the microstructure [96], and coalescence of smaller grains at high solid fraction [96], [97] It is then difficult to relate the grain size to the time of the fractional solidification experiments. Also, during the deformation the solid grains are pushed, forced to rearrange to accommodate the strain, and packed together due to a densification of the mush [78].

So, ultrasonic vibrations may help, under certain conditions, in easing the liquid flow through the mush, as well the squeezing by steps and the grain refinement. What is necessary to look at now, is the combined effect of US vibration on a grain refined sample in a squeezing procedure by steps.

Figure 44 and Table 10 present the results for an Al-3 wt% Si alloy purified with a squeezing procedure by steps in three different conditions: without ultrasound or grain refinement, with ultrasound but no grain refinement, and finally with ultrasound and grain refinement. The three samples show very different results. When the alloy was purified without the application of US vibration and with no grain refinement, the grains are quite big, and the shape factor is the lowest because there is no refinement to the structure.

Even though it was discussed that the deformation may cause the breaking of the dendritic structure, the coarsening upon isothermal holding seems to be a much more powerful factor. It would be expected that the shape factor closest to 1 was achieved in the sample that was grain refined before undergoing the squeezing procedure. From the values in Table 10, it is, however, clear that the sample treated with US vibrations has the highest value of shape factor, confirming a structure made of rounded grains in which the liquid can flow easier inside the mush. This also correlates to the value of the volume fraction liquid, that is very small in the

sample treated with US only. But, the application of US to a sample that has been grain refined seems not to be as efficient as in the case of not grain refined sample. The eutectic regions represent the liquid fraction that remains entrapped at the grain boundaries. In the case of the sample with US but without grain refinement, the thickness of these eutectic patches is the smallest (6 µm), testifying for the good evacuation of the liquid from the mush that is able to re-arrange small round grains and move then closer together. While in the other two cases, the thickness of eutectic channels is about 3-times larger (Table 10). This is a result of significant amount of liquid being trapped between grains preventing the grains from coming together.

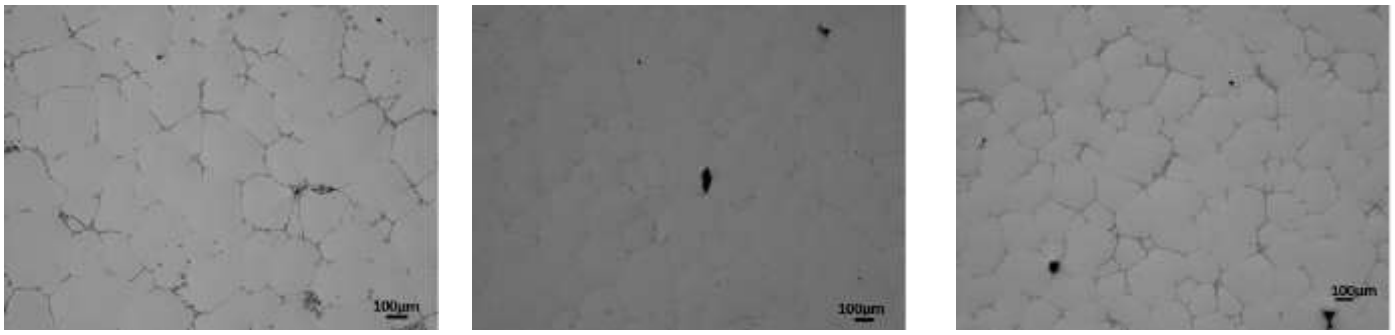

a) b) c)

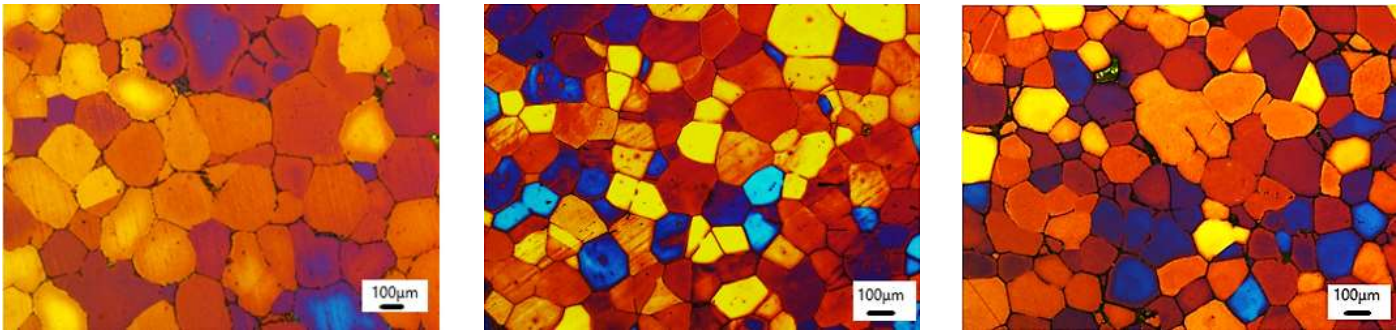

d) e) g)

Figure 44: Microstructure of a central area of the cross sections of purified fractions of an Al-3 wt% Si squeezed by steps: a, d) no US no GR; b, e) with US no GR; c, g) US+GR.

As we have discussed before, different mechanisms on a phenomenological level, take place during the time of our experiments. As discussed in Section 4.2, the initial structure of the alloy is lost at the end of the process, and this is due to the deformation, grain coarsening, ultrasonic vibrations, and isothermal holding.

So, in order to proceed further with the investigation, we will have a look now on the evolution of the structure in three scenarios (taking an Al-5 wt% Cu alloy as an example):

1. The sample is quenched from the liquid state at 700 °C
2. The sample is quenched from the semisolid state when it is 25% solid.
3. The sample is the purified fraction obtained at the end of the experiment.

Table 10: Grain size, liquid volume fraction, shape factor for the purified fraction of Al- 3 wt% Si squeezed by steps in different conditions.

	Squeezing by step No US no GR	**Squeezing by steps US no GR**	**Squeezing by steps GR+US**
Average grain size, µm	460±20	361±9	397±13
Average volume fraction, %	2.2	1.2	3.2
Shape factor	0.78	0.85	0.8
Liquid channels width, µm	19±1	6±1	17±2

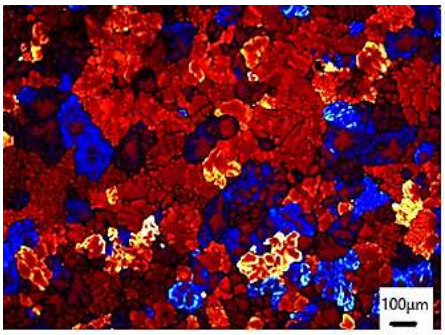

a) 191±4 µm

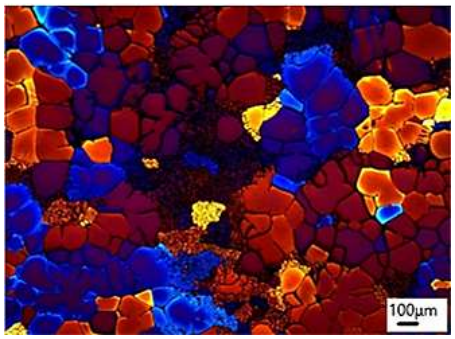

b) 310±7 µm

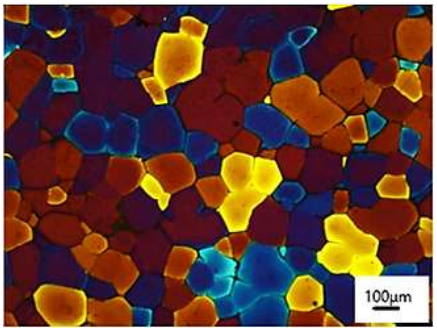

c) 339±8 µm

Figure 45: Microstructure of a central area in the anodized samples of an Al-5 wt% Cu alloy: a) cast from the liquid state at 700 °C; b) quenched from the semisolid state at 25% solid fraction; c) purified fraction obtained at the end of the multistep squeezing procedure with the application of US.

From Figure 45 is immediately clear that the structure is very much different in all the three conditions. The initial structure is rather dendritic with an average grain size less than 200 μm. When the sample is quenched from the semisolid state, the grain size is increasing to an average value of 310 μm and the dendritic shape is gradually disappearing, more rounded grains are visible. According to Atkinson and Liu [96], initially the coarsening happens only predominantly as coalescence of dendrites arms, especially when a large liquid fraction is presents like in Fig 45 b). Therefore, coarsening already happens before the alloy is subjected to isothermal squeezing. The rounded shape is even more visible in Figure 45c, where the dendritic shape is completely lost during squeezing. The biggest value of grain size in 45 c) can be explained as due to the coarsening effect caused by the ultrasonic treatment [98], and coalescence of smaller grains upon isothermal holding [82], [96]. This coarsening effect is also visible when the sample has been grain refined. Figure 46 shows three structures of a grain refined Al-5 wt% Cu alloy taken in the different conditions: cast at 700 °C, quenched at 25% solid fraction, and finally after the purification process.

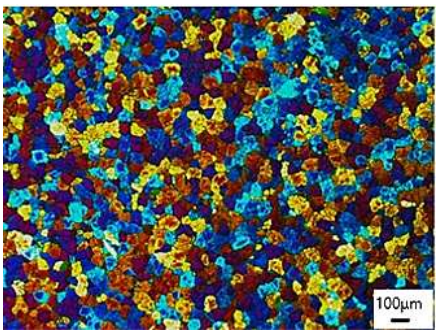

a) 118±2 μm

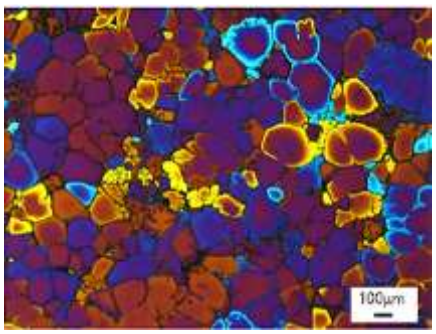

b) 300±9 μm

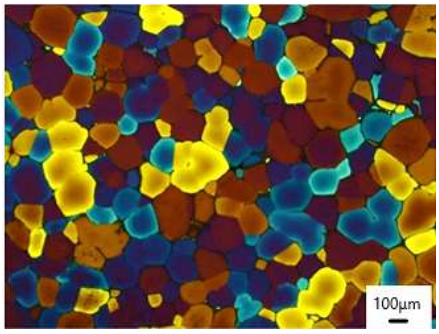

c) 304 ±8 μm

Figure 46: Microstructure of the anodized samples of a grain refined Al- 5 wt% Cu alloy: a) cast from the liquid state at 700 °C; b) quenched from the semisolid state at 25% solid fraction; c) purified fraction obtained at the end of the multistep squeezing procedure.

Initially (Figure 46a) the alloy has an average grain size of 118 μm with a fine dendritic structure. When the sample is quenched at the semisolid state, the grain size increases considerably to 300 μm with significant portion of the grains getting round. At the end of the squeezing process, the grains are completely nondendritic with the average grain size similar to that quenched at the semisolid alloy. It has been mentioned previously that a fine structure made of smaller, round grains facilitates the liquid flow through the mush. If this structure is lost during the multi-step squeezing process, then the grain refinement does not serve the purpose. What makes the difference in terms of facilitating the migration of the liquid, is the ultrasonic vibrations which push the liquid through the mush despite the coarsening effect and the resistance of the increasing solid volume as consequence of the squeezing.

4.5 Permeability assessment in different alloying systems

In the previous sections the effects of the initial microstructure and the processing conditions (number of steps and application of US during squeezing) on the deformation of the mush and the liquid flow through the mush were discussed. The effect of US vibrations seems to be beneficial in a multi-step squeezing mode because they help the migration of the liquid towards the filter. An important parameter to take into consideration in the evaluation of the behaviour of the liquid flow inside a semi-solid matrix, is the permeability.

The concept of permeability has been widely investigated through the years in material science. Piwonka and Flemings [99] for example, measured the permeability of a solidifying Al-4.5 wt% Cu alloy inside a U-shaped tube forcing molten lead or a gaseous nitrogen inside the tube. Later on, Poirier and Ganesan [100] measured the permeability of Al-Cu alloy using a permeameter. They considered the mush zone as made by a solid network in which the interdendritic liquid moves in. They found out that the permeability of a globular structure is an order of magnitude greater than the permeability of a dendritic-globular structure. Nielsen *at al*. [101] used experimental data and the Kozeny-Carman equation to calculate the permeability of an Al-Cu alloy with a globular structure. Their results, however, are a bit scattered due to the coarsening of the microstructure during the experiments which made it difficult to evaluate the surface area of solid. Oryshchyn and Dogan [102] developed a model to describe the development of the dendritic structure and the liquid flow in a mushy zone of a

dendritically freezing alloy. They found out that the tortuosity of a dendritic mushy zone depends on both liquid volume fraction and dendrite arm spacing.

However, despite the numerous amount of works found in literature, according to D. Bernard *et al*. [103] there is a lack of reliable data for metallic alloys because such measurements are difficult to perform due to the evolution of the solid/liquid interface morphology with time. The Kozeny-Carman equation, on the other hand, has been demonstrated to be applicable to most of metallic systems with adequate results on permeability values.

In this work, permeability was calculated according to the Kozeny–Carman equation [103]

$$K = \frac{1}{5S_v} \frac{(1-g_s)^3}{g_s^2} \tag{21}$$

Here S_v is the specific grain surface and g_s is the solid fraction. Both S_v and g_s have been calculated from the grey-scale versions of the micrographs. S_v was calculated as the number of intercepts for line length, g_s as the fraction of light grey regions in the micrographs. All the parameters in the Eq. (21) are obtained from image analysis and the calculation where performed on 5 images for each sample considered. The choice of 5 images was done in order to follow the procedure done by Nielsen *at al*. [101].

The results are given in Table 11 for two states, before and after the squeezing; and for several processing conditions.

The permeability of samples quenched at the semisolid state before the purification processing is quite high because the volume fraction of quenched liquid is higher than 50%. The liquid fraction in the quenched samples is calculated considering the eutectic liquid visible at the grain boundaries and the small dendritic structure formed as results of the quenching (Fig 47).

The Figure 48a shows that the highest value of permeability is for the Al-5 wt% Cu alloy even though the highest values of liquid fraction is in Al-3 wt% Si. According to Nicom and Nocura [51] the variation of morphology of the semisolid slurry has huge influence on the permeability even for samples with the same solid fraction. This could explain the differences shown in Fig. 48a. The two mush structures have different values of surface area (Table 11) which consequently influences the permeability.

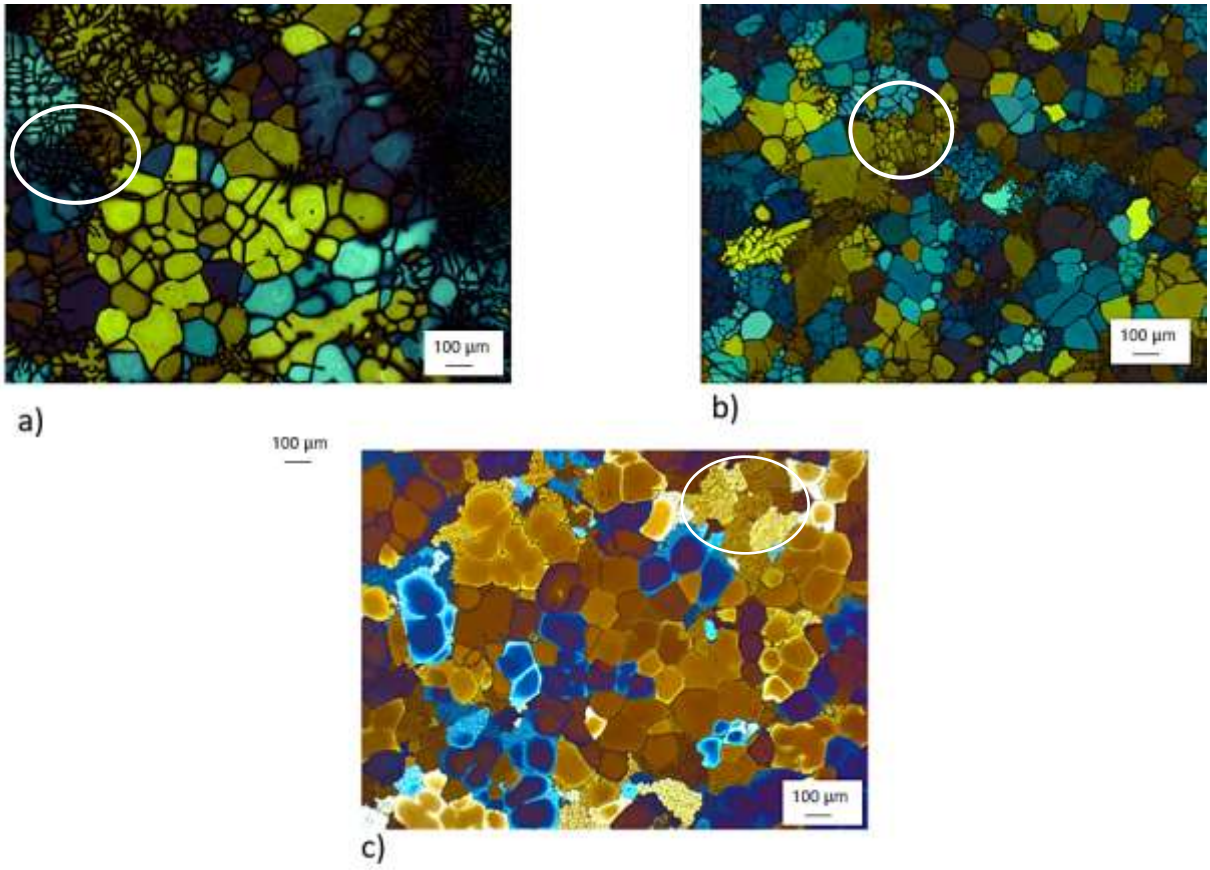

Figure 47: Semisolid microstructures of the Al-3 wt% Si, Al-3 wt% Ni and Al-5 wt% Cu alloys quenched at 30% solid fraction prior to the experiment. Fine dendritic structures as well as dark veins between grains represent liquid fraction prior to quenching.

The differences in the liquid volume fraction between the nominal (70%) and the measured one, can be explained considering that the quenching was done using a refractory rod to collect the semisolid alloy and then quenching into water. The quenching is not done with fast solidification rate, so the structure is not frozen exactly at the temperature corresponding at 70% liquid fraction. There is always overestimation of the solid fraction in quenching experiments as has been shown elsewhere [62].

Table 11: Values of permeability and grain size calculated from the microstructure of the purified fraction and from samples quenched at 30% solid phase

	Permeability (m^{-1})	**Specific surface (m^{-1})**	**Liquid fraction**
Al-5 wt% Cu quenched	K= 3.1 e–10	5.58 e-4	58%
Al- 3 wt% Ni quenched	K=2.67 e–10	2.14 e-4	54%
Al- 3 wt% Si quenched	K= 2.21e–10	1.82 e-4	65%
Al-5 wt% Cu US	K= 2.92 e–12	3.60 e-4	5%
Al-5 wt% Cu no US	K=5.8e–12	4.74e-4	5%
Al-3 wt% Ni US	K=2.20 e–12	2.92e-4	4.7%
Al-3 wt% Ni no US	K=3.3e–12	3.16e-4	5%
Al- 3 wt% Si US	K=1.95 e–13	4.54e-4	1.7%
Al-3 wt% Si no US	K= 1.1 e–12	5.84 e-4	2.5%

After the purification process (Figure 48b) the trend is a bit different. First of all, the retained permeability is consistently lower for the alloys treated with ultrasonic vibrations, most notably in Al-Si and Al-Cu alloys. The retained permeability reflects the final structure, hence, the lower the permeability, the denser the structure and the less liquid retained in the mush. Moreover, in the discussion about the deformation in the semisolid alloy, it was also mentioned, that the deformation (or the squeezing in this case) can cause a densification of the mush, especially in the areas close to the point of application of the force. The densification of the mush decreases the permeability [74]. In addition to decreasing the capillary pressure, and enabling the liquid penetration through narrower channels [104], US vibrations can also facilitate re-arranging of solid grains and further ease the liquid flow, causing eventually closing of the empty gaps between the grains.

It needs to be noted that the calculation of the permeability is based on the purified samples obtained at the end of a procedure by steps in which the structure undergoes different mechanism: coarsening, globularisation, dendrite breaking, dendrites remelting, coalescence, and all these phenomena contributes to the final structure. It could happen that the values of

permeability do not decrease linearly with the decreasing of the liquid fraction because as mentioned in the literature [51] the difference in the morphology play a role as well.

To summarise, the permeability decreases in all the sample in which US vibrations are applied in comparison to the same samples treated without US. The differences among samples processed with the same processing conditions, could be explained from the different morphology that is the result of twelve minutes processing in which isothermal holding, change of composition, and deformation of the semisolid structure happen.

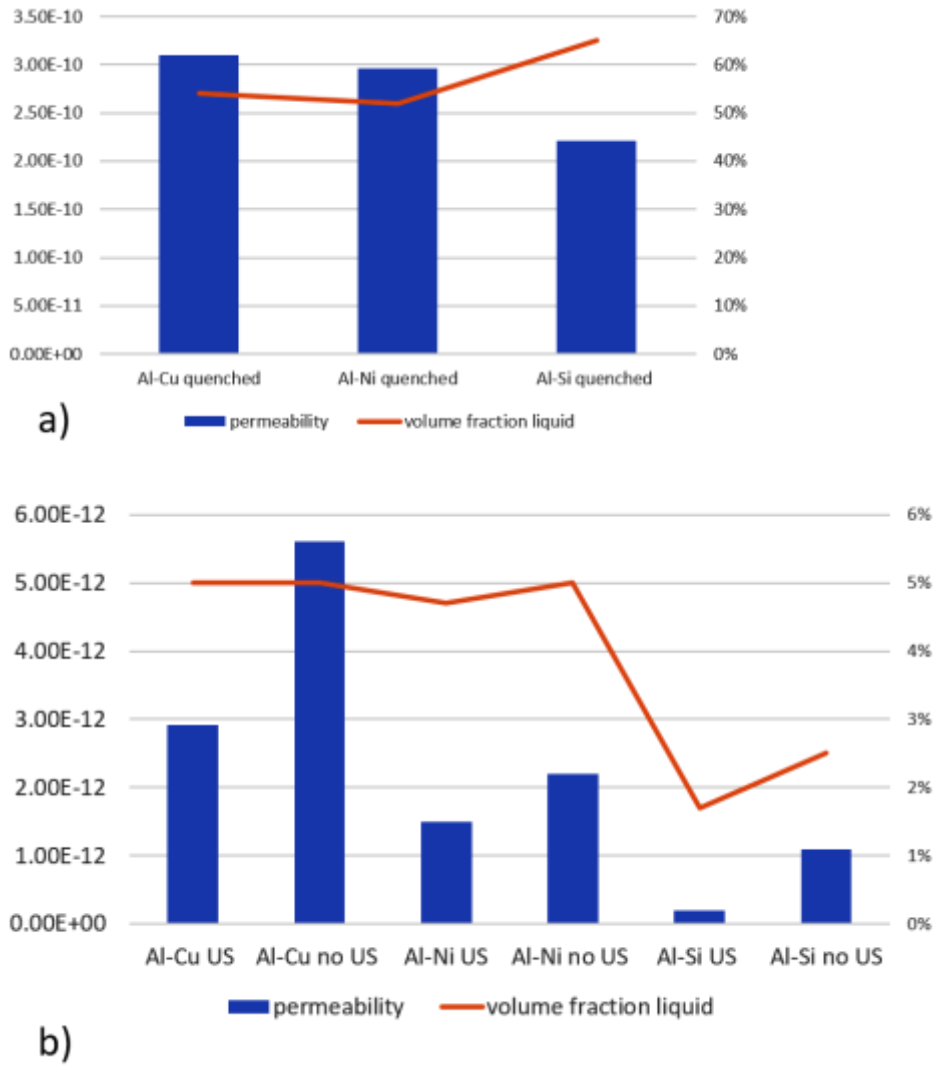

Figure 48: Permeability and volume fraction of liquid for Al- 3 wt% Si, Al-3 wt% Ni and Al-5 wt% Cu calculated from the micrographs obtained a) the quenching the mush at 30% solid and b) from the purified samples squeezed by steps with or without application of US.

4.6 Summary

During semisolid deformation different mechanisms take place: coarsening, coalescence, dendrites fragmentation; and these processes influence the final structure of the sample after the purification (which is also semi-solid deformation) process. The initial structure of the alloy prior to the deformation is lost at the end of the process, however the initial structure influences the amount of liquid fraction that remains entrapped at the end of the process. Having a structure made of smaller and rounded grains helps in the evacuation of the liquid from the mush especially in a squeezing procedure executed in one continuous step. In a squeezing procedure made by steps, ultrasonic vibrations facilitate the flow of the liquid inside the mush.

Also, permeability assessed at the end of the process is lower in samples treated with US, confirming that less liquid fraction remains entrapped at the grain boundaries.

The migration of the liquid inside a semisolid material is not homogenous and it follows a random path.

CHAPTER 5

Solutes redistribution during isothermal holding

When cooling down an alloy from its melting temperature, small grains of solid phase starts to nucleate and, with the progressing of solidification, these grains impinge into each other to form a continuous skeleton of solid phase. In the case of hypoeutectic alloys, the growing solid phase rejects solutes at the interface enriching the liquid fraction, and on this thermodynamic principle the fractional solidification is based on. This redistribution of solutes at the interface generates microsegregation. Microsegregation, in fact, is the inhomogeneous chemical distribution and concentration of alloying elements at the scale of cells or dendrites spacing and is the result of interaction of solute rejection with solutes diffusion in the liquid and solid phase [17], [105]. Microsegregation is an essential aspect to investigate in most of solidification processes because, in real conditions, there is not enough time for full equilibration of redistribution of solutes between the liquid and solid phases.

Experimental and analytical methods have been proposed to describe and evaluate the extent of microsegregation. The Scheil-Gulliver approximation considers solutes diffusion in the solid to be negligible, and the solid fraction is expressed according to Equation 9 in Section 2.2. The Scheil-Gulliver approach takes into account the reality in which the diffusion coefficient in the solid phase is several orders of magnitude smaller than that in the liquid, so solid diffusion happens much slower than the liquid one and can be neglected. However, the effect of solid diffusion needs to be considered and investigated, especially, but not only, when longer processing times are involved. The equilibration of the solid composition by the diffusion from the liquid to solid during solidification or isothermal holding is called back diffusion.

One of the first estimations of the amount of chemical segregation in the solid, taking into account back diffusion during solidification, was done by Brody and Flemings [17], [22] as follows

$$\frac{C_s}{C_0} = k_0[1 - f_s(1 - 2k_0F_{0s})]^{\frac{(1-k_0)}{1-2k_0F_{0s}}} \quad (22)$$

Where C_s is the concentration of solutes in the solid phase, C_0 is the initial concentration of the alloy, k_0 is the partition coefficient and F_{0s} is the dimensionless Fourier number for the solid fraction (Equation 10 in Section 2.2). The Fourier number depends on the ratio of the local solidification time to the time available for solute diffusion. So, the Brody–Flemings model,

depends on the partition coefficient, the development of solidification f_s and the time necessary to accomplish the solidification F_{0s}.

The drawback of the Brody-Flemings model is that it overestimates the solid-state diffusion, especially for slow solidification time when the Fourier number is closer to unity. But, when the Fourier number is much smaller than the nondimensional element $1/2k_0$, where k_0 is the partition coefficient, then the Brody-Flemings model reduces to the Scheil–Gulliver approach [17], [22].

More recent numerical treatments of the solute redistribution account for the right contribution of solid-state diffusion, and also consider the effect of coarsening [106]–[109]

In the previous chapter we evaluated the effect of ultrasonic vibrations and grain refinement as factors enhancing the purification buy facilitating the migration of the liquid through the mush, and the effect that the microstructure has on the purification process. In this chapter we analyse the extent of the microsegregation effects in the purification process considering first a modelling approach and then an experimental evaluation of the solid diffusion using SEM-EDX characterisation.

5.1 Numerical evaluation of the extent of back diffusion

In our experiments, the squeezing procedure was performed either in one continuous step, or in six steps applied every 2 minutes each. When the squeezing takes place in one continuous step, the process is rather quick, less than 5 minutes. Considered the short amount of time, diffusion from the liquid back to the solid is unlikely to happen on a significant scale. But, in the scenario in which the squeezing is performed by steps, 13 min (time in which the experiment takes place) at a rather high temperature, in the semi-solid region, may cause some diffusion from the liquid back to solid, effectively absorbing part of the unwanted solutes back to the solid phase. Considering how the experimental work was performed, an in-situ measurement of the back diffusion did not seem feasible. Also, according to the experimental procedure (Section 3.3.3) it was not possible to stop the experiment at different times to quench the mush and measure the extent of back diffusion. In order to estimate the solid diffusion, we decided to use a numerical model. Initially the idea was to find an approach that could relate the solute diffusion to the time and volume, in a form feasible to solve without the aid of professional software. After some literature investigation, all the models found were involving either the use of specialised software or a numerical approach that would have been out of the scope of this work [110]–[112]. It was decided, then, to use a model formulated by Professor Alain Jacot.

The model has been described in Section 3.5.3. Although the model does not account for all the mechanisms happening during semisolid holding, and described in chapter 4, it gives useful complementary information.

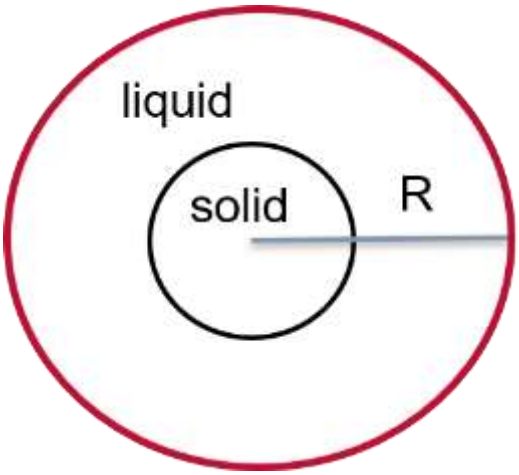

Figure 49: schematic representation in one dimension of a solid α Al grain surrounded by liquid. R is half the size of the domain (solid grain plus the liquid).

The model simulates the drainage of the liquid envelope around a solid grain. The microstructure is represented in one dimension using spherical symmetry (figure 49). The details about the input parameters in the model, have been described in 3.5.3. The values inserted in input command to run the model, are calculated either from the phase diagram and/or taken from the experimental results. The model was run for: Al-3 wt% Si, Al-5 wt% Cu, Al-3 wt% Ni alloys.

The model simulates the effect of squeezing by eliminating progressively the liquid around the solid grains. The initial size of the calculation domain was selected from the experimentally determined average distance between two grains surrounded by quenched liquid, measured from optical images of the semisolid quenched sample (e.g. Fig. 47 in 4.5). Starting from a negligibly small solid seed surrounded by liquid of nominal composition, solidification prior and during squeezing was described by solving the solute diffusion equations (Fick's Law) in the solid and liquid subdomains according to equation 18 in 2.5.1. The diffusion coefficients values were calculated from the Arrhenius equation (equation 14 in 2.5.1) using values of pre exponential factor and activation energy obtained from the literature [113], see Table 12. The position of the solid/liquid interface was updated at each time step from a local solute balance assuming local thermodynamic equilibrium at the interface. The squeezing was simulated by

eliminating progressively the liquid volume in the domain as it is visible on the right hand side of concentration profiles showed in Figures 50 and 51.

The time in every simulation was set as 13 minutes, which is the total time for the experimental procedure when the squeezing is performed by steps. However, the model simulated the draining of liquid as if it were done continuously for 13 minutes, and not in steps as happened in the real scenario.

Table 12: Assessed Arrhenius parameters for impurity diffusion coefficient in solid and liquid Al [113].

	$\mathbf{Q(KJ/mole)}$	$\mathbf{D_0(m^2/s)}$
Si (Fcc Al)	117.6	1.38×10^{-5}
Cu (Fcc Al)	133.9	4.44×10^{-5}
Ni (Fcc Al)	144.6	4.10×10^{-4}
Si (Liquid Al)	30.0	1.34×10^{-7}
Cu (liquid Al)	24.0	1.06×10^{-7}
Ni (liquid Al)	26.0	9.54×10^{-8}

Figures 50 and 51 show how the concentration changes in the domain at different times of the experiment: beginning (a, c) and end (b, d) with (a, b) and without (c, d) solid diffusion for Al-5 wt% Cu and Al-3 wt% Si alloys. Similar results were obtained for an Al-3 wt% Ni alloy.

In the profiles showed in Figures 50 and 51 there are only negligible differences when the simulation is run considering solid diffusion in comparison to the situation in which solid diffusion contribution is set as zero. This suggests that assuming the Scheil-Gulliver approach, correctly describes the redistribution of the solutes, and there is not much influence of the processing time on the purification efficiency. Table 13 shows that the calculated values of the Fourier number are close to zero, which suggests that the contribution of the back diffusion is very small. Moreover, these calculated Fourier numbers are well below the value of $1/2k_0$, (see Table 13). Therefore, as described in 5.1 and according to literature [22], we can assume that the Scheil-Gulliver approach is good enough for our application and does not underestimate the solid diffusion contribution affecting the purification efficiency.

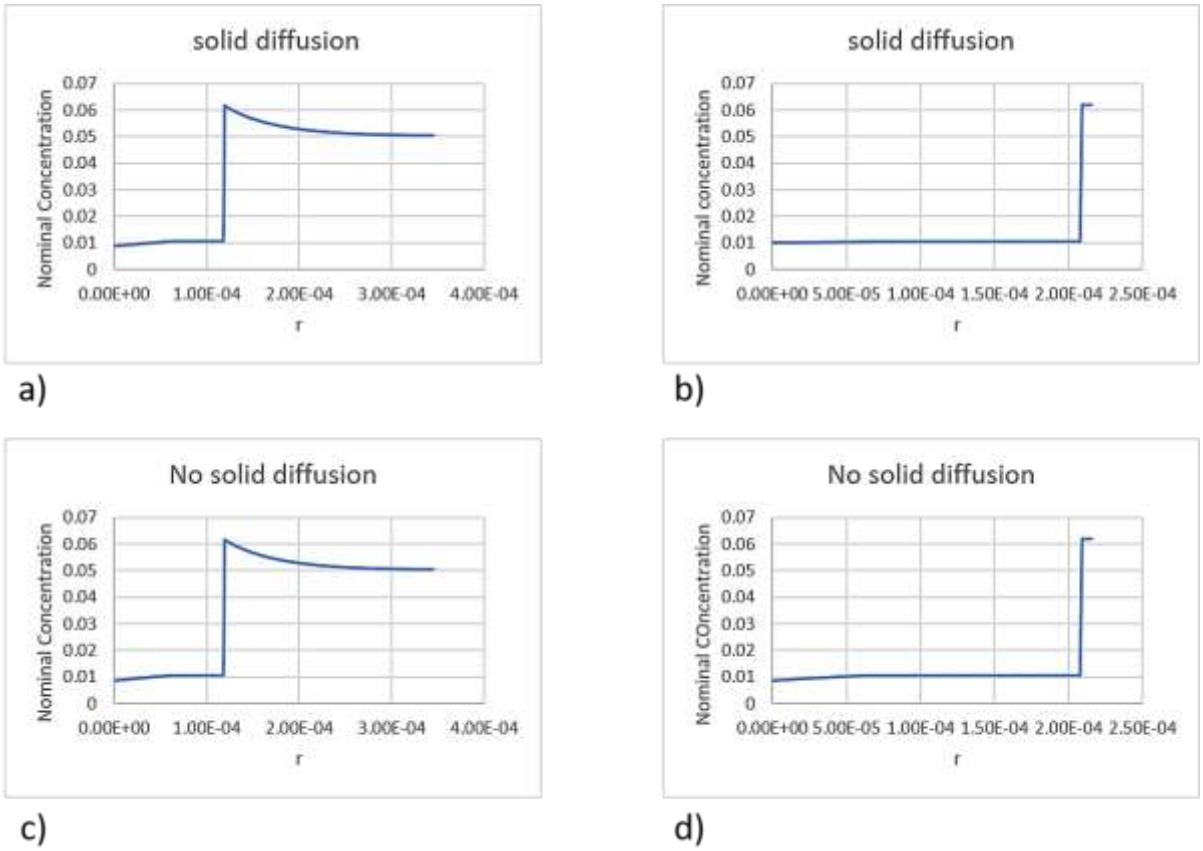

Figure 50: Profile of the change in the Cu composition in an Al-5 wt% Cu alloy vs the size of the domain at the start of the process (a, c) and at the end of the process (b, d): with taking into account the solid diffusion (a, b) and without solid diffusion (c, d).

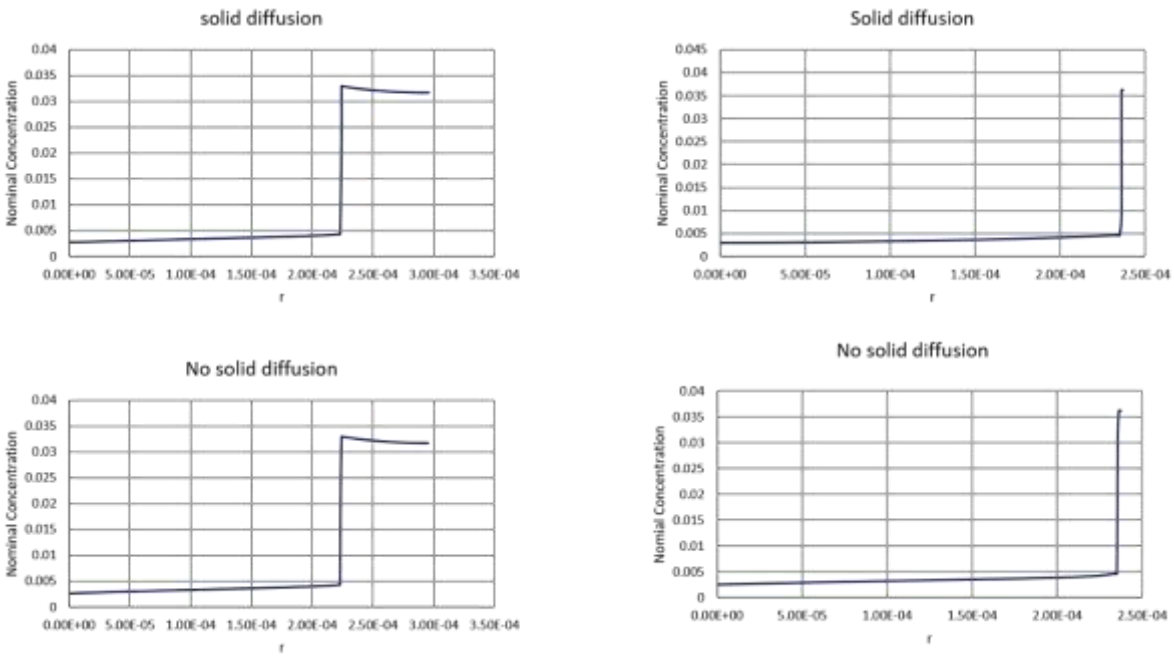

Figure 51: Profile of the change in the Si composition vs the size of the domain at the start of the process (a, c) and at the end of the process (b, d): with taking into account the solid diffusion (a, b) and without solid diffusion (c, d).

Table 13. Value of Fourier number and parameter 1/2k for the tested alloys.

	$\boldsymbol{\alpha}$	$\boldsymbol{1/2k}$
Al-5 wt% Cu	3.30 e–02	3.57
Al-3 wt% Ni	8.00 e–02	71.4
Al-3 wt% Si	6.44 e–02	3.57

5.2 Experimental evaluation of solid diffusion

In the previous section, the extent of solid diffusion during an experiment has been investigated by modelling, and the conclusion was that the Scheil- Gulliver approach is a good approximation for the evaluation of the solutes redistribution during solidification, and that the back diffusion can be considered negligible in the time frame of our experiment. Most of research concerning solid diffusion during solidification is based on calculations because it is quite challenging to have an experimental evaluation of the back diffusion. In this section, the solid diffusion was investigated through the line scan analysis performed at the SEM/EDX on the purified samples obtained at the end of the purification process. The purpose of the line scan analysis is to identify how the solute concentration evolves from the grain boundary towards the centre of the grain.

Figure 52 shows an SEM/EDX image of the purified fraction of the real scrap alloy whose composition is shown in table 5 (3.1). The real scrap was purified using a squeezing procedure by steps and applying US vibrations. It was decided to study the samples in which the squeezing procedure is performed by steps not only because it is the optimised procedure, but also to have some consistency with the modelling results. Figure 52 shows several points analysis, and these points are taken either inside a grain or at the grain boundaries. LG10 is the scan analysis performed along the entire length of a grain. This length is 87 μm and the highest percentage of elements can be found close to the origin and to the end of the x axis which means that the distribution of elements is mainly located at the perimeter of the grain.

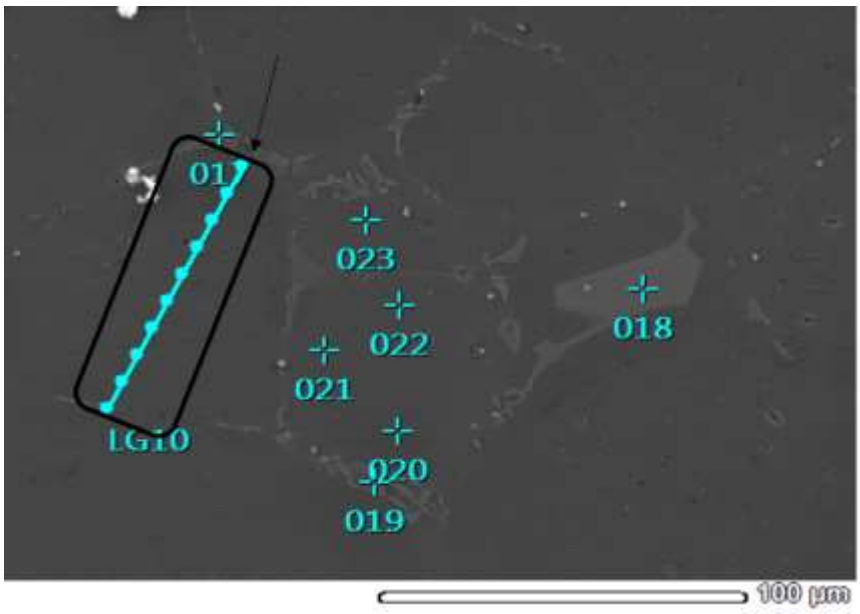

Figure 52: SEM/EDX image of the purified fraction of real scrap alloy treated with US and with multi steps squeezing procedure.

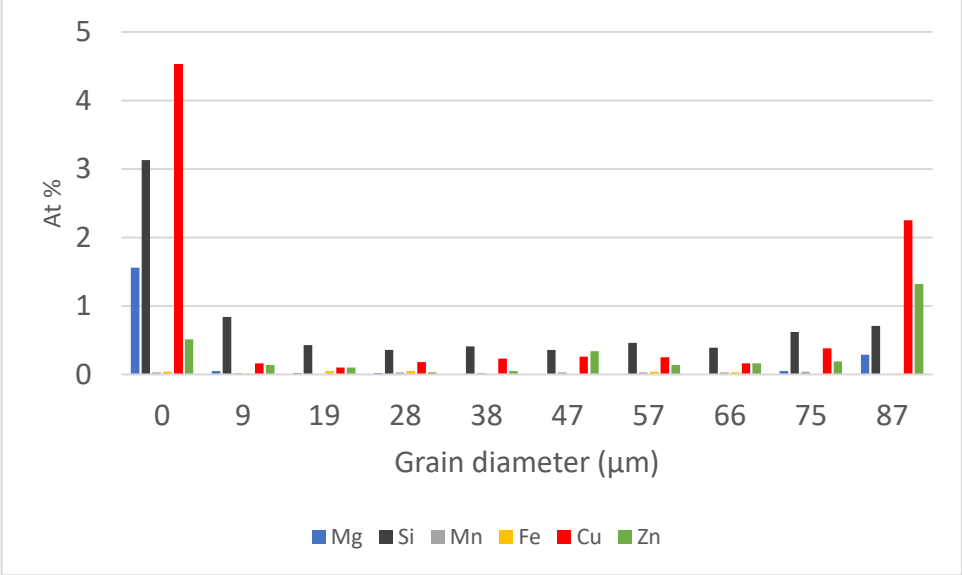

Figure 53: Distribution of atomic percentage (at. %) of elements obtained from the line scan analysis of LG10.

The percentage of Cu, Zn and Si gradually decrease from the side of the grain towards the centre. In fact, with the progressing of the solidification, the forming solid grain rejects solutes at the interface so it is quite expected that the concentration of solutes would be found more at the perimeter of the grains. Table 14 shows the diffusion coefficients for the alloying elements in solid Al calculated at 600 °C. The value of diffusion are obtained solving the Arrhenius equation (equation 14 in 2.5.1) using the value of the pre exponential factor and the activation energy found in literature [113] and shown in Table 12.

Table 14: Calculated diffusion coefficient of solutes elements in solid fcc Al

Cu	**Si**	**Fe**	**Mg**	**Mn**	**Zn**
4.27e-13	1.2e-12	5.7e-14	9.8e-13	3.2e-15	1.36e-12

Fe and Mn are the elements with the lowest diffusion coefficient and in fact their presence inside the grain is almost undetectable because the rate of the diffusion in the solid is very slow. Instead Zn and Si are the faster diffusers, and, in fact a small amount of those elements is present at the centre of the grain. In order to have a better visualization of the smaller peaks in the central area of the grain, Figure 54 gives an enlarged scale of composition.

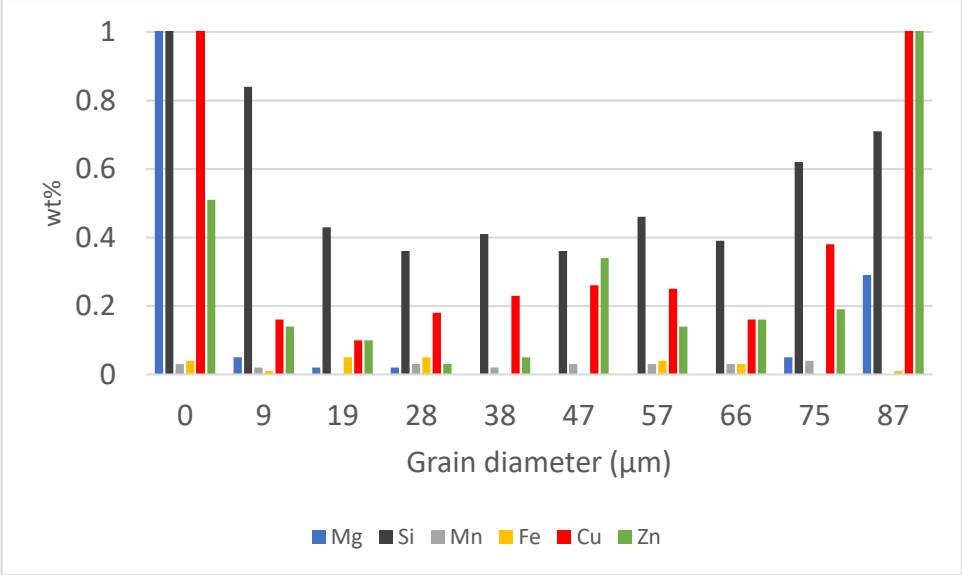

Figure 54: Enlargement of the graph showed in Figure 53 considering a smaller interval on the y axis to highlight the smaller peaks.

A similar trend can be found in a simple binary alloy like Al- 5 wt% Cu that underwent the procedure of squeezing by steps with the addition of US.

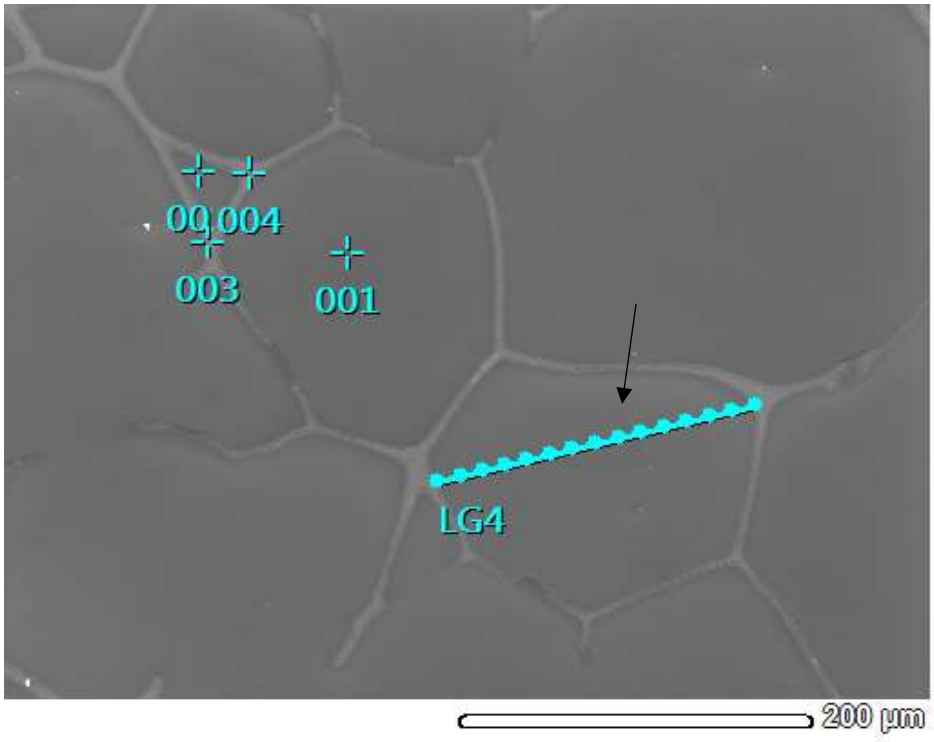

Figure 55: SEM/EDX image of the purified fraction of Al-5 wt% Cu alloy treated with US and with a multi-step squeezing procedure.

The arrow in figure 55 indicates where the line scan starts. The result of the line scan is reported in the graph in Figure 56, and it shows the fluctuation of the atomic percentage of Cu from the grain boundary to the central region. Clearly at the boundary of the grain (beginning and end of the x axis in Figure 56) the atomic percentage of Cu is higher and then gradually decreases moving towards the centre. As discussed for the analysis of the real scrap alloy, when the squeezing process is done in a multi-step procedure the time of the experiment is long enough to create some movement of atoms from the liquid fraction back to the solid. However, the number of atoms diffusing back to the solid is so small that does not affect the purification process.

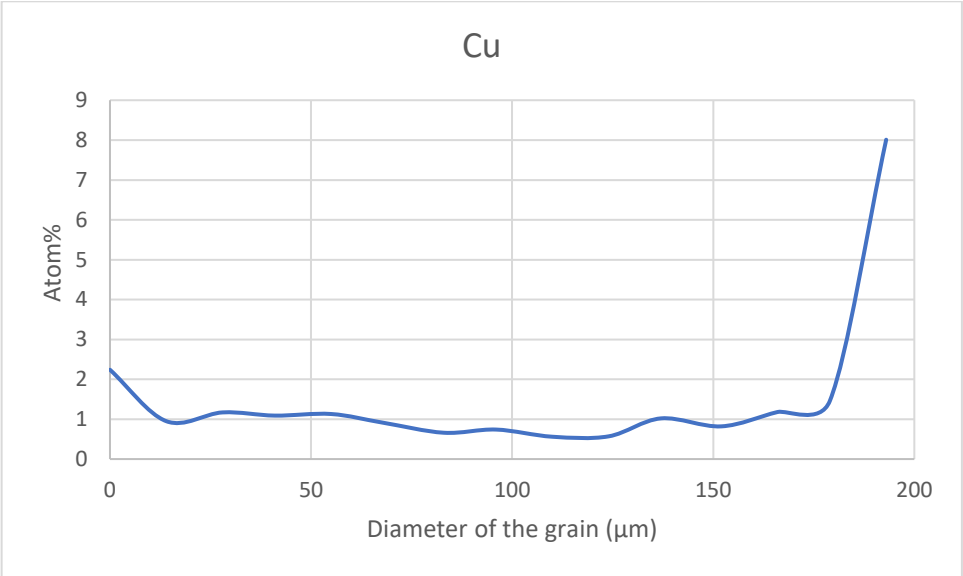

Figure 56: distribution of at % of Cu obtained from the line scan analysis of LG4.

5.3 Summary

- During fractional solidification solutes are redistributed between the solid and liquid phases and this distribution defines the microsegregation. Usually the redistribution of solutes during solidification is described by the Scheil-Gulliver approach in which the diffusion of the solute in the solid is considered negligible. However, there are modifications to this approach in which the solid diffusion is considered through adding the Fourier number to numerical models.
- In this chapter the back diffusion was, firstly, evaluated with a modelling approach which showed that, within the duration and diffusion length scale of our experiments, no significant back diffusion occurs. Obviously, back diffusion should be related to the value of the diffusion coefficient. However, within the processing window, the extent of back diffusion for all studied elements is not enough to compromise the purification efficiency.
- From the line scan analysis, the presence of solutes elements is mostly detected around the perimeter of the grain. A small atomic percentage of solutes detected inside the grain may indicate that some quick-diffusing solutes diffused back inside the solid.

CHAPTER 6

Efficiency of the purification technology in application to aluminium alloys

Fractional solidification consists in processing the material when it is in the semisolid state, in order to have the solutes partitioned between the solid and the liquid phases. In the case of hypoeutectic alloys, when cooled down from the liquidus temperature, the solid phase rejects solute elements at the interface enriching the liquid fraction. The solid fraction during solidification (between liquidus and solidus) has, therefore, a lower concentration of solutes than the initial composition of the alloy. The challenge is to remove the liquid fraction as completely as possible, in the process of this fractional solidification, in order to have a final alloy composition with lower concentrations of solute elements, hence, a purified alloy. In Chapter 2, different methodologies, and set-ups for implementing fractional solidification have been described. Most of the technologies are found in patents, and some of these patents do not even show experimental results, while the set-up designs are intricate and complex, which makes them not practical for a research. We have based our technology on the idea published by Lux and Flemings [50], [60] in which fractional solidification was realised by performing isothermal squeezing of a semisolid alloy toward a filter. Their set-up was tested only on a Sn-Pb alloy and in small quantities (500 g). In this work, the set-up is designed and tested on Al alloys, so the temperature involved is much higher and also the amount of material processed is larger, being 1 to 3 kg. Moreover, Lux and Flemings did not study the effects of process parameters on the purification efficiency like temperature or squeezing procedure, nor any additional effects (ultrasonic vibration and grain refiner) (see Chapter 4 for our research in this direction).

Once the set-up is designed, it is crucial to understand for which alloys it can be applied. First of all, an alloy has to be hypoeutectic in order to have fractional solidification with the depleted solid phase, and also the composition of the alloy is relevant. It was decided to choose simple alloy systems that could be a compromise between the most common impurities found in cast and wrought alloys, and the purpose of the scientific investigation. Table 2 in (2.5) shows the most common alloying elements for Al with a eutectic reaction in the Al corner of the phase diagram. It also shows the maximum solidification range calculated from the binary phase diagrams of these elements with aluminium. The thermodynamic purification efficiency is calculated from the phase diagram, assuming the solidus and the liquidus as straight lines, and it indicates the maximum purification efficiency that can be reached for a certain alloy. The purification efficiency depends on the difference of the composition between the initial alloy and the composition of the purified one that is calculated as the solid composition at the

eutectic temperature. In reality, a solid fraction of Al without any traces of solutes, cannot be achieved because even if the liquid fraction is all squeezed out, the remaining solid fraction still contains solutes reflecting the solid solubility. Also, processing a semisolid alloy close to the eutectic temperature, where the solutes partitioning is most pronounced, is not feasible because the mushy alloy behaves like almost solid, and performing squeezing on such a material is very challenging. In fact, semisolid material with a solid fraction higher than 0.6 is characterised by well-connected solid phase that behaves likes a solid having a certain yield strength [27]. Upon deformation this solid skeleton responds by densification leaving the liquid phase entrapped inside the mush decreasing the permeability as discussed in Section 4.4. Also, as discussed in Section 4.3, the liquid migration inside the semisolid material is facilitated when the liquid fraction is higher, and the structure is characterised by rounded solid grains. Since the scope of the purification is to eliminate the liquid fraction as much as possible a scenario in which the migration of the liquid is facilitated is better for the purpose of this work. It follows that, calculating the purification efficiency suggested by Sillekens et al. [39], [114], is not possible for our experimental work, so the values obtained in this work and shown in this chapter will be lower. In our work, the purification efficiency is also formulated taking into account the difference between the composition of the initial alloy and the purified one, and it is not theoretical one but obtained from the chemical composition measured on the purified sample obtained at the end of the squeezing process. Also, different parameters will be considered in this chapter that are the factors influencing the purification (temperature, time, squeezing procedure, ultrasonic vibrations, and grain size). According to the literature investigation, so far, no papers have been published in which there is a systematic analysis of these factors influencing purification.

6.1 Model alloy tested

- *Al-7 wt% Si*

Silicon is widely used in casting alloys because it (through the formation of Al-Si eutectics) improves the fluidity and other casting properties of the alloy, reduces the melting temperature, and is also relatively cheap as a raw material. Al-Si alloy forms a eutectic at 12.2 wt% Si [115]. Usually for automotive applications, cast alloys contain around 7 wt% (A356) so a binary alloy Al-7 wt% Si could represent a good explanatory model system for the purpose of this work. In real cast alloys additional elements are present as well, such as Mg, Fe and Mn in small

percentage, but these elements were not included in the alloy composition to not have a complex thermodynamic system to analyse.

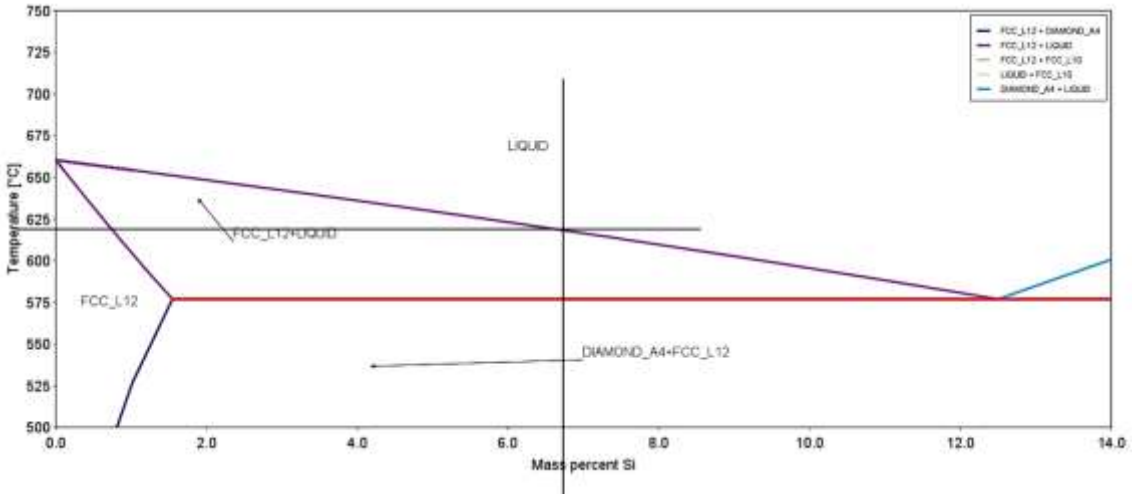

Figure 57: Al-Si phase diagram calculated by Thermocalc software

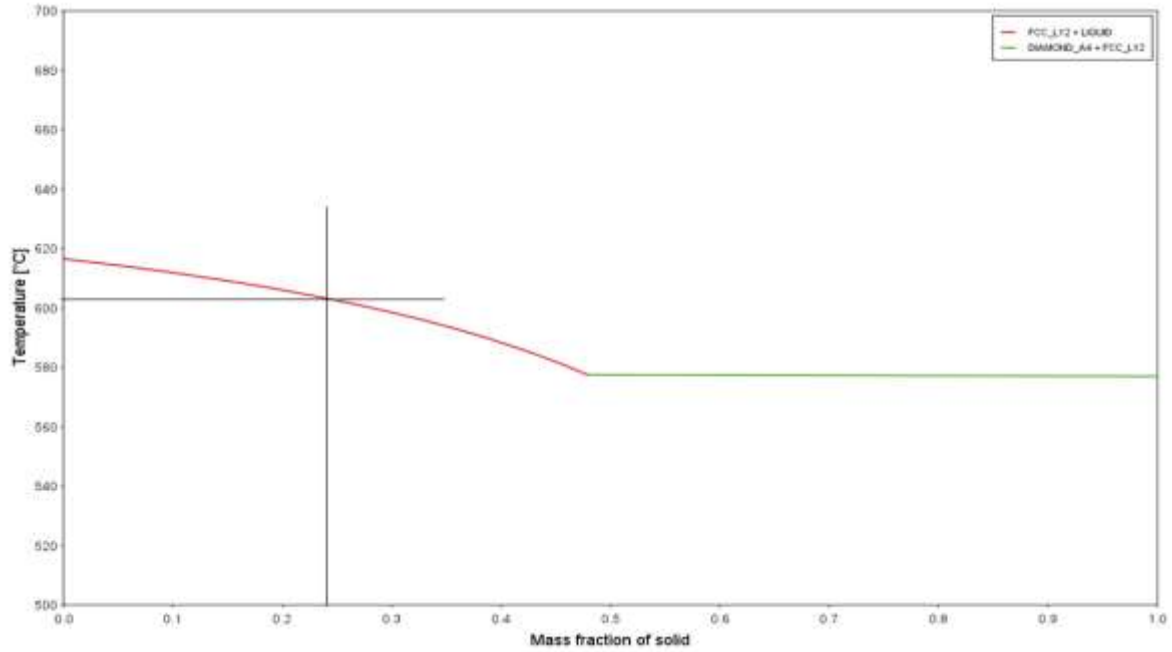

Figure 58: Evolution of the solid fraction in an Al-7 wt% Si alloy calculated using the Scheil equation estimated by Thermocalc.

The Al-Si phase diagram is shown in Figure 57, 617°C is the liquidus temperature for an Al-7 wt% Si and the eutectic temperature is 577 °C with a 38 °C of solidification range. This range is wide enough to give some flexibility in processing the semisolid material before it gets

completely solid. According to the evolution of the solid fraction by the Scheil-Gulliver approximation (Figure 58), the temperature in which the primary Al phase is 50% solid is 604 °C. This temperature actually corresponds to the situation in which the alloy is 25% solid with a lot of the remaining solid phase included in the eutectic. The goal is to process the alloy when only the primary Al phase is 50% solid so that, according to the thermodynamics, only relatively pure Al solidifies in the final product. In the real situation it was quite difficult to operate at the calculated semisolid temperature because the alloy appeared very mushy already some degrees below the liquidus temperature making it difficult to manipulate. In fact, when solidification proceeds, the dendrites in the solid structure start to impinge onto each other and the dendritic structure becomes coherent. At this point the semisolid alloy behaves more like a solid than a liquid [116].

- *Al- 4 wt% Mg*

Magnesium is widely applied in casting and wrought alloys. High weight percentage of Mg (5 - 6 wt%) are mostly employed for marine application and cryogenic tanks. In automotive applications the weight percentage is usually less than 3 wt%. The choice to make a model alloy Al-4 wt% Mg was due to the wider solidification range of Al- 4 wt% Mg over Al-3 wt% Mg. From the phase diagram in Figure 59, the liquidus temperature for Al-4 wt% Mg is at 639°C meanwhile the temperature at which the primary Al phase is 50% solid is 626°C (Figure 60).

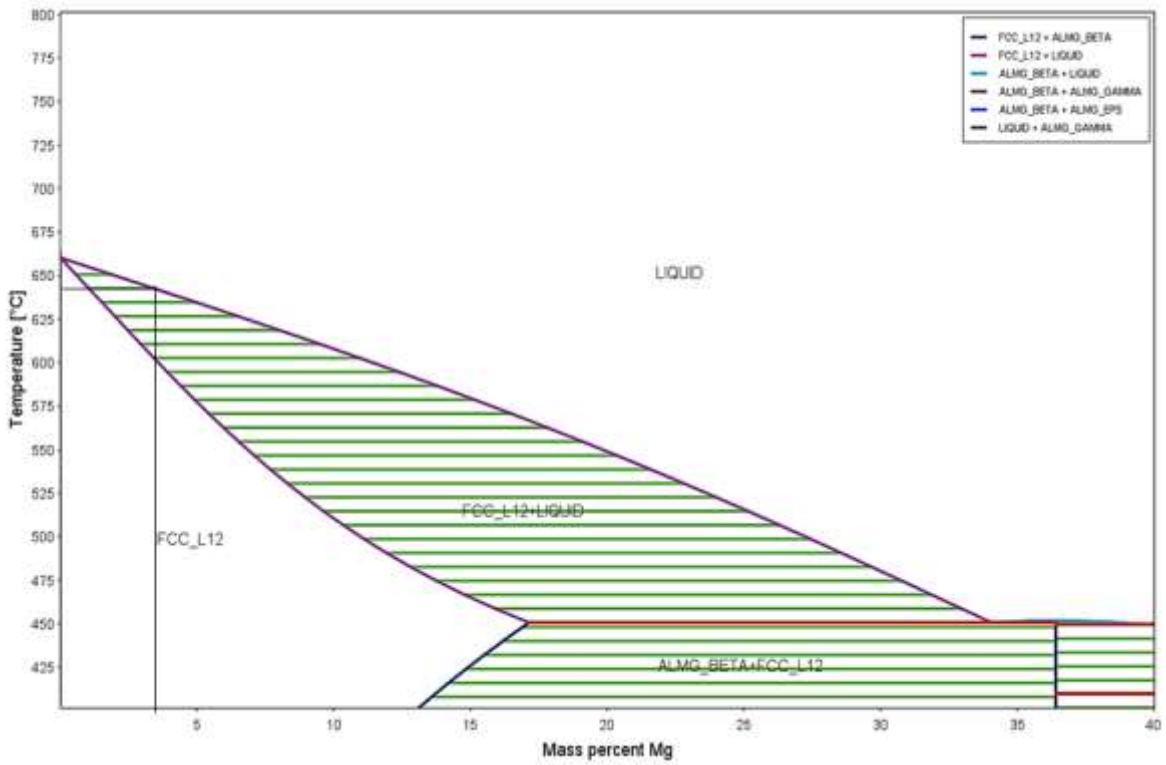

Figure 59: The Al-Mg phase diagram calculated by Thermocalc

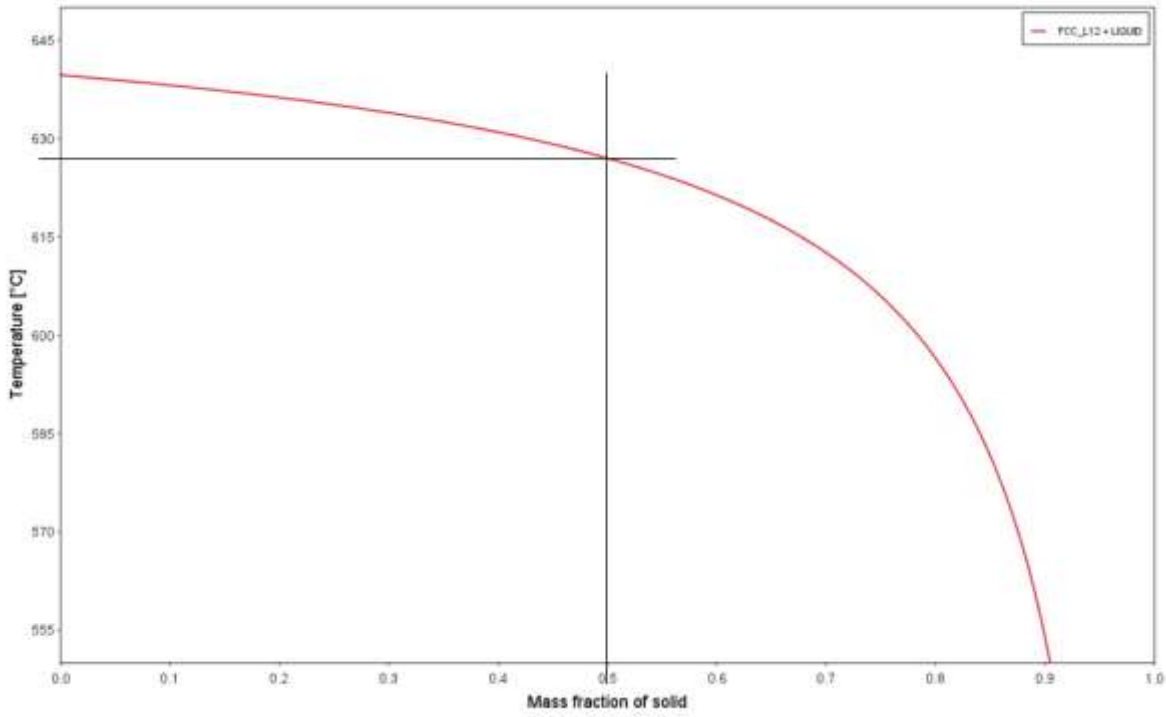

Figure 60: Evolution of the solid fraction in an Al-4 wt% Mg alloy calculated using the Scheil equation estimated by Thermocalc.

- *Al- 1wt% Si- 1 wt% Fe*

In most of wrought alloys commercially used for automotive applications, the weight percentage of Fe needs to be below 0.5% for cast alloys and below 0.2% for wrought alloys, while in scrap and recycled fraction it is usually more (see Table 1 in Introduction). An Al-1 wt% Fe-1 wt% Si alloy seems a suitable model alloy that could represent the composition of Fe and Si in scrap fraction, also the semisolid temperature range is wide enough to give time to operate during the experimental trials. Even though Figure 61 is only the vertical section of the phase diagram and cannot be used for direct calculation of the mass fractions, it is visible that the liquidus temperature is 650°C meanwhile the temperature in which the primary Al phase is 50% solid is 645°C (Figure 61). Here, as in the Al-Si system, most of the solid phases are formed though eutectic and peritectic reactions. Therefore 50% of primary solid Al corresponds to a much lower amount of total solid fraction (Figure 62).

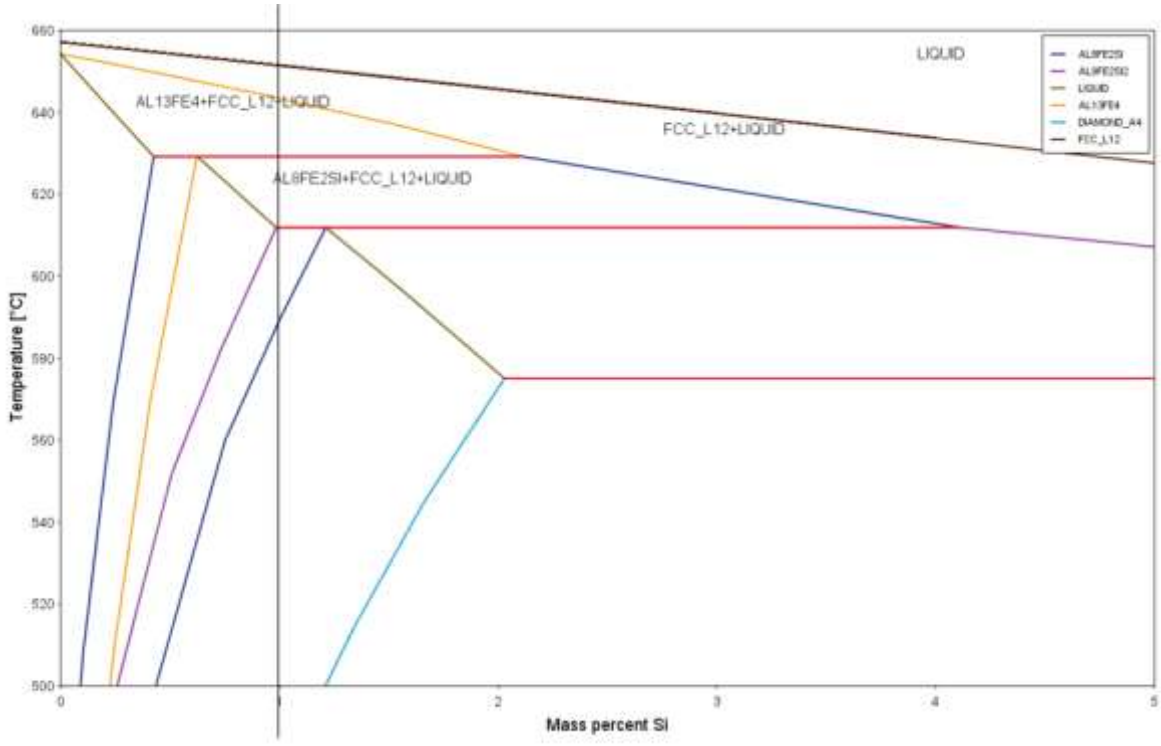

Figure 61: A vertical section of the phase diagram representing Si variation on Al-1 wt% Fe- x Si

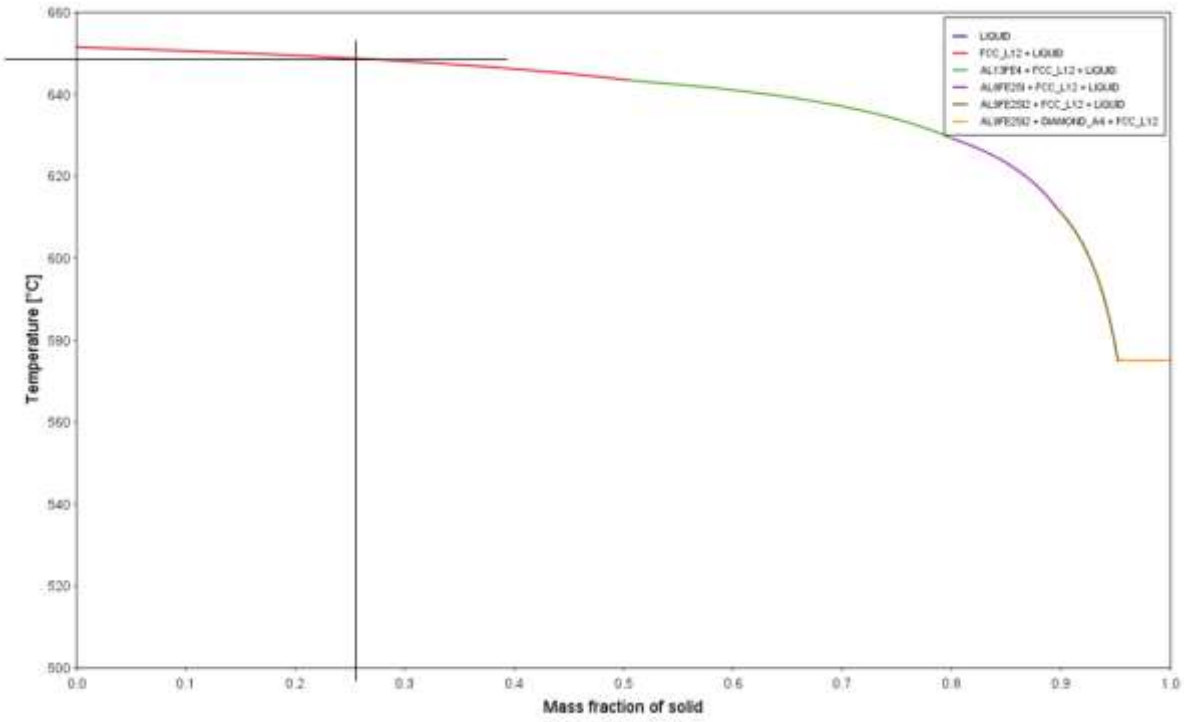

Figure 62: Evolution of the solid fraction in an Al-1 wt%Si-1 wt% Fe alloy calculated using the Scheil equation estimated by Thermocalc.

- *Al-2wt % Si-1.8 wt% Fe*

An Al-2 wt% Si-1.8 wt% Fe alloy was chosen to have a model alloy with a higher composition of Fe, to verify if is the final composition of the purified alloys is influenced by the initial composition. According to Figure 63 the liquidus temperature is 645°C and the temperature in which the primary Al phase is 50% solid is 643°C. This temperature corresponds to the situation in which only 7% of the Al-2 wt% Si-1.8 wt% Fe alloy is solid. However, the solidification range is very small so, even the drop of one degree in temperature brings to the formation of the intermetallic $Al_{13}Fe_4$ phase through a eutectic reaction. This means that the control of the temperature is essential for alloys with a narrow solidification range and processing such alloy with a set-up still in development, without an optimised control of the temperature, can lead to a low purification efficiency.

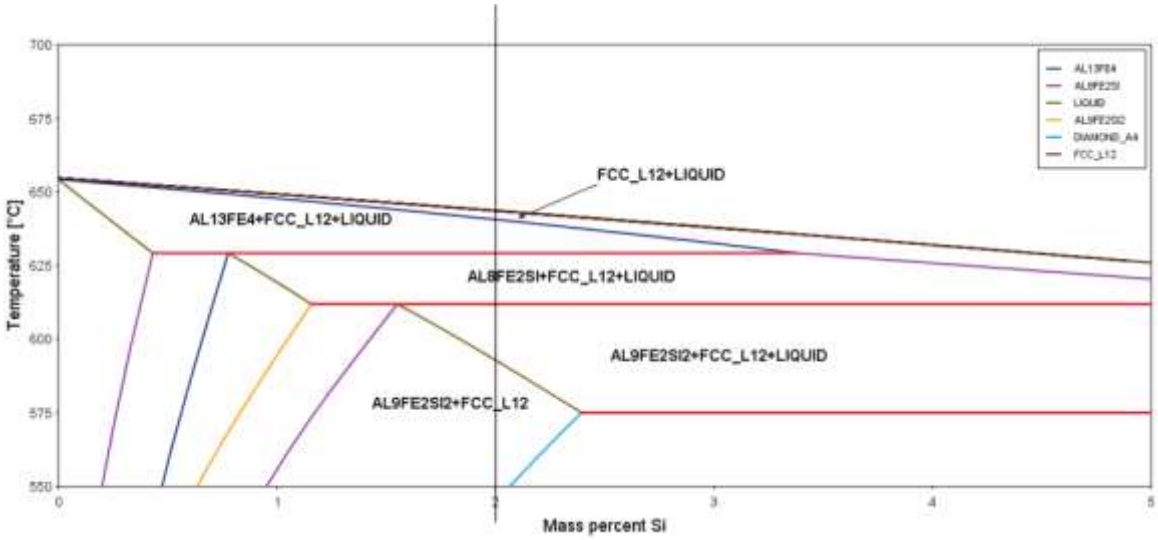

Figure 63: Vertical section of the phase diagram representing Si variation on Al-1.8 wt% Fe- x Si calculated by Thermocalc.

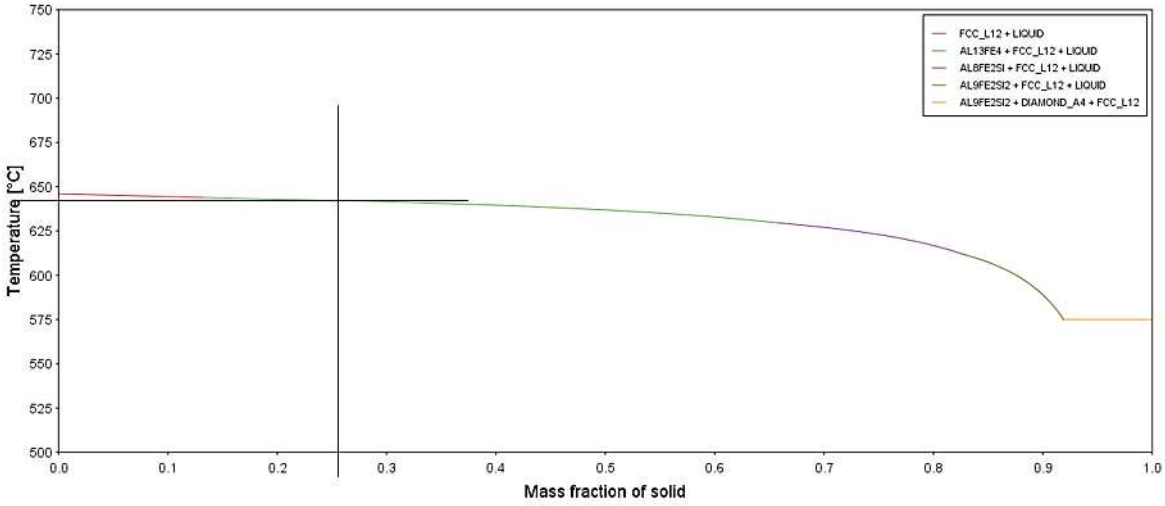

Figure 64: Evolution of the solid fraction for an Al- 2wt% Si-1.8 wt% Fe alloy calculated using the Scheil equation estimated by Thermocalc.

- *Al- 5 wt% Cu*

Al alloys in which Cu is the major alloying element, are usually employed for aerospace or engine applications. The Cu weight percentage is usually below 6 wt% in casting and wrought alloys. According to the phase diagram (Figure 65) the liquidus temperature for an Al-5 wt% Cu alloy is 647°C and the eutectic one is 548 °C resulting in a solidification range of 100°C.

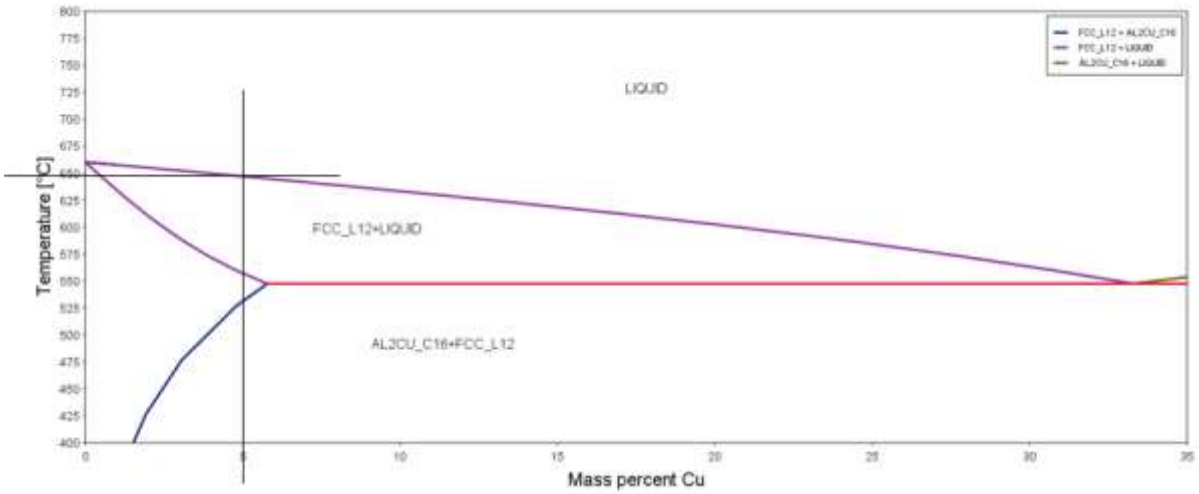

Figure 65: Al-Cu phase diagram calculated by Thermocalc.

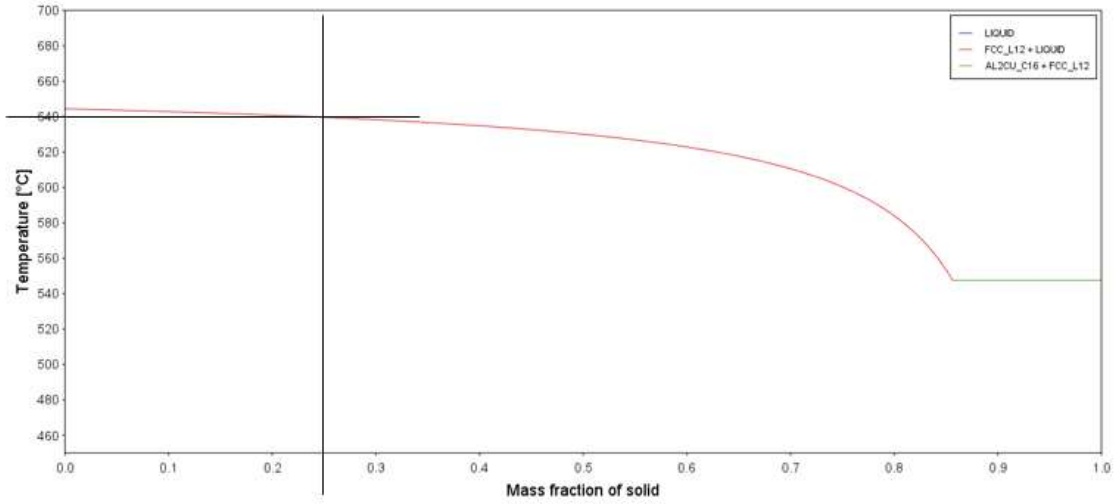

Figure 66: Evolution of the solid fraction for an Al-5 wt% Cu alloy.

As for the other alloys described so far, in this case as well, the purpose is to process the alloy when the primary aluminium is 50 wt% solid. Considering the wide solidification range, 50% primary aluminium is reached when the alloy is almost 50 wt% solid. As already mentioned, due to the coherency phenomenon, processing the alloy when it is 50 wt% solid can be quite difficult in practice. It was decided to choose as semisolid processing temperature (T= 638°C) the one in which the α aluminium is 25 wt% solid.

- *Al-3 wt% Ni*

Nickel is usually present in Al alloys together with elements like Si, Fe or Mg. Al-Ni binary alloys with a low percentage of Ni, are not really used in industrial applications. However, this binary system is very important for our fundamental studies on the purification process because it has a big enough solidification range and a small partition coefficient (k=0.07). Nickel forms a eutectic point with aluminium at 640°C for a composition equal to 5.7 wt%. The liquidus temperature for Al-3 wt% Ni is 652°C (Figure 67) and the temperature at which the alloy is processed is the one corresponding to 20 wt% solid fraction so 647°C (Figure 68).

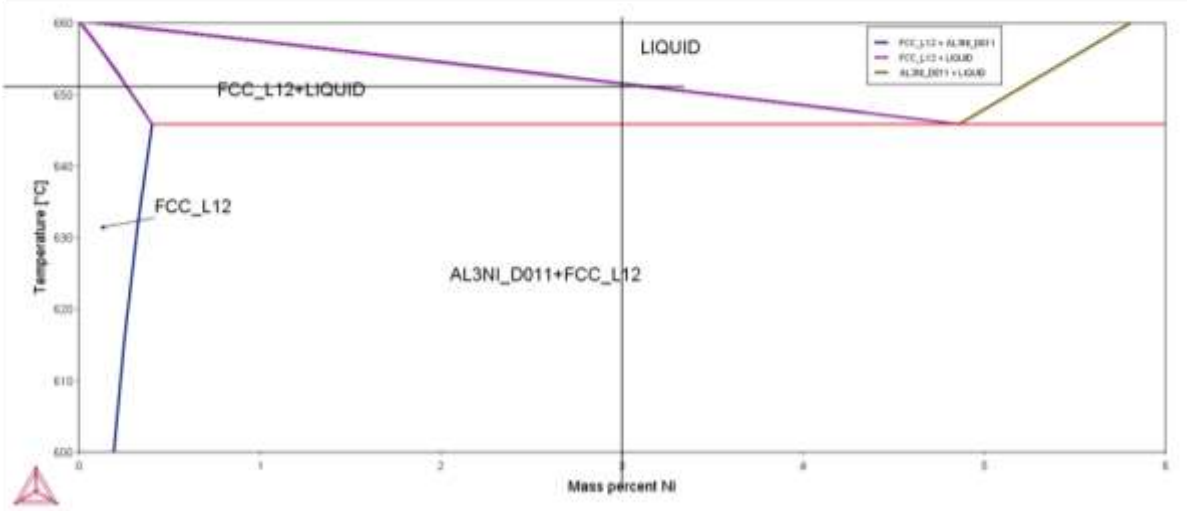

Figure 67: Al-Ni phase diagram calculated by Thermocalc.

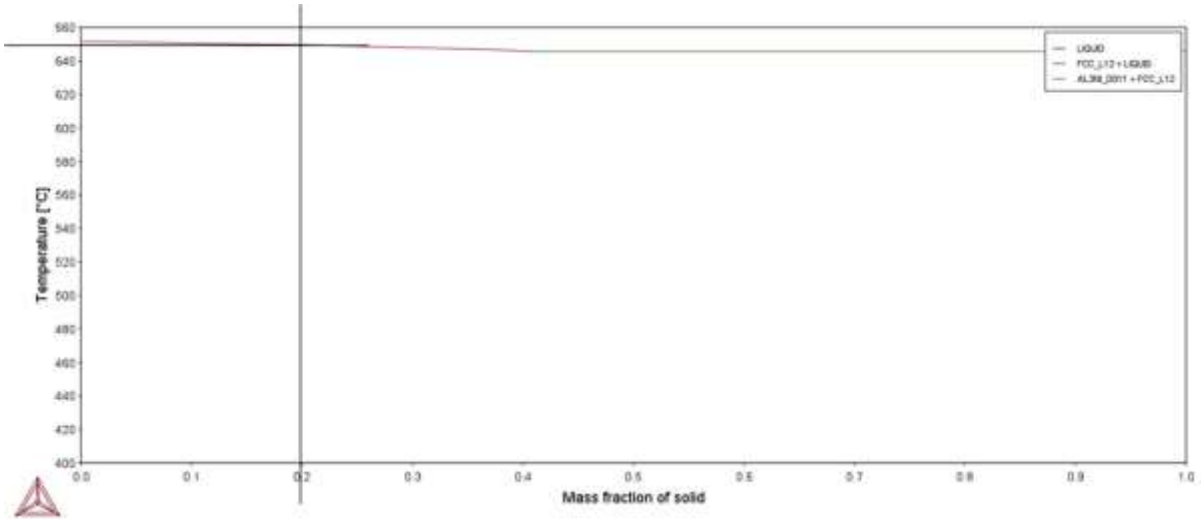

Figure 68: Evolution of the solid fraction for an Al-3 wt% Ni alloy.

- *Al-2 wt% Si*

With the first set-up, Al-7 wt% Si alloy was tested which represents the composition of one of the most used alloys in automotive application. With this upscaled set-up instead, it was decided to test an Al-Si model alloy which could represents the typical composition of a wrought alloy usually used in automotive application. Since the Al-Si phase diagram has already been shown (Figure 59), Figure 69 shows the evolution of the solid fraction according to the Scheil-Gulliver approximation. The liquidus temperature is identified at T= 648°C and the solidification range is 72 °C. Considering the wide solidification range, 50% primary solid Al is reached when the alloy is almost 50% solid. Due to the coherency phenomena, processing the alloy at 50 % solid fraction is challenging. So, as for the Al-5 wt% Cu alloy, in this case as well, the chosen semisolid temperature was the one in which the primary aluminium phase is 25 wt% so T=644 °C (Figure 69).

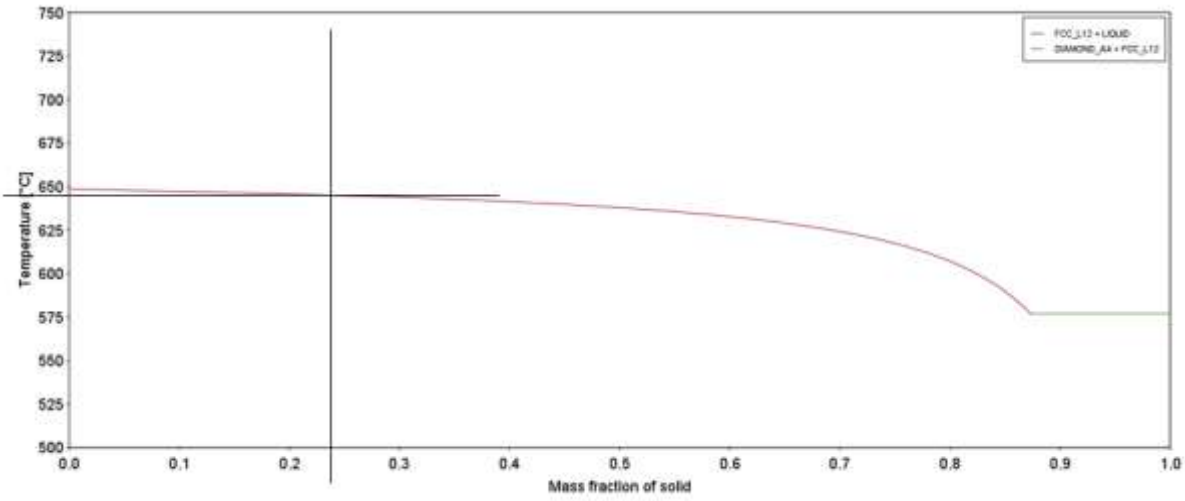

Figure 69: Evolution of the solid fraction in Al-3 wt% Si calculated by Thermocalc using Scheil equation.

6.2 Proof of concept

In order to verify the feasibility of performing fractional solidification with the isothermal squeezing procedure, an initial set up, described in Section 3.3.2, was designed. This first set-up was just a first step in the developing of the technology and was working on a small scale, able to process only a small amount of material. This set-up was tested only on three alloys: Al- 7 wt% Si, Al- 1 wt% Si- 1 wt% Fe and Al- 4 wt% Mg.

Table 15 shows the composition of the alloys as cast in the lab, before undergoing the purification procedure. Table 16 gives the results of chemical composition of the purified and scrap fraction obtained at the end of the purification process. The analysis was done using optical emission spectroscopy in order to get the difference in composition between prior to the purification process and after. The analysis was done as described in Section 3.5.1. The efficiency of purification was calculated using the experimental results obtained at the end of the process and represents the percentage of solutes that are eliminated with the squeezing procedure. It is calculated as follow:

$$E = 100 - \left(\frac{C_F}{C_0}\right) \times 100 \quad (23)$$

Where C_0 is the initial composition of the alloy and C_F is the composition of the final purified fraction.

For brevity only the selected results are shown.

Table 15: Initial compositions of the model alloys

	Al, wt%	**Si, wt%**	**Fe, wt%**	**Mg, wt%**
Al- 7% Si	92.8±0.2	7.04±0.25	0.02±0.01	-
Al- 1% Si- 1% Fe	95.7±0.07	1.27±0.04	1.08±0.06	-
Al- 4% Mg	95.7±0.1	0.02±0.01	0.02±0.01	4.13±0.09

Table 16: Average chemical compositions of the purified fraction, the liquid scrap fraction, and purification efficiency of the alloys processed with the application of ultrasonic vibration.

	Al, wt%	Si, wt%	Fe, wt%	Mg, wt%	Purification efficiency (E)
Al- 7wt% Si					
Purified US	95.8±0.4	3.9±0.4	0.010±0.01	-	47%
Residue	92.0±0.09	7.83±0.01	0.010±0.01	-	
Al- 1wt% Si-1wt %Fe					
Purified US	98.7±0.9	0.68±0.05	0.49±0.05	-	46% for Si; 55% for Fe
Residue	97.1±0.05	1.51±0.17	1.38±0.02	-	
Al- 4 wt% Mg					
Purified US	96.2±0.1	-	0.010±0.01	3.62±0.13	12%
Residue	94.5±0.1	-	0.010±0.01	5.24±0.10	

In the case of Al-7 wt% Si, E= 47% has been achieved and the purified fraction has less solute than the initial alloy. Consequently, there is a parallel increase in the percentage of solutes in the residue collected under the filter. From the value of Si in the residue fraction it is possible to verify if the temperature at which we were processing the material is the intended one. In fact, in the phase diagram a value of 7.83 wt% Si corresponds to the composition of the liquid at a temperature of 609°C that is exactly the one measured during the experiment. According to the Scheil-Gulliver equation the semisolid temperature in which α Al is 50% solid should be 604 °C, but it was very difficult to reach that temperature because the alloy started to solidify in the crucible and usually the solidification starts on the wall of the crucible moving towards the centre. This prevented some material to be poured in the set-up. This explains why the actual pouring temperature was few degrees higher than the calculated one (see experimental details in 3.4). Obviously, this has consequence on the amount of solid and liquid phase formed. Ideally the more the solid phase is formed, the more the partitioning and the better the purification achieved. However, processing higher amount of solid fraction is more difficult, so

during the experimental procedure the choice of the pouring temperature has to be a compromise between different factors: solid fraction, coherency, and viscosity.

For what concerns the alloy Al-1 wt% Si-1 wt% Fe, a good level of purification was achieved for both alloying elements: E_{Si}= 46% and E_{Fe}= 55%. The reason why the purification is not identical for two elements in the same alloy, can be attributed to the different partition coefficient of Si and Fe in aluminium. In the case of Fe, the value of the partition coefficient is 0.03, while for Si is 0.13. This means that Fe tend to remain in the liquid phase more than Si, facilitating the purification process. From Tables 15 and 16, the concentrations of Si and Fe in the purified fraction have decreased from the initial value, and the concentration of these solutes in the residue fraction has increased as expected from the theory. The concentrations of Fe and Si in the residue fraction correspond to a temperature of 647 °C which is 2 degrees higher than the calculated one.

For the Al- 4wt% Mg alloy the results achieved in terms of purification are not as good as for the other two alloying systems, with an efficiency value equal to 12%. In every trial, the purification efficiency for Al-4 wt% Mg remained very low and, as a result, testing of this alloy was discontinued. The explanation to the low value of E can be found again in the partition coefficient. In the case of Al-Mg the value of k is 0.45. This means that Mg tends to stay in the solid state as much in the liquid one, contributing as a limitation to the purification process. From the composition of the residue collected under the filter we can verify that the semisolid temperature at which we were working was 632°C, which is substantially higher than the targeted one calculated through the Scheil-Gulliver equation. In this case, the large partition coefficient coupled with a high solubility of Mg in solid Al influences the amount of eutectic formed and the solutes rejection at the interphase, lowering the purification achievable.

Every purified fraction was first cut off from the filter and cut in two halves. The analysis was done on the vertical cross section of the sample (Fig. 25 in Section 3.5.1) taking images in regions close and far from the filter. Optical microscope analysis was done to investigate the differences in microstructure in samples treated with US or without US.

As example, Figure 70 demonstrates images of an Al-1 wt% Si-1 wt% Fe alloy. The microstructure of the purified fraction is mainly characterised by the presence of some light grey regions representing the α-aluminium grains and dark grey areas (Figures 70a and 70b). These dark grey areas are the results of the solidification of the liquid fraction that could not be squeezed out. These dark grey areas might be attributed to the $Al_{13}Fe_4$ binary eutectic intermetallic and the Al_8Fe_2Si ternary eutectic intermetallic (see Figure 61). In fact, under equilibrium conditions, for the composition shown in Table 16 and with taking into account the

calculated phase diagram in Fig. 61, at T= 643°C the main transformation is the eutectic reaction

$$L = \alpha + Al_{13}Fe_4 \quad (24)$$

and at T= 630 °C the eutectic transformation

$$L = \alpha + Al_8Fe_2Si \quad (25)$$

In real situation, equilibrium conditions are not achieved so the two reaction may not happen exactly as shown as Equations 24 and 25.

a)

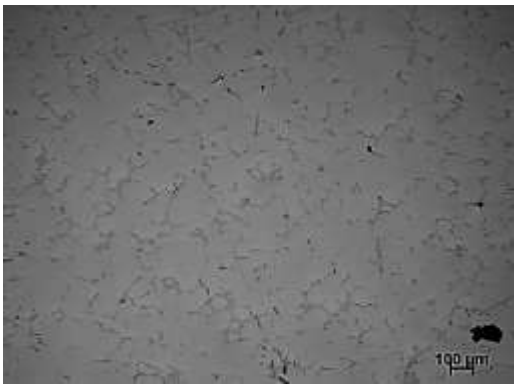

b)

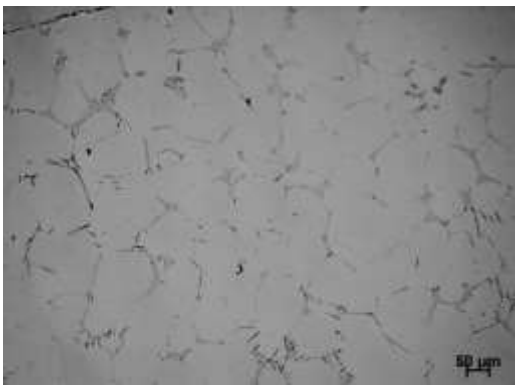

c)

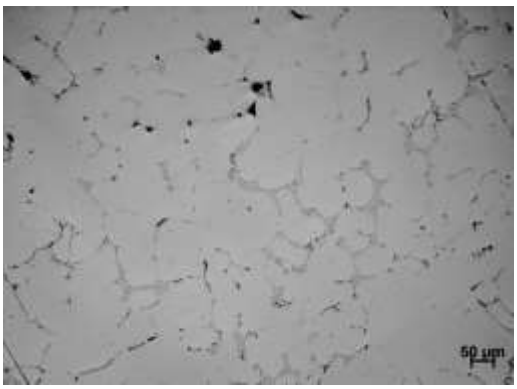

d)

Figure 70: Optical microscope image of the purified fraction of Al-1 wt% Si-1 wt% Fe a) No US treatment lower magnification b) US treatment lower magnification c) No US treatment higher magnification d) US treatment higher magnification

There are, however, no significant differences in the microstructure of samples treated with US or without it. From the anodized images (Figure 71) both samples seem to have a relatively

fine structure intermixed with some bigger grains. The inhomogeneous shape of the grains can be due to the fact that the squeezing process breaks some of the dendrites during the process, while other grains coarsen as a result of isothermal holding.

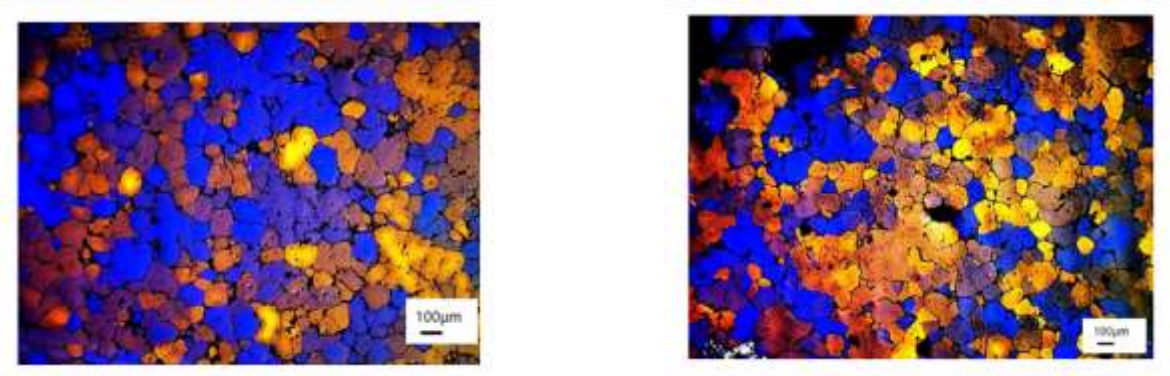

a) No US grain size: 197±18 µm b) with US 169 ±12 µm

Figure 71: Metallographic image of the anodized purified fraction of Al-1 wt% Si-1 wt% Fe with No US a) and US b).

It is interesting also to have a look at the metallographic image of the residue that was collected under the filter. Figure 72 shows a schematic of the shape of the sample. It consists of two parts (two disks) that probably were squeezed in two different moments through the filter. The bigger disk is probably the initial liquid fraction that passed though the filter during the pouring. The second disk, it can be the liquid that was actually squeezed out from the mush by the piston. In fact, as Table 17 shows, the lower disk which is the one that has been filtered first, has a lower mass fraction of Si and Fe because it represents the liquid fraction that come put first from crucible at the moment of pouring. The upper disk has higher content of Fe and Si because is the actual liquid fraction squeezed out of the mush that has a higher amount of impurities due to the solute enrichment in the liquid phase. Also, the microstructure shown in Figure 73b has quite coarse grain structure and needle shaped intermetallics at the grain boundaries. This lower portion was separated as first and filtered out from the semisolid material. This melt was then collected in the reservoir that is heated to the semisolid temperature. This would explain why the lower disk has so big and coarse grains due to slow solidification rate. The structure of the upper disk shows smaller grains with finer intermetallics. The structure might be affected by the fact that this melt was actually squeezed by the piston, passed through the filter, and fell on top of the lower disk. Apparently, it solidified at a higher cooling rate.

Table 17: Average chemical compositions of the residue collected under the filer and showed in Figure 72.

	Al (wt%)	Si (wt%)	Fe (wt%)
Upper disk	96.0±0.1	1.99±0.12	1.88±0.08
Lower disk	96.4±0.2	1.77±0.15	1.72±0.12

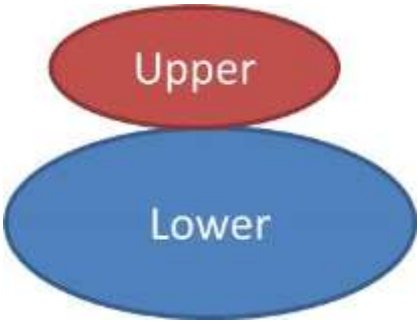

Figure 72: Schematic of the shape of the residue fraction of Al- 1wt% Si-1 wt% Fe.

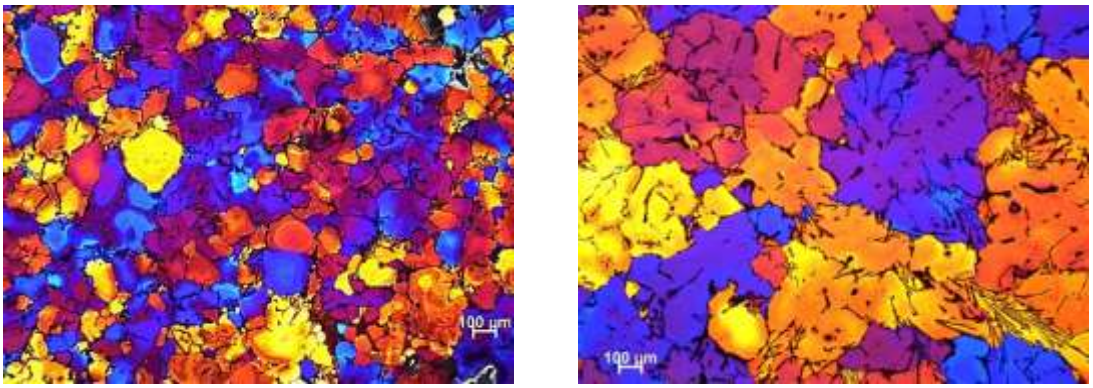

a) Grain size: 140 µm b) Grain size: 350 µm

Figure 73: a) Metallographic image of the upper disk of the residue fraction of Al- 1wt% Si-1 wt% Fe, b) Metallographic image of the lower disk of the residue fraction of Al- 1wt% Si-1 wt% Fe

The results in Table 16 show that a good level of purification is achievable and that the isothermal squeezing is a feasible way to perform fractional solidification. Also, from Figure 73 and Table 17, it is clear that the amount of liquid fraction collected under the filter is not just the one obtained by filtering the initial slurry but there is a contribution of the liquid fraction

squeezed out of the mush, confirming that the squeezing is actually effective for the purification. Processing the material in the semisolid state is very complex and several parameters need to be taken into consideration. However, this set-up was a good starting point to develop a new upscaled technology in order to optimise the parameters that could affect the purification.

6.3 Technical parameters influencing purification

Isothermal squeezing proved to be a valid idea to perform fractional solidification. We decided, then, to upscale the setup to have a more robust and reliable technology in which the control of the variables (like temperature) would be more efficient. Most of experimental work in this thesis was done using this upscaled setup. With the initial setup, a purification level around 50% from the initial composition was achieved by processing about 0.5 kg of an alloy. With the use of the new setup it was possible to obtain a good level of purification for several alloys with different partition coefficients, and taking into consideration different parameters, while also processing up to 2 kg of an alloy. In this Section we will analyse the role of the process parameters.

6.3.1 Squeezing in one step

As described in the experimental procedure in Section 3.3.3, two different ways of performing the squeezing have been adopted. Initially the squeezing was done dropping the piston/sonotrode in contact with the semisolid material inside the processing channel, and then lifting the entire setup as quick as possible towards the sonotrode until it was not possible to squeeze any more. Since this procedure was proven effective in the first setup built, it was decided to keep it that way and to explore if the purification efficiency could be improved through manipulating the structure prior to the purification process. In fact, a finer and round structure in the semisolid mush can help the flow of the liquid, as explained in Section 4.3. A smaller grain structure has less liquid fraction surrounding the grains so the amount of liquid that can remain entrapped is less than in a dendritic structure with big grains. Also, a fine and globular grain structure facilitate the migration of the liquid inside the mush.

Table 18 reports the results of the fractional solidification of an Al-5 wt% Cu alloy in three different conditions: superheating the alloy to 820°C before the purification, superheating to 720°C before the purification, and grain refining it before the purification process. The corresponding analysis of the structure is given in 4.3.

A purification efficiency of 39% was obtained when the alloys had been grain refined and it was also the highest value of purification efficiency in this series of experiments. Note that the purification efficiency is calculated in the same way explained in Section 6.1 for the results obtained with the first set-up.

The lowest value of purification is obtained when the alloy has been superheated to 820 °C. It follows that the purification efficiency increases with the decreasing of the grain sizes. Also, as discussed in Section 4.4 (Fig. 36, Tables 6 and 7), when the alloy has been grain refined, the volume fraction of liquid entrapped is less than in the other two conditions. The less liquid entrapped, the more purification achieved, as shown in Table 18.

Table 18: Average chemical composition of the purified and residue fraction an Al-Cu alloy processed under standard condition, after grain refining, and after superheating.

	Al, wt%	**Cu, wt%**	**Purification efficiency (E)**
Al-Cu	94.4±0.1	5.42±0.09	
Purified no Gr	96.3±0.1	3.55±0.12	34%
Residue no Gr	93.4±0.1	6.4±0.1	
Purified yes Gr	96.3±0.4	3.33±0.3	39%
Residue yes Gr	92.7±0.1	7.0±0.1	
Purified Superheated	96.1±0.2	3.65±0.15	33%
Residue Superheated	93.3±0.2	6.4±0.2	

The second parameter that was studied in order to increase the purification efficiency, was the application of ultrasonic vibrations during the squeezing. Using US vibration is very well documented in literature and it has been applied to Al alloys with various purposes: refinement of the structure, improving the mechanical properties, producing semisolid slurry for thixoforming applications (Section 2.5.6). But the purpose of using US vibration in this work, is to facilitate the migration of the melt inside the mush. The scope of the technology is to eliminate as much liquid fraction as possible and the US vibrations, due to the sonocapillary effect, might help.

Because the addition of GR proved to give good results, the testing was done considering both the parameters but not simultaneously.

Table 19 presents the compositions of the purified fraction and the residue without US treatment, with US treatment, and with grain refining, for an Al-Fe-Si alloy.

Table 19: Average chemical compositions of the purified and residue fraction for an Al-1.6 wt% Si-1.7 wt% Fe when no ultrasonic vibrations are applied, when US are applied and when the alloys has been grain refined.

	Al, wt%	**Si, wt%**	**Fe, wt%**	**Purification efficiency (E)**
Initial alloy	96.1±0.05	1.66±0.02	1.7±0.02	
Purified no US	97.8±0.1	1.04±0.04	0.98±0.07	36 % Si 42% Fe
Residue no US	96.0±0.1	1.81 ±0.07	2.04±0.05	
Purified yes US	97.1±0.1	1.08±0.05	1.05±0.09	35% Si 38% Fe
Residue yes US	96.0±0.1	1.87 ±0.09	2.0±0.1	
Purified GR	97.9±0.1	1.02±0.05	0.87±0.05	39 % Si 47% Fe
Residue GR	96.1±0.1	1.8±0.1	1.94±0.05	

The application of US vibration does not improve the purification efficiency as with the process without US applied. The best purification efficiency for Fe and Si is achieved (in the one step procedure) with the addition of grain refiner.

Figure 74 gives optical microscope images for the purified fraction of the alloy, processed in the three different conditions. When the US is applied (Fig. 74b) the resulting microstructure is different than in the other two conditions. The structure is made of grains alternated with pockets of liquid that solidified at the grain boundaries showing a eutectic structure and finer elongated intermetallics then in Figs. 74a and c.

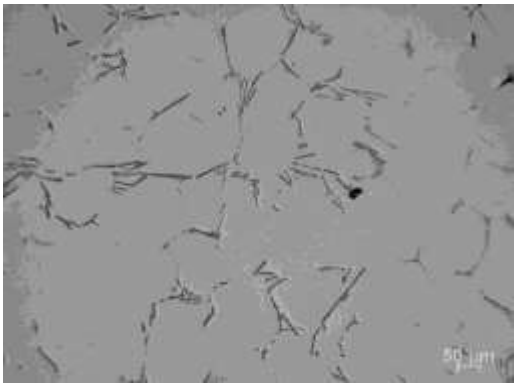

a)

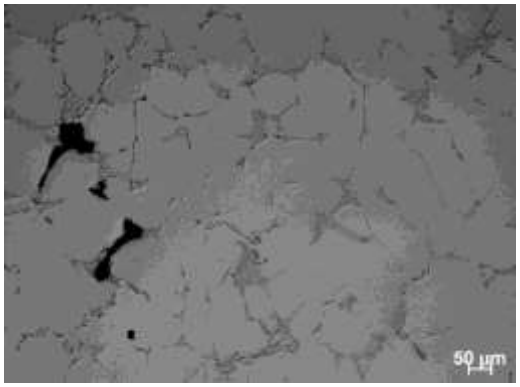

b)

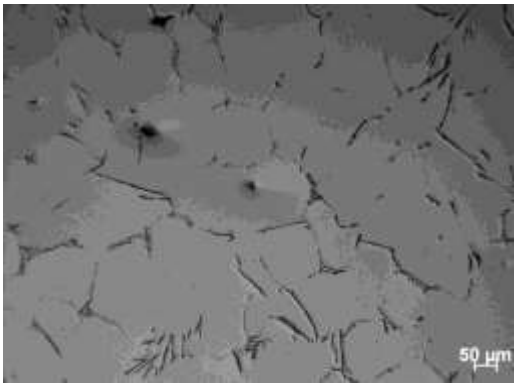

c)

Figure 74: Optical microscope images of the purified fraction Al-1.7 wt% Fe-1.7 wt% Si alloy for three different condition a) one step squeezing no US no GR b) one step squeezing US c) one step squeezing GR

According to the literature [117] [118], the application of US can affect the formation and growth of Fe intermetallics and this would explain why the microstructure is different when US is applied. Probably, in a one-step procedure, the US does not facilitate the purification from Fe because the conditions of the experiment do not allow for the sonocapillary effect to act. As discussed in 4.3, at the beginning of the experiment the alloy is 75% liquid, and the morphology is a fluid like slurry, made of grains dispersed in the liquid. When the squeezing starts, substantial part of the liquid is drained out and the mush is compacted. At this point liquid channels are formed in the mush, but they remain entrapped in the dendritic solid skeleton without much interconnection. Maybe, when a squeezing procedure is done in steps, this would avoid the immediate compacting of the mush and would give time for the liquid channels to form and allow the sonocapillary effect to happen.

Also, according to the phase diagram in Fig. 63, at a solid fraction equal to 30%, the intermetallic phase $Al_{13}Fe_4$ starts to form. Probably nucleation of this intermetallic is enhanced

by the US and this would explain the lower purification achieved for Fe and for Si. Also, considering that in real life the solidification does not happen according to the equilibrium phase diagram, along with the formation of $Al_{13}Fe_{14}$ also Al_8Fe_2Si forms. The Fe and Si contained in these intermetallics, that solidify at the grain boundaries, contribute to the lower level of purification.

Instead when the alloy is grain refined, the morphology is made of rounded grains which would facilitate the migration of the liquid improving the purification. It is documented that ultrasonic vibration refine the grain structure [70], but when US is applied above or across the liquidus temperature and not in the semisolid range [65].

So, in a squeezing procedure done in one step, a better purification is achieved by grain refining the alloy but not with US vibration applied.

6.3.2 Squeezing by steps

In the squeezing procedure via steps, the application of the US vibration was further investigated. A longer processing time allows the US vibration to push the liquid inside the mush towards the filter.

Selected results, out of a series of experiments, obtained for four different alloys purified in a procedure by steps and with the application of the ultrasonic vibrations are given below.

The values showed in Table 20 demonstrate that the purification has clearly increased with a squeezing procedure via steps and the application of ultrasonic vibrations, in comparison to a single step procedure. In a multi-step squeezing, the semisolid alloy is deformed gradually, grains rearrange because of the deformation, and the liquid fraction is squeezed gradually. In such a scenario, the effect of the sonocapillary effect is much more likely to happen. As discussed in Section 4.3, during the deformation process, the solid fraction is a semisolid alloy gradually increases, and the deformation becomes a plastic deformation of solid particles. At this point, the structure should resemble the one shown in Figure 43d, and if bubbles produced by cavitation collapse at the entrance of this narrow channels created by the solid grains, the liquid is forced to move through (sonocapillary effect). This phenomenon cannot happen at smaller processing times because the semisolid alloy is compacted too quickly not allowing the liquid channels to be formed.

Interesting to note that the purification efficiency achieved for Fe and Si in the Al-Fe-Si alloy is the lowest. Probably, as has been mentioned for the one step squeezing procedure, the

ultrasonic vibrations still enhance the nucleation of the $Al_{13}Fe_4$ and Al_8Fe_2Si intermetallics, clogging the liquid channels and removing Fe and Si from the liquid phase, lowering the purification efficiency.

Table 20: Chemical composition of the purified fraction and the residue of the samples squeezed step by step with US application

	Al, wt%	**Cu, wt%**	**Si, wt%**	**Fe, wt%**	**Ni, wt%**	**Purification efficiency (E)**
Al-Cu	94.5±0.1	5.33±0.06	0.02	0.01		
purified	92.8±0.3	2.03±0.15	0.02	0.01		62%
Residue	94.9±0.1	6.54±0.13	0.02	0.01		
Al-Si	97.3±0.1	-	2.5±0.1	0.01		
Purified	99.0±0.09	-	0.8±0.1	0.01		68%
Residue	96.0±0.1	-	3.79±0.1	0.01		
Al-Fe-Si	97.1±0.1	-	1.33±0.03	1.41±0.02		
Purified	98.2±0.1	-	0.77±0.04	0.82±0.06		42%Si 41%Fe
Residue	96.2±0.1	-	1.79±0.03	1.87±0.05		
Al- Ni	97.7±0.1	-	0.02	0.01	2.9±0.1	
Purified	93.8±0.2	-	0.02	0.01	1.3±0.3	55%
Residue	95.3±0.2	-	0.02	0.01	4.4±0.2	

As discussed in Section 6.2.2 grain refiner was beneficial in increasing the purification efficiency in a one-step procedure. We decided to test the effect of the grain refiner and the ultrasonic vibration together. Tables 21 and 22 show that the efficiency of purification is around 30% for all grain refined tested alloys and elements, which is slightly less than achieved for the one step procedure (Tables 18 and 19) and significantly less than for US only in the multi-step procedure (Table 20). Also, the purification efficiency for Fe is the lowest one (table 22).

According to the literature [118], [119] there are conflicting results about the influence of Al-Ti-B on the formation mechanism of Fe bearing phases and it is still not clear yet how the mechanism happens.

Table 21: Purification efficiency for an Al-5 wt% Cu in a multi-step squeezing procedure in three different condition: GR no US, US, US+GR

	Al, wt%	**Cu, wt%**	**Purification efficiency (E)**
Al-Cu	94.5±0.1	5.3±0.1	
Purified US	97.7±0.2	1.5±0.1	70%
Residue US	92.9±0.1	6.5±0.1	
Purified Gr no US	95.3±0.1	4.41±0.08	26 %
Residue Gr no US	93.7±0.1	5.7±0.1	
Purified US+Gr	95.5±0.2	3.83±0.15	29%
Residue US+Gr	93.3±0.2	5.7±0.2	

It appears that the combination of grain refiner and ultrasonic vibration does not help the purification when it is done in several steps. It has to be remembered that the material is processed in a semisolid state, during deformation and with changes in composition after every squeezing step. The mechanisms that happen on a microstructure level are many (dendrite fragmentation, coalescence, Ostwald ripening, adjustment of grains) and these may also interfere in the purification efficiency. Probably when only US vibrations are applied, the sonocapillary effect is the prevailing mechanism, but when GR are added as well, other mechanisms play a role, with liquid channels being too narrow for US action. It would be interesting, in future research, to explore more the combinations on grain refinement with US.

Table 22: Chemical composition of the purified fraction and the residue of the sample squeezed step by step when grain refiner was added before the purification process

	Al, wt%	Cu, wt%	Si, wt%	Fe, wt%	Ni, wt%	Purification efficiency (E)
Al-Cu	95.1±0.1	4.7±0.1	0.02	0.01		
purified	96.7±0.2	3.09±0.17	0.02	0.01		34%
Residue	93.3±0.2	6.42±0.27	0.02	0.01		
Al-Si	97.2±0.1	-	2.6±0.1	0.01		
Purified	98.0±0.01	-	1.80±0.05	0.01		30%
Residue	96.5±0.1	-	3.31±0.1	0.01		
Al-Fe-Si	97.2±0	-	1.30±0.02		1.39±0.02	
Purified	97.9±0.1	-	0.87±0.06		1.10±0.07	33% Si 21%Fe
Residue	96.2±0.1	-	1.9±0.1		1.83±0.07	
Al- Ni	97.7±0.1	-	0.02	0.01	3.0±0.1	
Purified	97.6±0.2	-	0.02	0.01	2.1±0.2	30%
Residue	96.1±0.1	-	0.02	0.01	3.6±0.1	

6.3.3 Temperature

Temperature is a key parameter in the fractional solidification process. Temperature influences the diffusion rate and the partitioning of solute elements. From a thermodynamic point of view, the compositional gap between the solid and the liquid phases increases with the decreasing temperature. However, for aluminium alloys, a solid fraction higher than 30% exceeds the coherency threshold making progressively difficult to drain the liquid. So, the choice of the right temperature has to be a compromise between the coherency point and the difference in solute concentration in the solid and liquid fractions. For this reason, as showed in Section 6.1, the temperature at which every alloy was processed is the one corresponding to 50% solid fraction of primary aluminium, which is approximately 20-25% of the solid phase in the system. Also, the process should take place isothermally, which means that the temperature of the processed alloy and the temperature of the set-up need to be the same.

A series of experiments were done to optimise the temperature and to verify the outcome of a change in temperature. Table 23 summarises the results for an Al-5 wt% Cu alloy processed with three different temperature settings for the setup:

1. Temperature equal to the chosen temperature reflecting 25% solid.
2. Temperature 5 degrees higher.
3. Temperature 5 degrees lower.

Table 23: Purification efficiency values for an Al-5 wt% Cu processed at three different temperatures of the set-up using a squeezing procedure by steps and ultrasound.

Temperature °C	**Purification efficiency**
645	34%
650	76%
641	24%

Let us now have a look at the temperature changes measured during the experiment. Figure 75 shows the changes of temperature in the processing channel during the time of the experiment when it is performed in a multi-step procedure. Table 23 shows the purification efficiency.

As mentioned earlier, the temperature initially drops (0 min is the moment of pouring). When US only is applied, the temperature drops and starts to raise back half-way through the experiment. This actually facilitates the squeezing, and the process itself, because the rising of temperature induces some remelting of eutectics enriched in solutes that remained entrapped at the grain boundaries and started to solidify. This reheating is a result of the energy introduced into the system by ultrasonic vibrations and cavitation.

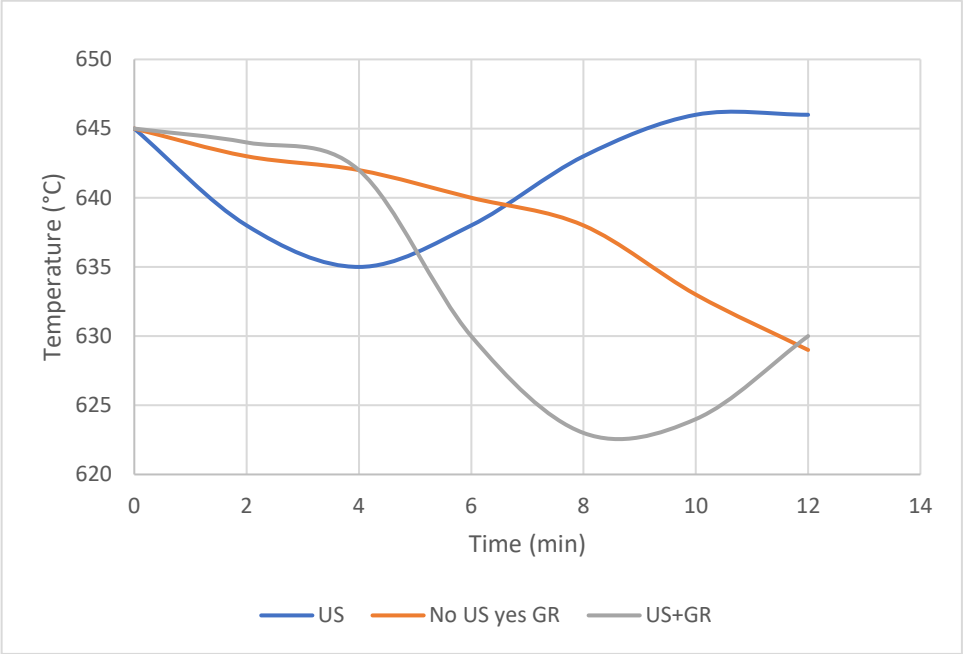

Figure 75: Variation of temperature in the processing channel during the multi-steps squeezing procedure for Al-5 wt% Cu in three different conditions: No US yes GR, US only, US+GR

When ultrasound is not applied, the temperature decreases until the end of the experiment. The piston/ sonotrode is a massive piece of steel and, although pre-heated, it tends to absorb the heat and cool down the alloy. When US is on, this cooling effect is reduced due to the energy introduced by US vibrations into the mushy alloy.

The results shown in Table 21 confirm that the rising in temperature measured with US processing benefits the purification efficiency. This effect is additional and assistant to the sonocapillary mechanism that facilitates moving the liquid in the channels between grains.

6.4 Fractional solidification processing of a real scrap alloy

Our experiments on model alloys demonstrated that the best purification efficiency was reached when the squeezing procedure was done in steps and when US was applied, also when the initial temperature of the setup was set 5 °C above the calculated semi-solid temperature to compensate for the initial cooling. It was decided that these conditions would be the optimised procedure.

The further step in the development of the fractional solidification as a purification technology, was to test the optimised procedure on real scrap alloys.

The composition of the real scrap alloy, obtained by remelting the end-of-life automotive scrap, has been shown in Table 5 in Section 3.2. Figure 76 shows the respective phase diagram section for the composition shown in Table 5. Since Fe is the most harmful impurity and the most import to eliminate, it was appropriate to represent the phase diagram considering the mass fraction of Fe.

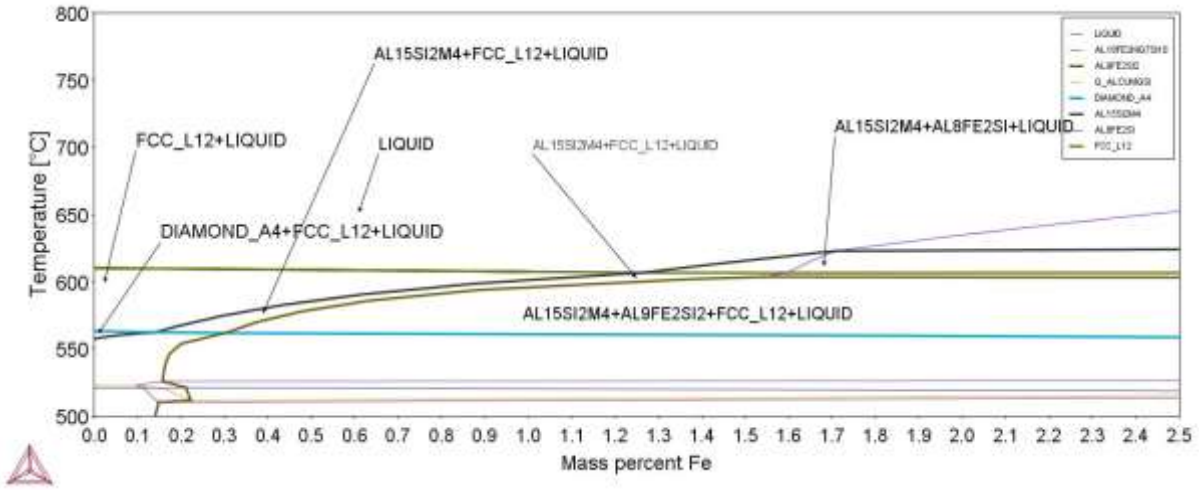

Figure 76: A vertical section of the phase diagram for the real scrap Al-2.34 wt% Cu- 6.32 wt% Si-0.5wt% Mg-0.90 wt% Zn- 0.2 wt% Mn- x wt% Fe alloy.

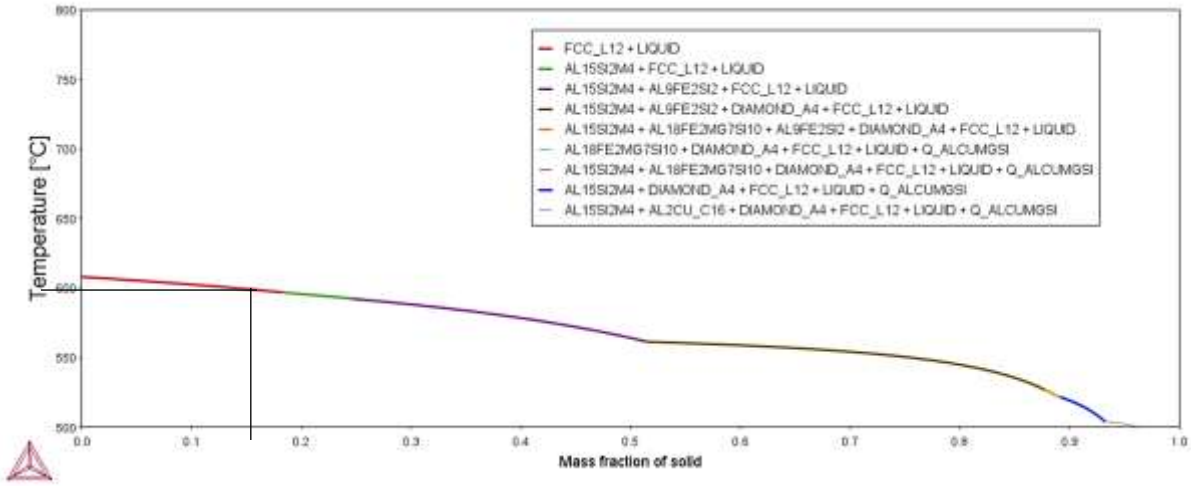

Figure 77: Evolution of the solid fraction in the real-scrap alloy calculated by Thermocalc using the Scheil equation.

Figure 77 shows the evolution of the solid fraction according to the Scheil approximation. When the mass fraction of solid phase is close to 20%, in addition to the Al grains there is already the formation of the $Al_{15}Si_2Mn_4$ intermetallic phase from the liquid. This takes part of Si and Mn from the liquid and interferes with the purification. So, the temperature at which we chose to operate was T=595 °C and it corresponds to a mass fraction of solid of 15%. Although the model alloys described in Section 6.1 were poured, in the set-up, at semisolid temperatures equal to 50% of primary aluminium, this guideline is more difficult to apply it here. Processing the real scrap at 50% primary Al, means pouring the semisolid alloy when the total solid fraction is 8%. This mean losing almost all the material through the filter before even starting the squeezing procedure. For this reason, we decide to process the alloy at the 15% solid fraction.

As Table 24 demonstrates, the set-up designed works efficiently in removing Si, Cu, Mg and Zn. It is interesting that this time, Mg was actually purified from the alloy. Obviously the two alloys processed (Al- 4 wt% Mg and real scrap) are completely different and so is the amount of Mg present in the liquid phase at the processing temperature.

Fe and Mn did not get removed, their composition even slightly increased in the purified fraction in comparison to the residue fraction. This is probably because we did not manage to avoid the formation of the quaternary intermetallic phase $Al_{15}(FeMn)_3Si_2$ which is usually called shortly α-AlFeSi.

Table 25: Average chemical composition of the real scrap alloy before processing and after the optimised purification procedure (US vibrations are applied). Note that the composition of the real scrap alloy before processing differs slightly from the one shown in Table 5 in Section

3.2. This is because the real scrap was manually sorted and molten before every experiment, so it is quite difficult to obtain every time the same composition.

	Al	**Si**	**Cu**	**Fe**	**Mg**	**Mn**	**Zn**
Real scrap	86.6±0.1	7.4±0.1	3.0±0.1	0.8±0.1	0.6±0.1	0.2±0.1	0.9±0.1
Purified fraction	89.9±0.1	5.0±0.1	1.9±0.1	0.91±0.08	0.4±0.1	0.3±0.1	0.6±0.1
Residue fraction	84.4±0.1	8.28±0.09	3.6±0.1	0.78±0.08	0.7±0.1	0.2±0.1	1.0±0.1
efficiency (E)	-	32%	37%	-	33%	-	33%

The intermetallic structure circled in Figure 78 a) and b) can be the polygonal α-AlFeSi phase particles which formation is facilitated by US processing [117].

The overall degree of purification is not as high as the results seen in Section 6.2 because the real alloy is a complex thermodynamic system, where the dynamic changing of the composition upon squeezing, changes the ratio between phases and solid and liquid fractions in the way that is difficult to account for at the moment. Also, the operational window of temperature is very small, which makes it difficult to control the process.

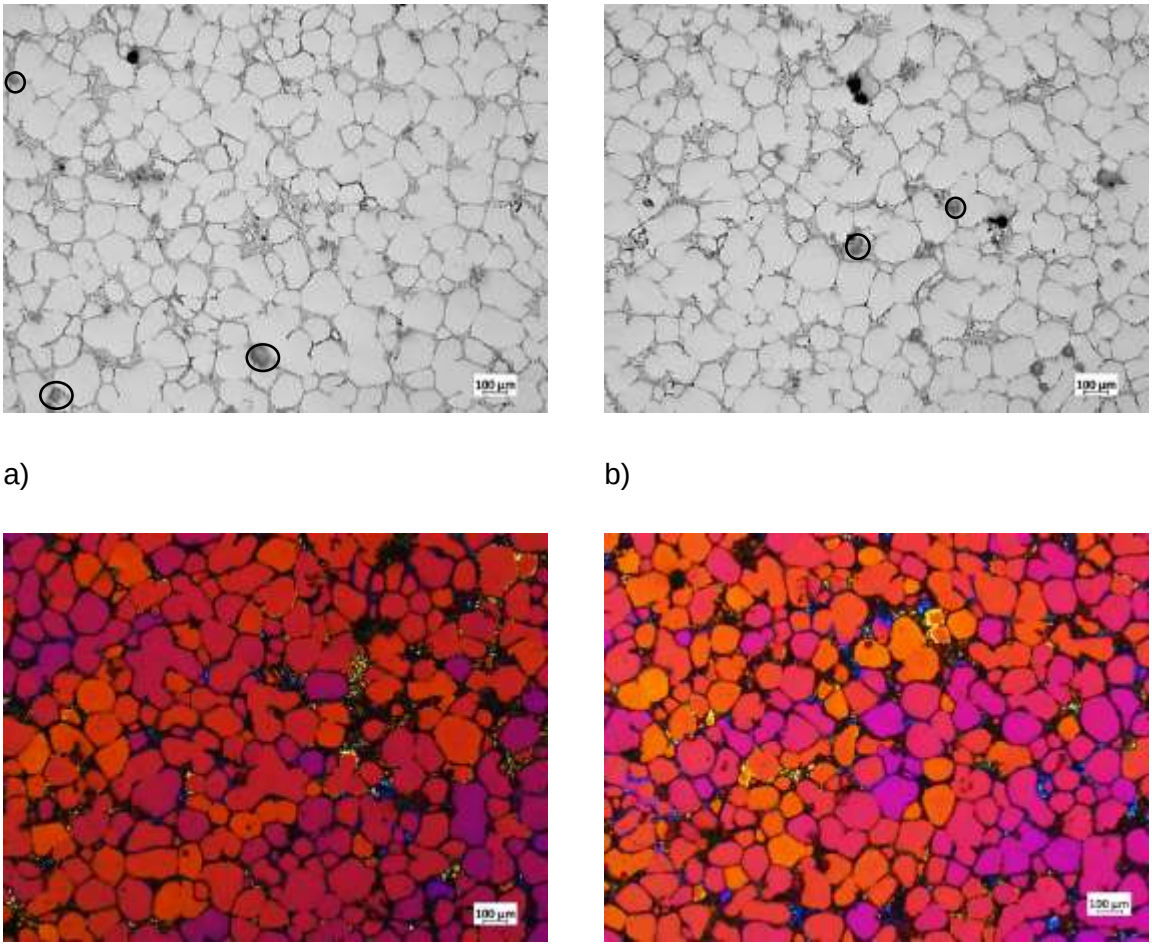

a) b)

c) 230±6 d) 239±5 µm

Figure 78: Microstructures and anodized images of purified real scrap alloy taken close to the filter a) and c) and far from the filter b) and d)

Since the Fe content was not possible to eliminate in the first purification stage, it was decided to repeat the purification process on the residue fraction collected at the end of the process. This residue fraction has a different composition of the initial alloy, so the phase diagram is slightly different. This might help in the purification process. Also, the temperature at which the semisolid alloy has been initially processed is the one corresponding at 15% solid fraction, consequently the amount of residue fraction that passes through the filter is large. So, reprocessing the residue is also a technological way to avoid wasting of material.

The chemical composition in Table 26 is somewhat different from the one showed in the residue fraction in Table 25 because Table 25 shows the selected result out of a series of experiments. The residues fraction collected from these experiments were mixed together to be processed in this second trial and have the composition shown in Table 26. This alloy was poured in the set-up at 15% solid fraction at 590 °C.

As it appears from Table 26, the process works again very well for Si, Cu and Mg. Iron is difficult to eliminate also in this second trial due to the same reason: the early formation of the quaternary intermetallic phase $Al_{15}(FeMn)_3Si_2$ shown in Fig 79.

In future works it would be interesting to investigate the role of ultrasound on the formation of Fe containing intermetallic phase. Another option is to change the temperature of processing to avoid the formation of Fe-containing phases.

Table 26: Chemical analysis of the residue fraction collected at the end of the first purification process that is process in a new purification process.

	Al	**Si**	**Cu**	**Fe**	**Mg**	**Mn**	**Zn**
Initial composition	85.2±0.2	7.91±0.1	3.2±0.1	0.8±0.1	0.5±0.1	0.2±0.1	0.9±0.1
Purified fraction	89.4±0.2	5.5±0.2	2.0±0.1	1.0±0.1	0.3±0.2	0.3±0.1	0.8±0.1
Residue fraction	85.4±0.2	8.75±0.08	3.6±0.1	0.8±0.1	0.60±0.1	0.2±0.1	1.0±0.1
Purification efficiency (E)	-	30%	38%	-	40%	-	11%

Even if it was not possible to decrease the concentration of Fe and Mn in this particular scrap composition, the technology developed in this work demonstrated the capability of purifying a range of alloying elements, also in real scrap alloys

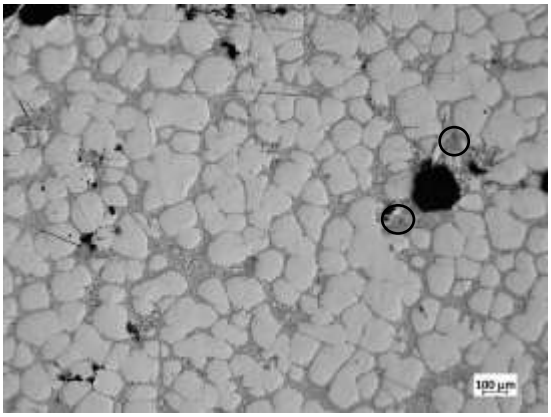

a)

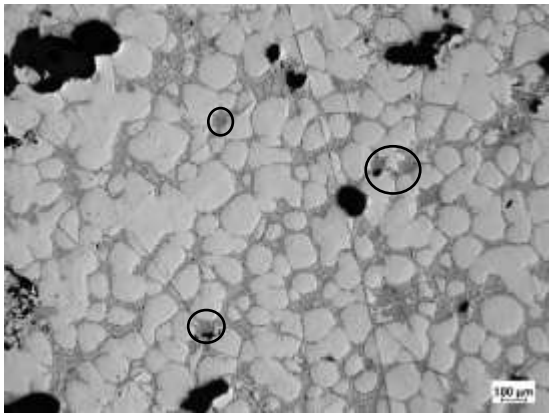

b)

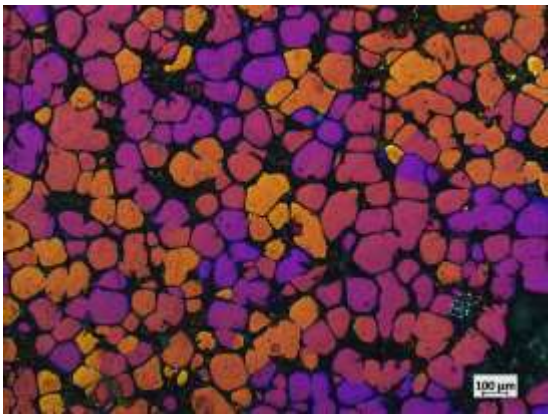

c) 275±12 µm

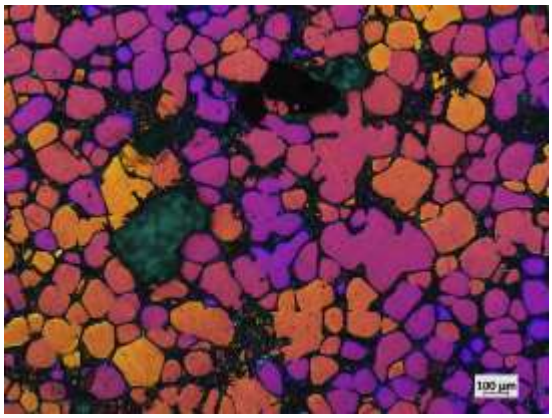

d) 284±17 µm

Figure 79: Microstructures and anodized images of purified real scrap alloy taken close to the filter a) and c) and far from the filter b) and d)

6.5 Summary

- Fractional solidification is performed through an isothermal squeezing of a semisolid alloy towards a filter
- An initial set-up, able to process 500g of material, was built to verify the feasibility of the process and it was proven successful on Al-7 wt% Si and Al-1 wt% Si- wt% Fe
- An optimised upscaled set-up able to process up to 3 kg of semisolid alloy was built.
- The upscaled set-up has been optimised for a procedure of squeezing by steps and with the application of US vibrations.
- The upscaled set-up was successfully applied on Al-Si, Al-Cu, Al-Ni and Al-Si-Fe alloys.
- The optimised upscaled set-up was successfully applied to purification of a real scrap alloy with the efficiency 30-40% depending on the alloying element.

7. Conclusions

This thesis focuses on the application of the fractional solidification principle in order to purify Al alloys. There are, currently, established methods for the purification of cast and wrought alloys; however the application of these procedures will lead to a non- recyclable surplus in the long ran. After careful literature investigation and taking inspiration from an idea developed in 1979 by A.L. Lux and M.C Flemings, a small-scale set-up able to process 500 g of material, was built. In this set-up a semisolid alloy was isothermally squeezed towards a filter by a piston. A purification efficiency close to 50% was achieved for Al-7 wt% Si and Al-1 wt% Si-1 wt% Fe alloys. In the second stage of the thesis, an upscaled and more robust set-up was built. This made it possible to process up to 3 kg of material. The set-us was tested on a wider selection of model alloys: Al-3 wt% Si, Al-5 wt% Cu, Al-1 wt% Si-1 wt% Fe, Al-3 wt% Ni. With this new set-up, the scientific investigation was focused on evaluating the effect of the processing parameters that could influence the solidification and hence the purification achievable, in order to develop an optimise procedure to apply for the purification of real scrap alloys from Jaguar and Land Rover. The process parameters, and their effect, are listed below.

- Grain size: the structure and the grain size influence the purification achievable. Although the semisolid alloy during the deformation process loses the initial structure due to effects like coarsening, dendrites fragmentation and coalescence, a structure made of small and rounded grains facilitate the migration of the liquid inside the mush towards the filter. This eases the squeezing process and prevent the liquid fraction to remain entrapped at the grain boundaries lowering the purification efficiency. So, grain refining of an alloy prior to isothermal squeezing process, enhances the purification. This effect is more pronounced in a one-step squeezing procedure.

- Ultrasonic vibrations: the application of ultrasonic vibrations was proven beneficial in increasing the purification efficiency in a multi-squeezing procedure. The ultrasonic vibrations, due to the sonocapillary effect, help the liquid to move through narrow channels, i.e. the ones created between solid grains that impinge on each other. The application of US was more effective when the squeezing procedure was performed by steps. This is probably due to several factors. A squeezing procedure by steps takes place over a longer time than the one done in one step only. During this time, the US vibrations increase the temperature of the melt compensating for the initial cooling of the slurry by the piston, causing some dendrites to remelt and facilitating the migration of the liquid. Also, a longer processing time prevents the semisolid material from being immediately compacted by the piston without giving sufficient time to the liquid fraction

to actually be pushed by the cavitation bubbles. The effect of US vibrations on a semisolid material is not very much investigated in literature, so some open questions may still remain. It would be interesting to have a deeper understanding of the effect of the US on semisolid material with different percentage of liquid or solid fractions.

Along with the process parameters, there are some technological parameters that influence the procedure and the purification

- A squeezing procedure by steps is preferred over a procedure done in one step only. This is to avoid that the semisolid alloy is compacted to soon, entrapping liquid fraction between the impinged grains and not allowing the liquid to migrate inside the mush to reach the filter.
- The temperature of the set-up set at 5 degrees higher than the semisolid calculated one, compensate for some temperature drop registered during the experiments.

It was demonstrated that within the time frame of the experiment, the back diffusion did not play significant role and did not affect the distribution of the solutes between the liquid and the solid phases. Finally, it was demonstrated by in-situ experiments that the migration of the liquid inside the mush in not homogenous and follows a random path. In fact, during the deformation of a semisolid alloy several phenomena takes place (dendrites fragmentation, coalescence, coarsening, Ostwald ripening) and it is quite hard to understand which one is prevailing and this has to be taken into consideration in the future work.

7.1 Future work

As described the previously, an upscaled set-up was built and optimised considering the effect of process parameters and technological parameters. Some aspects of the research done in this thesis, can be further investigated to improve the study in the field.

- The effect of the ultrasonic vibrations on different semisolid materials, not just aluminium alloys. Specifically, it could be very interesting, to consider a semisolid transparent organic system because it does not involve high processing temperatures and it allows to visualise, with a high-resolution camera, the response of the system upon vibrations. A transparent system could also be considered to study, in situ, the behaviour of the semisolid material upon deformation.
- A deeper understanding of the combined effect of ultrasonic vibrations and grain refiner on aluminium alloys with different concentration of alloying elements.
- The temperature of the set-up was optimised for a value five degrees higher than the calculated semisolid temperature. The choice was done taking into account the sensibility of the measuring instruments available and the scope of the research. However, a further investigation considering different temperature increments could be very interesting for industrial applications.
- Finally, it would be very interesting to test the technology on real scrap alloys with different concentration of alloying elements and, potentially, to use this technology in tandem with new emerging technologies on aluminium recycling. This could improve the quality of the recycled (or purified) material.

Acknowledgements

I would express my gratitude to Professor Dmitry Eskin for giving me the opportunity of this PhD, for actively taking part in every experiment, and for helping in the editing of this thesis. I had the chance to learn a lot.

I would like to thank Professor Alain Jacot for the import help with the modelling part.

I would like to thank EPSRC and Jaguar and Land Rover for the huge opportunity given to me with this PhD project. This work, in fact, is part of an Industrial Case PhD project jointly funded by Engineering and Physical Sciences Research Council of UK (voucher no 16000068) and Jaguar Land Rover. Particularly I would like to express my gratitude to my industrial advisors Adrian Tauscher, Michael Lough, and Paul Blake, for the precious suggestions during these four years.

I would like to thank Professor Peter Lee and Dr. Biao Cai for the kindness in giving us some their in-situ synchrotron data for further analysis. Thank you, also, to Dr Nima E. Gorij for the image analysis support. I would like also to express my gratitude to Dr Chamini Mendis for the help with the computed tomography acquisition and analysis, and for being a constant and reliable presence during these four years.

I would like to express my appreciation to Dr. Feng Wang, for helping me to move my first steps in the metallurgical labs, and to Dr. Tungky Subroto for being an amazing scientist and colleague, as well a good friend.

A deep and sincere thank you, to all the technicians in BCAST for dealing with me and for being such a good support. Particularly I would like to thank Graham Mitchell for the huge help in building and improving the set-ups day by day, and Peter Lloyd for machining a huge number of samples. I would like to thank, also, Sam Melvin for never refusing to help me, and for being a friend during these years.

I would also like to thank Dr. Lorna Anguilano, meeting you has been a revelation. Your scientific advice, your life tips, and your charismatic personality, are source of inspiration every day.

On a more personal note there are few people that I would like to thank.

To Kilian, Jaime, Elena, Alberto, Paula, Arnas, Florencia and German, thanks for sharing with me lots of fun moments. To Paula, especially, for your friendship, your precious advice, and your work ethic. You are a role model.

I would like to express my gratitude to Lauren and Susan, meeting you has been a gift that I want to preserve and cherish for a long, long, time. You girls are amazing beyond words.

A special thanks to Amy, your presence, your friendship, and your joy, have been my constant strength in this journey. Everything would have been different without you. I can’t wait to toast together to the life that is awaiting us.

Last, but not least, I would like to express my gratitude to a person who came into my life towards the end of this journey but has made it all different and more beautiful.

Infine, un grazie speciale alla mia famiglia, loro sono il mio faro nella notte e i pilastri della mia anima, e un grazie, dal profondo del mio cuore, ai Daniletti, Giulia, ed Alessandra. Grazie per scegliere sempre di condividere le vostre vite come me e per non avermi mai dimenticato. A Diletta, grazie per moltissime cose, ma soprattutto al fato (o chi per lui) per averci fatto incontrare.

Bibliography

[1] 'Hall Process Production and Commercialization of Aluminum - National Historic Chemical Landmark', *American Chemical Society*. https://www.acs.org/content/acs/en/education/whatischemistry/landmarks/aluminumprocess.html.

[2] A. Association, 'International alloy designations and chemical composition limits for wrought aluminum and wrought aluminum alloys', *Teal Sheets*, pp. 1–28, 2009.

[3] M. C. Santos, A. R. Machado, W. F. Sales, M. A. S. Barrozo, and E. O. Ezugwu, 'Machining of aluminum alloys: a review', *Int. J. Adv. Manuf. Technol.*, vol. 86, no. 9, pp. 3067–3080, Oct. 2016, doi: 10.1007/s00170-016-8431-9.

[4] T. Monetta, A. Acquesta, and F. Bellucci, 'A multifactor approach to evaluate the sealing of "smooth-wall" containers for food packaging', *Surf. Coat. Technol.*, vol. 310, pp. 33–37, Jan. 2017, doi: 10.1016/j.surfcoat.2016.12.041.

[5] 'Recycling | The Aluminum Association'. https://www.aluminum.org/industries/production/recycling.

[6] 'BIR - Home of BIR'. https://www.bir.org/.

[7] S. Capuzzi and G. Timelli, 'Preparation and Melting of Scrap in Aluminum Recycling: A Review', *Metals*, vol. 8, no. 4, Art. no. 4, Apr. 2018, doi: 10.3390/met8040249.

[8] E. David and J. Kopac, 'Use of Separation and Impurity Removal Methods to Improve Aluminium Waste Recycling Process', *Mater. Today Proc.*, vol. 2, no. 10, Part A, pp. 5071–5079, Jan. 2015, doi: 10.1016/j.matpr.2015.10.098.

[9] Mark. E. Schlesinger, *Aluminium recycling*, Second edition. CRC press, 2013.

[10] G. Coates and S. Rahimifard, 'Modelling of post-fragmentation waste stream processing within UK shredder facilities', *Waste Manag.*, vol. 29, no. 1, pp. 44–53, Jan. 2009, doi: 10.1016/j.wasman.2008.03.006.

[11] D. Montagna, F. Ambrose, and R.D.J Brown, 'Separation of cast and wrought alloys by Thermomecanical Processing'. Department of interior, Bureau of Mines Washington DC USA, 1985.

[12] B. Noharet, T. Irebo, and H. Karlsson, 'Compact industrial LIBS systems can assist aluminum recycling', p. 3.

[13] A. Gesing, L. Berry, R. Dalton, and R. Wolanski, 'Assuring continued recyclability of automotive aluminum alloys: Grouping of wrought alloys by color, x-ray absorption and chemical composition-based sorting', *TMS Annu. Meet.*, pp. 3–17, Jan. 2002.

[14] M. Ohtaki, T. Arakawa, and F. Murata, 'A new proposal of continuous agitation vacuum distillation process (CAVP) to remove Zn from aluminium scrap melt', *Fourth International symposium on recycling metal and engineering materials*, TMS, 2000.

[15] Y. Bao *et al.*, 'Simultaneous Removal of Silicon and Iron-Rich Phases from Coarse Al-Si Alloys Using Manganese Under Electromagnetic Field', *Metall. Mater. Trans. B*, vol. 49, no. 6, pp. 3413–3423, Dec. 2018, doi: 10.1007/s11663-018-1412-7.

[16] Jaime Lazaro-Nebreda, Jayesh B. Patel, Ian Stone, Geoff M. Scamans, and Zhongyun Fan, 'De-ironing of Aluminium alloy scrap by high shear melt conditioning technology', *6th Decenn. Int. Conf. Solidif. Process.*, pp. 601–604, Jul. 2017.

[17] Jonathan A. Dantzig and Michel Rappaz, *Solidification*. Lausanne, Switzerland: EPFL Press, 2009.

[18] William D. Callister Jr and David G. Rethwisch, *Materials Science and Engineering*, 7th Edition. John Wiley & Sons, 2007.

[19] S. Giorgini, 'Lecture Notes on Statistical Mechanics - Course for the Master degree in Physics at the University of Trento from 2010 to 2015 (misprints amended and solution to problems added)'. Accessed: Jul. 09, 2020. [Online]. Available:

https://www.researchgate.net/publication/291075075_Lecture_Notes_on_Statistical_Mechanics_-_Course_for_the_Master_degree_in_Physics_at_the_University_of_Trento_from_2010_to_2015_misprints_amended_and_solution_to_problems_added.
[20] William G. Boettinger and Dilip K. Banerjee, 'Solidification', Material Science and Engineering Division, Material Measurements Laboratory NIST, USA: Elsevier, 2014, p. 212.
[21] TS Prasanna Kumar, 'Casting Simulation Methods', Indian Institute of Technology, Madras, Chennai India: Elsevier, 2014.
[22] Martin Eden Glicksman, *Principles of solidification*. Springer, 2011.
[23] 'DoITPoMS - TLP Library Solidification of Alloys - Dendritic Growth'. https://www.doitpoms.ac.uk/tlplib/solidification_alloys/dendritic.php.
[24] Bedri Drini, 'Aluminium scrap refining with fractional layer crystallization', Technische Universiteit Delft, 2006.
[25] V.R. Voller and C. Beckermann, 'A unified model of micosegregation and coarsening', *Metall and Materi Trans A*, vol. 30, pp. 2183–2189, 1999.
[26] H. V. Atkinson, 'Semisolid processing of metallic materials', *Mater. Sci. Technol.*, vol. 26, no. 12, pp. 1401–1413, Dec. 2010, doi: 10.1179/026708310X12815992418012.
[27] Z. Fan, 'Semisolid metal processing', *Int. Mater. Rev.*, vol. 47, no. 2, pp. 49–85, Apr. 2002, doi: 10.1179/095066001225001076.
[28] B. Cantor and A. Vogel, 'Dendritic solidification and fluid flow', *J. Cryst. Growth*, vol. 41, no. 1, pp. 109–123, 1977.
[29] D. M. Smith, J. A. Eady, L. M. Hogan, and D. W. Irwin, 'Crystallization of a faceted primary phase in a stirred slurry', *Metall. Trans. A*, vol. 22, no. 2, pp. 575–584, 1991.
[30] S. Ji and Z. Fan, 'Solidification behavior of Sn-15 wt pct Pb alloy under a high shear rate and high intensity of turbulence during semisolid processing', *Metall. Mater. Trans. A*, vol. 33, no. 11, pp. 3511–3520, 2002.
[31] A. Vogel, R. D. Doherty, and B. Cantor, 'Solidification and casting of metals', *Met. Soc. Lond.*, vol. 518, p. 525, 1979.
[32] Q. Han and A. Hellawell, 'Primary particle melting rates and equiaxed grain nucleation', *Metall. Mater. Trans. B*, vol. 28, no. 1, pp. 169–173, 1997.
[33] A. M. Mullis, 'Growth induced dendritic bending and rosette formation during solidification in a shearing flow', *Acta Mater.*, vol. 47, no. 6, pp. 1783–1789, 1999.
[34] R. S. Qin and Z. Fan, 'Fractal theory study on morphological dependence of viscosity of semisolid slurries', *Mater. Sci. Technol.*, vol. 17, no. 9, pp. 1149–1152, 2001.
[35] K. F. Griffiths, 'Method of and apparatus for segregating by fractional solidification', US3005691A, Oct. 24, 1961.
[36] G. Calliauw *et al.*, 'On the fractional crystallization of palm olein: solid solutions and eutectic solidification', *Food Res. Int.*, vol. 43, no. 4, pp. 972–981, 2010.
[37] M. Garcia-Arias and G. Stevens, 'Phase equilibrium modelling of granite magma petrogenesis: A. An evaluation of the magma compositions produced by crystal entrainment in the source', *Lithos*, vol. 277, pp. 131–153, 2017.
[38] M. Garcia-Arias and G. Stevens, 'Phase equilibrium modelling of granite magma petrogenesis: B. An evaluation of the magma compositions that result from fractional crystallization', *Lithos*, vol. 277, pp. 109–130, 2017.
[39] W. H. Sillekens, D. Verdoes, and J. S. Van WESTURM, 'Refining aluminium scrap by means of fractional crystallisation: technical feasibility', in *Proceeding of the Fourth ASM International Conference and Exhibition on the Recycling of Metals, ASM Europe*, 1999, pp. 105–113.
[40] H. L. Pattinson, 'An Improved Method of Separating Silver from Lead', *G. B. Pat.*, no. 6497, 1833.
[41] X. Zhang, S. Friedrich, and B. Friedrich, 'Production of high purity metals: a review on zone refining process', *J. Cryst. Process Technol.*, vol. 8, no. 01, p. 33, 2018.
[42] D. Geiger, M. Flemings, and R. Mehrabian, 'Methods of refining metal alloys', Oct. 08, 1974.

[43] R. K. Dawless, R. E. Graziano, and A. A. Bonarett, 'Fractional crystallization process', Sep. 09, 1980.
[44] K. Qiu, W. Duan, and Q. Chen, 'Basic principles of control of continuous crystallizer in metal refining', *Miner. Process. Extr. Metall.*, vol. 110, no. 3, pp. 161–164, 2001.
[45] J. D. Esdaile and G. W. Walters, 'Continuous reflux refining of metals', Jan. 09, 1979.
[46] R.F Boutin, 'Process for the Continuous Purification of Metals by Fractional. Crystallization on a Rotary Drum', US 4581062, Apr. 1986.
[47] P. A. De Vries and H. A. Wouters, 'Method for fractional crystallisation of a molten metal', Sep. 02, 2008.
[48] C. Celik and G. Dube, 'Process and apparatus for producing high purity aluminum', EP0375308A1, Jun. 27, 1990.
[49] B. Mehmetaj, O. S. L. Bruinsma, W. H. Kool, P. J. Jansens, and L. Katgerman, 'Aluminium scrap recycling with solid layer fractional crystallization', in *15th International Symposium on Industrial Crystallization (ISIC-15), Sorrento, Italy*, 2002, pp. 15–18.
[50] A. L. Lux and M. C. Flemings, 'Refining by fractional solidification', *Metall. Trans. B*, vol. 10, no. 1, pp. 71–78, 1979.
[51] N. Nicom and H. Nomura, 'Molten Metal Flow through Solid Network in Semi-Solid Al–Si Alloy', *Mater. Trans.*, vol. 46, no. 8, pp. 1897–1902, 2005.
[52] A. T. Ali, N. M. Stubina, and J. M. Toguri, 'Silicon removal from cast aluminum scrap using an isothermal compression technique', *Resour. Conserv. Recycl.*, vol. 2, no. 2, pp. 87–98, 1989.
[53] T. Sotome and M. Ohtaki, 'Application of fractional crystallization for refining of molten aluminum scrap', in *ICAA-6: 6 th International Conference on Aluminium Alloys*, 1998, pp. 351–356.
[54] K. Ichikawa, M. Katoh, F. Asuke, and Y. Nakazawa, 'High efficient recovery of pure aluminum from Al–Sn and Al–Ni alloys by rheorefining process', *Mater. Trans. JIM*, vol. 38, no. 7, pp. 622–629, 1997.
[55] V. N. Nurni, B. N. Ballal, and S. Seetharaman, 'Mass Diffusion in Process Metallurgy', in *Diffusion Foundations*, 2015, vol. 4, pp. 139–157.
[56] E. Machlin, *An introduction to aspects of thermodynamics and kinetics relevant to materials science*. Elsevier, 2010.
[57] S. Geng *et al.*, 'Effects of back-diffusion on solidification cracking susceptibility of Al-Mg alloys during welding: A phase-field study', *Acta Mater.*, vol. 160, pp. 85–96, 2018.
[58] M. Ganesan, L. Thuinet, D. Dye, and P. D. Lee, 'Quantification of microsegregation in cast Al-Si-Cu alloys', *Metall. Mater. Trans. B*, vol. 38, no. 4, pp. 557–566, 2007.
[59] D. Larouche, 'Computation of solidification paths in multiphase alloys with back-diffusion', *Calphad*, vol. 31, no. 4, pp. 490–504, 2007.
[60] A. L. Lux and M. C. Flemings, 'Refining by fractional melting', *Metall. Trans. B*, vol. 10, no. 1, pp. 79–84, 1979.
[61] G. K. Sigworth, 'Fundamentals of solidification in aluminum castings', *Int. J. Met.*, vol. 8, no. 1, pp. 7–20, 2014.
[62] Demian Gibran Ruvalcaba Jimenez, 'Microstructure Development during Solidification of Aluminium Alloys', Delft University of Technology, 2009.
[63] M. A. Easton, M. Qian, A. Prasad, and D. H. StJohn, 'Recent advances in grain refinement of light metals and alloys', *Curr. Opin. Solid State Mater. Sci.*, vol. 20, no. 1, pp. 13–24, 2016.
[64] G. K. Sigworth and T. A. Kuhn, 'Grain refinement of aluminum casting alloys', *Int. J. Met.*, vol. 1, no. 1, pp. 31–40, 2007.
[65] T. V. Atamanenko, D. G. Eskin, L. Zhang, and L. Katgerman, 'Criteria of grain refinement induced by ultrasonic melt treatment of aluminum alloys containing Zr and Ti', *Metall. Mater. Trans. A*, vol. 41, no. 8, pp. 2056–2066, 2010.

[66] G. Wang, M. S. Dargusch, M. Qian, D. G. Eskin, and D. H. StJohn, 'The role of ultrasonic treatment in refining the as-cast grain structure during the solidification of an Al–2Cu alloy', *J. Cryst. Growth*, vol. 408, pp. 119–124, 2014.
[67] Z. Y. Fan, Y. B. Zuo, and B. Jiang, 'A new technology for treating liquid metals with intensive melt shearing', in *Materials Science Forum*, 2011, vol. 690, pp. 141–144.
[68] H. Men, B. Jiang, and Z. Fan, 'Mechanisms of grain refinement by intensive shearing of AZ91 alloy melt', *Acta Mater.*, vol. 58, no. 19, pp. 6526–6534, 2010.
[69] G. I. Eskin and D. G. Eskin, *Ultrasonic Treatment of Light Alloy Melts, Second Edition*. CRC Press, 2014.
[70] N. Balasubramani, D. StJohn, M. Dargusch, and G. Wang, 'Ultrasonic Processing for Structure Refinement: An Overview of Mechanisms and Application of the Interdependence Theory', *Materials*, vol. 12, no. 19, p. 3187, 2019.
[71] C. J. Todaro, M. A. Easton, D. Qiu, G. Wang, D. H. StJohn, and M. Qian, 'Effect of ultrasonic melt treatment on intermetallic phase formation in a manganese-modified Al-17Si-2Fe alloy', *J. Mater. Process. Technol.*, vol. 271, pp. 346–356, 2019.
[72] H. K. Feng, S. R. Yu, Y. L. Li, and L. Y. Gong, 'Effect of ultrasonic treatment on microstructures of hypereutectic Al–Si alloy', *J. Mater. Process. Technol.*, vol. 208, no. 1–3, pp. 330–335, 2008.
[73] I. Tzanakis, W. W. Xu, D. G. Eskin, P. D. Lee, and N. Kotsovinos, 'In situ observation and analysis of ultrasonic capillary effect in molten aluminium', *Ultrason. Sonochem.*, vol. 27, pp. 72–80, 2015.
[74] B. Cai, S. Karagadde, D. Rowley, T. J. Marrow, T. Connolley, and P. D. Lee, 'Time-resolved synchrotron tomographic quantification of deformation-induced flow in a semi-solid equiaxed dendritic Al–Cu alloy', *Scr. Mater.*, vol. 103, pp. 69–72, 2015.
[75] R. F. Katz, M. Spiegelman, and B. Holtzman, 'The dynamics of melt and shear localization in partially molten aggregates', *Nature*, vol. 442, no. 7103, pp. 676–679, 2006.
[76] Y. Lavallée *et al.*, 'Seismogenic lavas and explosive eruption forecasting', *Nature*, vol. 453, no. 7194, pp. 507–510, 2008.
[77] T. Rølland, R. Flatval, and L. Arnberg, 'Strain induced macrosegregation in squeeze cast Al Mg and Al Si alloys', *Mater. Sci. Eng. A*, vol. 173, no. 1–2, pp. 267–270, 1993.
[78] B. Cai, P. D. Lee, S. Karagadde, T. J. Marrow, and T. Connolley, 'Time-resolved synchrotron tomographic quantification of deformation during indentation of an equiaxed semi-solid granular alloy', *Acta Mater.*, vol. 105, pp. 338–346, 2016.
[79] K. M. Kareh, P. D. Lee, R. C. Atwood, T. Connolley, and C. M. Gourlay, 'Revealing the micromechanisms behind semi-solid metal deformation with time-resolved X-ray tomography', *Nat. Commun.*, vol. 5, no. 1, pp. 1–7, 2014.
[80] R. Pastor-Satorras and M.-C. Miguel, 'Percolation analysis of force networks in anisotropic granular matter', *J. Stat. Mech. Theory Exp.*, vol. 2012, no. 02, p. P02008, 2012.
[81] Z. L. Ning, H. Wang, and J. F. Sun, 'Deformation Behavior of Semisolid A356 Alloy Prepared by Low Temperature Pouring', *Mater. Manuf. Process.*, vol. 25, no. 7, pp. 648–653, Jul. 2010, doi: 10.1080/10426910903447279.
[82] C. P. Chen and C.-Y. Tsao, 'Semi-solid deformation of non-dendritic structures—I. Phenomenological behavior', *Acta Mater.*, vol. 45, no. 5, pp. 1955–1968, 1997.
[83] S. Wasco, A. Orris, S.L Semiatin, and P. Raghupathi, *Forging Handbook*, T. G. Byrer, S. L. Semiatin and D. C. Vollmer. ASM, Metals Park, OH, 1985.
[84] H. Mohammadi, M. Ketabchi, and A. Kalaki, 'Microstructure evolution of semi-solid 7075 aluminum alloy during reheating process', *J. Mater. Eng. Perform.*, vol. 20, no. 7, pp. 1256–1263, 2011.
[85] S. Terzi, L. Salvo, M. Suery, and A. K. Dahle, 'Coarsening mechanisms during isothermal holding of a dendritic Al-10wt% Cu alloy', *Trans. Indian Inst. Met.*, vol. 62, no. 4–5, pp. 447–449, 2009.
[86] J. F. Seconde and M. Suery, 'Effect of solidification conditions on deformation behaviour of semi-solid Sn-Pb alloys', *J. Mater. Sci.*, vol. 19, no. 12, pp. 3995–4006, 1984.

[87] S. Annavarapu and R. D. Doherty, 'Inhibited coarsening of solid-liquid microstructures in spray casting at high volume fractions of solid', *Acta Metall. Mater.*, vol. 43, no. 8, pp. 3207–3230, 1995.
[88] A. Benabbou, H. Borouchaki, P. Laug, and J. Lu, 'Sphere packing and applications to granular structure modeling', in *Proceedings of the 17th International Meshing Roundtable*, Springer, 2008, pp. 1–18.
[89] R. Gupta, A. Sharma, and S. Kumar, 'Characterization Study of Al Alloy Cast through Strain Induced Melt Activated (SIMA) Process'.
[90] I. G. Brodova, P. S. Popel, and G. I. Eskin, *Liquid metal processing: applications to aluminium alloy production*. CRC Press, 2001.
[91] D. Eskin and F. Wang, 'Joint effect of ultrasonic vibrations and solid metal addition on the grain refinement of an aluminium alloy', *Metals*, vol. 9, no. 2, p. 161, 2019.
[92] N. V. Dezhkunov, A. Francescutto, P. Ciuti, and P. Ignatenko, 'Ultrasonic capillary effect and sonoluminescence', in *Proc. of 5-th World Congress on Ultrasonics (WCU 2003). Paris*, 2003, pp. 597–600.
[93] O. G. Martynenko and V. V. Levdansky, *PP Prokhorenko, NV Dezhkunov, GE Konovalov, Ultrasonic Capillary Effect, Nauka i Tekhnika, Minsk (1981)*. Pergamon, 1983.
[94] J.-C. Hung, Y.-C. Tsai, and C. Hung, 'Frictional effect of ultrasonic-vibration on upsetting', *Ultrasonics*, vol. 46, no. 3, pp. 277–284, 2007.
[95] J.-C. Hung and C. Hung, 'The influence of ultrasonic-vibration on hot upsetting of aluminum alloy', *Ultrasonics*, vol. 43, no. 8, pp. 692–698, 2005.
[96] H. V. Atkinson and D. Liu, 'Microstructural coarsening of semi-solid aluminium alloys', *Mater. Sci. Eng. A*, vol. 496, no. 1–2, pp. 439–446, 2008.
[97] E. Tzimas and A. Zavaliangos, 'Evaluation of volume fraction of solid in alloys formed by semisolid processing', *J. Mater. Sci.*, vol. 35, no. 21, pp. 5319–5330, 2000.
[98] O. Kudryashova and S. Vorozhtsov, 'On the mechanism of ultrasound-driven deagglomeration of nanoparticle agglomerates in aluminum melt', *Jom*, vol. 68, no. 5, pp. 1307–1311, 2016.
[99] T. S. Piwonka and M. C. Flemings, 'Pore formation in solidification', *Aime Met Soc Trans*, vol. 236, no. 8, pp. 1157–1165, 1966.
[100] D. R. Poirier and S. Ganesan, 'Permeabilities for flow of interdendritic liquid in equiaxial structures', *Mater. Sci. Eng. A*, vol. 157, no. 1, pp. 113–123, 1992.
[101] Ø. Nielsen, S. L. Arnberg, A. Mo, and H. Thevik, 'Experimental determination of mushy zone permeability in aluminum-copper alloys with equiaxed microstructures', *Metall. Mater. Trans. A*, vol. 30, no. 9, pp. 2455–2462, 1999.
[102] D. B. Oryshchyn and Ö. N. Doğan, 'An examination of effects of solidification parameters on permeability of a mushy zone in castings', *J. Mater. Sci.*, vol. 43, no. 4, pp. 1471–1479, 2008.
[103] D. Bernard, Ø. Nielsen, L. Salvo, and P. Cloetens, 'Permeability assessment by 3D interdendritic flow simulations on microtomography mappings of Al–Cu alloys', *Mater. Sci. Eng. A*, vol. 392, no. 1–2, pp. 112–120, 2005.
[104] G. I. Eskin, 'Prospects of ultrasonic (cavitational) treatment of the melt in the manufacture of aluminum alloy products', *Metallurgist*, vol. 42, no. 8, pp. 284–291, 1998.
[105] T. W. Clyne and W. Kurz, 'Solute redistribution during solidification with rapid solid state diffusion', *Metall. Trans. A*, vol. 12, no. 6, pp. 965–971, 1981.
[106] I. Ohnaka, 'Mathematical analysis of solute redistribution during solidification with diffusion in solid phase', *Trans. Iron Steel Inst. Jpn.*, vol. 26, no. 12, pp. 1045–1051, 1986.
[107] C. Y. Wang and C. Beckermann, 'A unified solute diffusion model for columnar and equiaxed dendritic alloy solidification', *Mater. Sci. Eng. A*, vol. 171, no. 1–2, pp. 199–211, 1993.
[108] A. Roosz, E. Halder, and H. E. Exner, 'Numerical calculation of microsegregation in coarsened dendritic microstructures', *Mater. Sci. Technol.*, vol. 2, no. 11, pp. 1149–1155, 1986.

[109] A. J. W. Ogilvy and D. H. Kirkwood, 'A model for the numerical computation of microsegregation in alloys', in *Modelling the Flow and Solidification of Metals*, Springer, 1987, pp. 43–49.
[110] I. Vusanovic and M. J. M. Krane, 'MICROSEGREGATION DURING SOLIDIFICATION OF AI-Cu-Mg ALLOYS WITH VARYING COMPOSITION', 2002.
[111] V. R. Voller and S. Sundarraj, 'Modelling of microsegregation', *Mater. Sci. Technol.*, vol. 9, no. 6, pp. 474–482, 1993.
[112] T. P. Battle and R. D. Pehlke, 'Mathematical modeling of microsegregation in binary metallic alloys', *Metall. Trans. B*, vol. 21, no. 2, pp. 357–375, 1990.
[113] Y. Du *et al.*, 'Diffusion coefficients of some solutes in fcc and liquid Al: critical evaluation and correlation', *Mater. Sci. Eng. A*, vol. 363, no. 1–2, pp. 140–151, 2003.
[114] W. H. Sillekens, D. Verdoes, and W. Boender, 'Refining aluminium scrap by means of fractional crystallisation: Status and prospects for development', *Met.-Berl.-*, vol. 56, no. 7/8, pp. 468–473, 2002.
[115] S. Ikhmayies, 'Phase Diagrams of Al–Si System', in *Energy Technology 2019*, Cham, 2019, pp. 231–237, doi: 10.1007/978-3-030-06209-5_24.
[116] G. Chai, L. BÄckerud, T. RØlland, and L. Arnberg, 'Dendrite coherency during equiaxed solidification in binary aluminum alloys', *Metall. Mater. Trans. A*, vol. 26, no. 4, pp. 965–970, 1995.
[117] Y. Osawa, S. Takamori, T. Kimura, K. Minagawa, and H. Kakisawa, 'Morphology of intermetallic compounds in Al-Si-Fe alloy and its control by ultrasonic vibration', *Mater. Trans.*, vol. 48, no. 9, pp. 2467–2475, 2007.
[118] W. Khalifa, F. H. Samuel, J. E. Gruzleski, H. W. Doty, and S. Valtierra, 'Nucleation of Fe-intermetallic phases in the Al-Si-Fe alloys', *Metall. Mater. Trans. A*, vol. 36, no. 4, pp. 1017–1032, 2005.
[119] L. A. Narayanan, F. H. Samuel, and J. E. Gruzleski, 'Crystallization behavior of iron-containing intermetallic compounds in 319 aluminum alloy', *Metall. Mater. Trans. A*, vol. 25, no. 8, pp. 1761–1773, 1994.